# MICROFABRICATED BRAIN ORGAN-ON-A-CHIP SYSTEMS FOR NEUROPHYSIOLOGICAL STUDIES

A Dissertation

by

SEHOON JEONG

Submitted to the Office of Graduate and Professional Studies of
Texas A&M University
in partial fulfillment of the requirements for the degree of

DOCTOR OF PHILOSOPHY

| | |
|---|---|
| Co-Chairs of Committee, | Arum Han |
| | Jianrong Li |
| Committee Members, | Mike J. McShane |
| | Akhilesh K. Gaharwar |
| Head of Department, | Mike J. McShane |

May 2018

Major Subject: Biomedical Engineering

ABSTRACT

Neurological diseases are a major challenge to reach new therapies. However, physiological signals that regulate neurodegeneration in the central nervous system (CNS) are still little known since there is no suitable in vitro model for studying the basis of localized cells and molecules. Here this dissertation presents the development of biomimetic microsystems that reconstitute neurophysiologically important functional brain and neurovascular interface in the CNS.

The brain organs-on-chips can recapitulate pharmacological responses and complex interactions between different types of cells that are mediated by the extracellular matrix and intercellular junctions within the organ model. Since the developed microsystems have a biomimetic tissue structure, it is possible to more accurately function and simulate the delivery and penetration of the drug compound in vivo than the 2D cell monolayer in the conventional culture model or the prior microfluidics.

The developed brain chip is composed of four culture chambers with 10 aggregate traps and multi-electrode arrays enable electrical stimulation for 40 neuronal aggregates as well as drug stimulation. Uniform 150 μm aggregates from the microwell can be cultured for 4 weeks. This system developed for the study of CNS myelin formation showed that the 10Hz of electrical stimulation for the promotion of myelination was successfully confirmed with 500 nM retinoic acid treatment results in the automatic image analysis.

The other developed blood-brain barrier (BBB) chip consists of 4 × 4 microfluidic channel arrays and 16 channel multi-electrode arrays, able to electrically analyze 16 sites. Co-culture BBB-on-a-chip contains neurovascular endothelium separated from primary astrocyte by a porous membrane that allows cell-cell interactions through the membrane. In this platform, the effects of astrocyte-coculture, extracellular matrix, and *in vivo* shear stress level on barrier permeability were characterized through TEER measurements and dextran permeability assays.

Also, despite the presence of BBB, monocyte infiltration into the CNS was observed by monocyte chemotactic protein (CCL2), which corresponds to the early event of brain injury. Finally, the system developed to address these pharmacological problems for drug development showed how drugs work in brain vessels (histamine) and brain tissues (tetrodotoxin), as well as delivering drugs from brain vessels to brain tissue (atenolol).

# DEDICATION

*I would like to dedicate this work to my wonderful wife, Sohun for her patience, love, and solid support through the harsh period of my graduate years. I am very lucky that there was somebody on my side who experienced everything in parallel with me. If she was not in my life, I am convinced that I would not be the person I am today. As we approach this new chapter of our lives, I am looking forward to a happy future with my wife, daughter, and son.*

# ACKNOWLEDGEMENTS

I would like to express my deep appreciation to Dr. Arum Han for his thorough guidance and support as my advisor and committee chair. He was an exceptional leader and gave me precious encouragement and suggestions throughout my research. I also deeply appreciate my co-advisor and my co-chair, Dr. Jianrong Li for her thoughtful guidance and support. I was interested in biomedical research when I became a graduate student, and I would like to thank both advisors, Dr. Han and Dr. Li, for helping me grow into other independent research areas. I am grateful for the guidance and support of my committee members, Dr. Michael McShane and Dr. Akhilesh Gaharwar throughout this research.

I thank all our group members in Dr. Han's and Dr. Li's laboratory for their support, help, and opinions from different perspectives. I want to express special thanks to Dr. Sanja Kim and John Buonocore for their wonderful work and valuable discussion. I also want to thank both group members, Hyunsoo Kim, Jing Dai, Song-I Han, Lanchun He, Can Huang, Adrian Guzman, Sergio Waqued, Nebras Sobahi, Jose Wippold, Sinan Yigit, Amirali Selahi, Prof. Younghak Cho, Prof. Jaewon Park, Prof. Chiwan Koo, Sungman Kim, Han Wang, Celal Erbay, Yusuf Dogan, Keith Krenek, Mijin Choi, Changwoo Ban, Shenyang Yang, Sungjin Kim, Felix Lu, Danielle Michaud, Bianca Barth, and Prof. Andrew Steelman. Also, I thank my friends, colleagues, faculty, and staff that helped make my time at Texas A&M University a wonderful experience.

Finally, without the strong support system of my family, we could not have done this. In particular, I would like to thank my parents and parents-in-law for their love, guidance, support, and encouragement in everything I have done. My brother and my brother-in-law have always supported me. My wife, my love and close friend always supports and encourages me, no matter what happens. My beloved daughter and son, the most grateful gifts in my life, brighten my life with so much happiness. To them, I dedicated this dissertation.

CONTRIBUTORS AND FUNDING SOURCES

## Contributors

This work was supervised by a dissertation committee consisting of Dr. Arum Han of the Department of Electrical & Computer Engineering and Dr. Jianrong Li of the Department of Veterinary Integrative Biosciences at Texas A&M University.

Preparing primary neurovascular endothelial cells was completed with the assistance of Dr. Jane Welsh of the Department of Veterinary Integrative Biosciences at Texas A&M University.

## Funding Sources

This work was partially supported by the National Institutes of Health (NIH) Grant #1R21EB021005-01.

# NOMENCLATURE

| | |
|---|---|
| 2D | Two-dimensional |
| 3D | Three-dimensional |
| CNS | Central Nervous System |
| BBB | Blood-brain Barrier |
| TEER | Transendothelial Electrical Resistance |
| MS | Multiple Sclerosis |
| CSF | Cerebrospinal Fluid |
| BOE | Buffered Oxide Etch |
| DRIE | Deep Reactive Ion Etching |
| ES | Electrical Stimulation |
| RA | Retinoic Acid |
| ROI | Region of Interest |
| MBP | Myelin Basic Protein |
| NF | Neurofilament |
| ROS | Reactive Oxygen Species |
| MMP | Matrix Metalloproteinases |
| CAM | Cell Adhesion Molecule |
| TTX | Tetrodotoxin |

TABLE OF CONTENTS

Page

LIST OF FIGURES

Page

# 1. INTRODUCTION

## 1.1 Objective and Motivation

The objective of this work is to demonstrate microfabricated organ-on-a-chip systems for neurophysiological studies. The research focuses on both a microelectrode array-based 3D CNS neural aggregate culture platform, as well as a biomimetic co-culture microfluidic BBB-on-a-chip that provides interactions between neuronal cells and neurovascular endothelial cells mimicking *in vivo* conditions.

A microelectrode array-based 3D neural aggregate culture platform can provide unprecedented control over the aggregate culture microenvironment. This is because the platform allows the formation of a large number of uniformly sized aggregates, and allows these aggregates to be loaded into an array of culture chambers where the inter-aggregate distances and number of aggregates in each culture chamber are accurately controlled with predetermined dimensions. The microfluidic platform also allows cultured aggregates to be easily treated with various biomolecules that promote *in vitro* myelin sheath formation. Since acute electrical stimulation aids in myelinogenesis, the platform has integrated microelectrodes within each microfluidic culture chamber.

On the other hand, the multi-compartment microfluidic BBB chip can recapitulate the critical functional astrocyte–capillary interface of the brain. This bioinspired microsystem is a multi–cellular integrated organ level analytical platform that mimics the brain–capillary interface. It uses only mouse primary endothelial cells and mouse primary astrocytes, co-cultured on each side of a porous membrane and

connected through a microfluidic network which allows physiologically relevant levels of shear stress. Each BBB compartment is equipped with integrated electrical impedance sensors that measure the permeability barrier function continuously and non–invasively.

Such developed systems are expected to eliminate the labor-intensive nature of conventional neuroscience research, enable control over the intracellular and extracellular fluid environment, enable fast and accurate characterization neurovascular units through microfluidics, and achieve high throughput by utilizing an array format. Automated and miniaturized multifunctional CNS neural aggregate chips and neurovascular BBB chips are expected to provide an in-depth look at neurophysiological events occurring at the organ level and pathological status with high throughput. The systems can be easily expanded to have additional functionalities including animal or human organs such as the liver, heart, kidney, and gut by creating various primary cell cultures on the system. The result of this study is expected to be applied for high-throughput drug screening and various disease model diagnosis by providing an accurate and effective analytical instrument.

## 1.2 Multiple Sclerosis

Multiple sclerosis (MS) is a chronic neurological disorder, characterized by demyelination of the CNS with consequent plaque formation (Figure 1). Although the course of the disease is often progressive, it is highly unpredictable and varies significantly between individuals. MS has been categorized by the number and severity of relapses, recovery, and progression of the disease but these categories are not distinct [1]. The cause of MS is unknown, but there is evidence indicating that an autoimmune mechanism is involved. It is also possible that other factors, including viral infection, may play a role in the pathogenesis of this disease [2-4]. People with MS may experience a variety of symptoms and side effects including bowel and bladder problems, fatigue, pain, sexual problems, spasticity, speech and swallowing difficulties, tremors, visual and cognitive problems [5].

MS causes demyelination plaque with glial scar formation. Although the process is characterized by demyelination, destruction of axons is also observed. There is evidence that the extent of axonal loss correlates with the reduction of N-acetyl aspartate in quantitative magnetic resonance spectroscopy, as well as with T1-weighted hypointensity in MRI and with the extent of CNS atrophy [6-9]. This has led to the concept that irreversible axonal damage is an essential cause of non-remitting clinical disability and disease progression. Most studies on the axonal injury, however, have been performed on autopsy tissue of patients, who died either from fulminant MS or after many years of a chronic disease course. Based on the analysis of this limited material, axon reduction was thought to occur early in the course of the disease and to

correlate with the extent of inflammation [10, 11]. Although there is some evidence from magnetic resonance spectroscopy that axonal reduction also appears in the normal white matter, most axons that undergo transection are demyelinated and located within MS lesions [9, 12]. However, it is still unknown whether the same pathogenetic mechanisms cause both demyelination and axonal injury. Thus, to clarify the cause of MS, a creative approach and an investigative way of thinking are needed rather than trying to support the hypothesis that is considered to be difficult to verify.

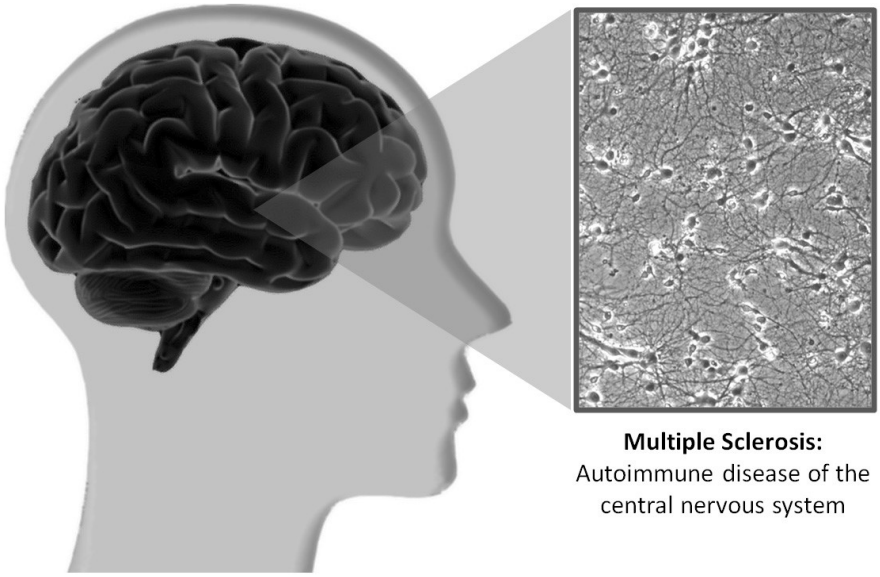


**Figure 1 Multiple sclerosis (MS) in the CNS.** MS is an autoimmune disease in which the immune system attacks the central nervous system. In MS, the immune system surrounds the nerves and attacks, damages or destroys the insulator myelin. The destruction of the myelin causes distortion or collapse of nerve impulses entering the brain and causes a variety of symptoms.

### 1.3 The Blood-brain Barrier and Multiple Sclerosis

The BBB establishes both physical and metabolic barriers to isolate the CNS from the systemic circulation and creates a unique and stable environment for optimal neural activity. It exerts bidirectional control on regulatory proteins, nutrients and electrolytes, and the passage of a wide variety of potential neurotoxins. Also, BBB exercises CNS defense by efflux transporters preventing the invasion of toxins in blood vessels and promoting the removal of toxic substances from the bloodstream [13]. In certain areas of the CNS, classical BBB structure is replaced by a blood-cerebrospinal fluid (CSF) barrier, which, although more permeable than the BBB, still prevents the free passage of serum proteins from the blood into CSF. This is because in the area of neurosecretory areas such as the posterior pituitary gland and chemoreceptor functions such as pineal gland, pituitary gland organ, central superiority, precordial, pituitary organ and pedicle organ vessels [14].

MS is an inflammatory demyelinating disease of the CNS and is characterized at the tissue level primarily by multifocal perivascular infiltrates of lymphocytes and macrophages. Demyelination in MS is indeed most prominent in the area adjacent to CSF and plaque tends to gather around small vessels. Cell recruitment activated across BBB endothelial cells appears to be an essential step to induce CNS inflammation and subsequent tissue damage (Figure 2) [15]. The burst of inflammation observed in MS appears to be regulated by circulating monocytes [16]. These monocytes also constitute the major cell type of perivascular infiltration characteristic of MS [17, 18]. In addition, cell migration across the membrane representing the BBB is facilitated by monocytes

[19]. These data show that monocytes can contribute to the pathological-anatomical features observed in the CNS of MS patients. Therefore, elucidating the molecular pathway into which different cell populations enter the CNS not only understands intrathecal immunoreactivity, but also prevents inflammatory cell infiltration into the CNS by rational treatment to control the disease. Converting it into a strategy is important.

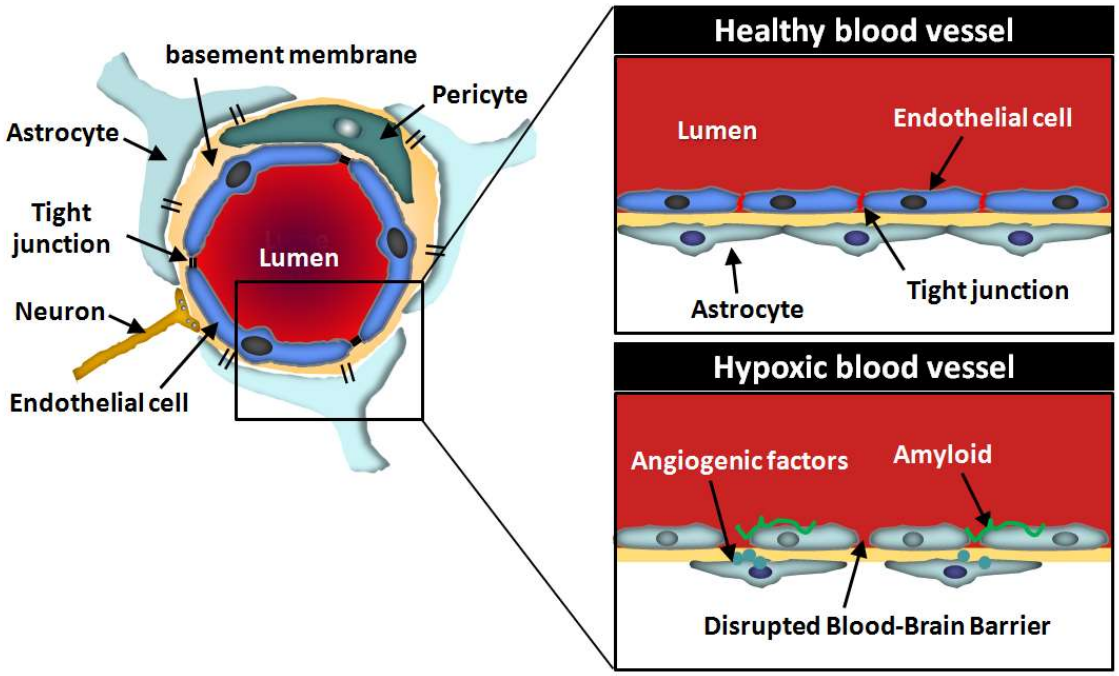


**Figure 2 An illustration of Blood-brain Barrier (BBB).** BBB establishes both physical and metabolic barriers to isolate the CNS from the systemic circulation and creates a unique and stable environment for optimal neural activity. Proper maintenance of BBB is essential for maintaining brain homeostasis. Otherwise, it can cause neurological impairment.

## 1.4 The Needs of Organ-on-a-chips

Organ-on-a-chip is a microfluidic device for culturing live cells in a continuously perfused micrometer-sized chamber to model the physiological functions of tissues and organs. The goal is not to build the whole living organism but rather to synthesize the smallest functional unit that requires organizational and organ level functions. These systems can incorporate physical forces, including physiologically relevant levels of shear stress, periodic strain and mechanical compression, and analysis of organ-specific responses including recruitment of circulating immune cells, in response to drugs or toxins. Mimicking the physiological interactions between different organs *in vitro*, one interstitial tissue compartment is fluidly connected from another interstitial tissue compartment directly or via a second channel lined with vascular endothelium. A similar analysis can be done with chips backed by cells from different organs [20].

## 1.5 Pharmaceutical Alternative in Preclinical Stages

Currently, the pharmaceutical and biotechnology industries are facing increased research and development expenses, shrinking pipelines, and pressures on public health policy [21]. Organ-on-chip microfluidic systems will have a significant impact on the future of the pharmaceutical industry by streamlining the drug discovery process and pretesting efficacy and toxicity before animal experiments. One of the main goals of organs-on-chips is to reduce or replace animal models significantly. Animal testing is necessary for judgments on therapeutic effect and safety. The disadvantages of animal testing are one of the big bottlenecks in drug development, as it is costly, time-

consuming and requires a lot of compounds. Also, traditional animal testing methods are unable to predict the toxicity and efficacy on humans and often the ethical question of sacrificing animals if they cannot reliably predict the clinical outcome arises [22]. Therefore, there is a strong pressure to find an effective means to improve the success of the drug development process and to identify appropriate alternatives that can replace the need for animal research. Organ-on-chip technology is a more predictable human-related model for toxicity and efficacy testing and has the potential to provide insight into the mechanism of action at the tissue and organ level. Such models may affect different stages of the drug development process, including the identification and prioritization of lead compounds and the verification of targets in preclinical stages.

# 2. A MICROELECTRODE ARRAY-BASED 3D NEURAL AGGREGATE ORGAN-ON-A-CHIP

## 2.1 Motivation

In many fields, including tissue engineering, stem cell biology, and cancer biology, 3D cell culture is accepted to provide physiologically relevant functional development of living tissues and cells, providing more *in vivo*-like functions, such as in a cell culture environment. These 3D culture models represent physiologically relevant responses and are considered to be a better model system in drug discovery applications. We have developed a method of CNS neural culture using 3D neural cell aggregation models; Myelin was formed more robustly than myelin in a conventional dissociation culture in which little myelin formation was observed. The 3D nature of the aggregate culture system is believed to provide a microenvironment that closely resembles that *in vivo*, thereby allowing proper generation and differentiation of neural progenitor cells into mature neurons and glia. However, the extent of myelination using spontaneously formed aggregates cultured on conventional multi-well cell culture plates depends on the size of the aggregates, the number of aggregates per culture well, and the distance between the aggregates, which is similar to the axon connectivity. Therefore, we developed a microelectrode array-based *in vitro* three-dimensional neural aggregate culture platform, which provides unprecedented control over aggregate culture microenvironment. The platform allows for the formation of a large number of uniformly sized aggregates which are loaded into the array of each culture chamber. And

the aggregate distance and the number of aggregates in each culture chamber can precisely be controlled. The microfluidic platform also makes it possible to easily process cultured aggregates with various biomolecules to directly investigate the effect of promoting *in vitro* myelin sheath formation. Also, the platform integrates microelectrodes within each microfluidic culture chamber for electrical stimulation during culture, as electrical stimulation is believed to improve myelinogenesis [23-25]. All operations of this 3D aggregate culture platform can be done using pipettes without requiring complicated tubing connections common in microfluidic systems, greatly simplifying operation and attracting attention to a broad research community.

## 2.2 Chip Design

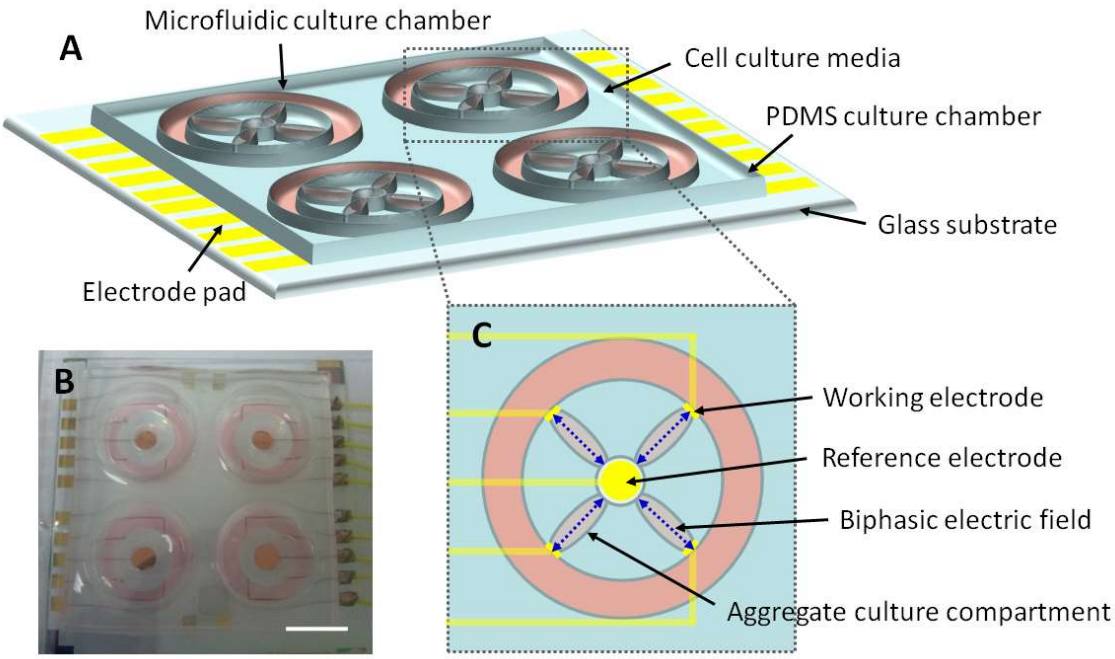


**Figure 3 Illustrations of a microfluidic 3D neural aggregate culture platform.** (A) The microfluidic platform based on the microelectrode array for neural aggregate culture is fabricated from a PDMS layer assembled on a microelectrode patterned glass substrate. (B) Actual device filled with culture media. Scale bar: 1 mm. (C) The PDMS layer of the platform consists of four culture chambers arranged radially.

A microfluidic 3D neural aggregate culture platform based on a microelectrode array is fabricated from a PDMS layer assembled on a microelectrode patterned glass substrate (Figure 3). The PDMS layer of the platform consists of four culture chambers (height: 200 μm) arranged radially. Each culture chamber has 10 aggregate trap sites consisting of three pillar structures (Figure 4). Based on an initial platform based

preliminary test with a single chamber with 100 traps, we showed damage to axon processes and loss of glial cells in the chamber, but this is due to a large number of aggregates are difficult to supply proper nutrition. Therefore, the number of cell aggregate traps in each culture chamber decreased to 10, so the distance from the inlet of the chamber to the center of the chamber was only 1.5 mm.

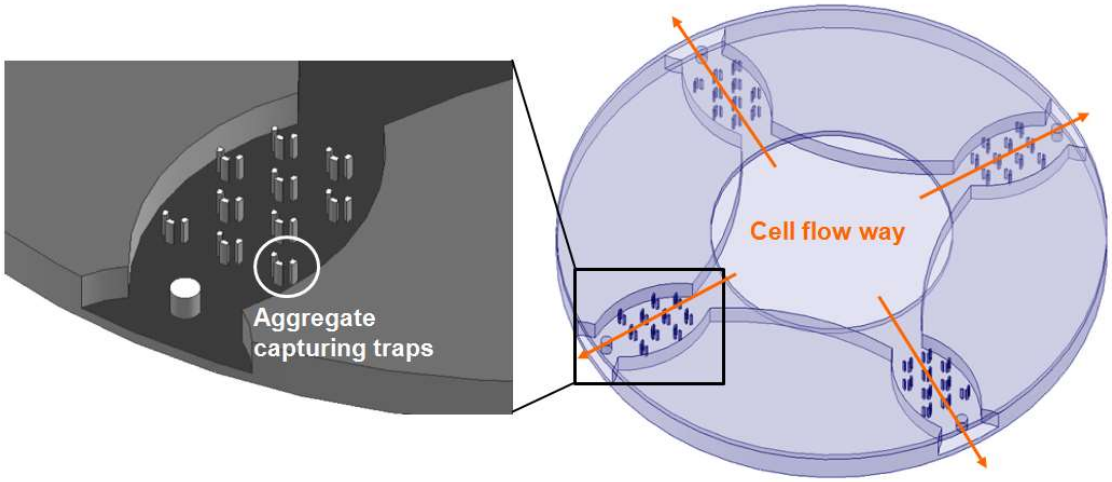


**Figure 4 Schematic design of a 3D microfluidic culture platform with four culture chambers with 10 aggregate traps (total 40 traps per a PDMS device).**

## 2.3 Chip Fabrication

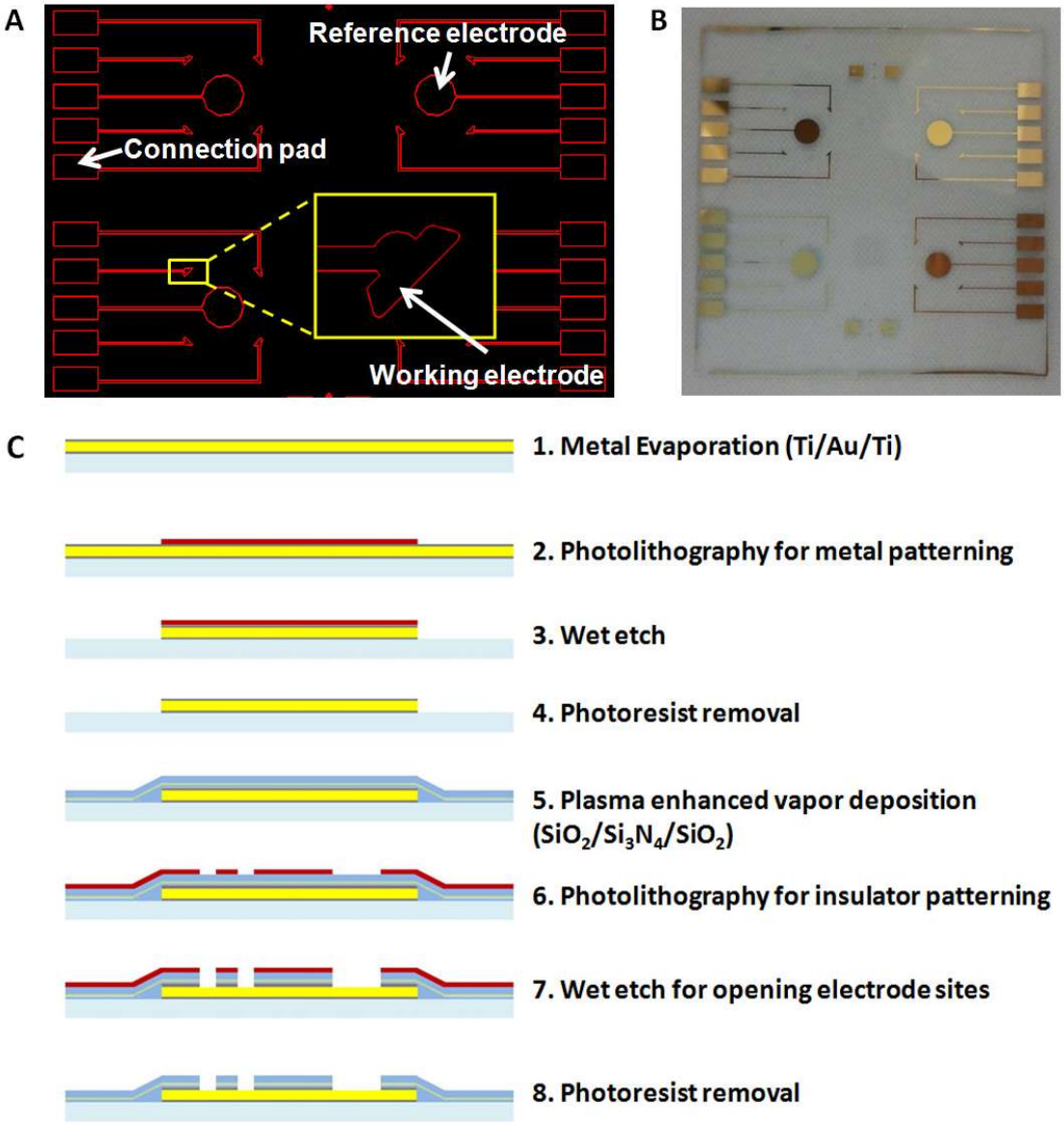


**Figure 5 Chip Electrode Fabrication.** (A) Design of the microelectrode array for 3D aggregate culture platform. (B) Actual electrode, Scale bar: 10 mm (C) Fabrication procedure.

The microelectrode array was patterned on a glass substrate using standard photolithography. The MEA was designed to have four sets of electrodes (four outer electrodes in the middle and one circular reference electrode) (Figure 5). Briefly, a Ti / Au (20 nm / 200 nm) layer is deposited on a 2 × 2 inch glass substrate, and an additional Ti layer (10 nm) is deposited on the gold layer and subsequently deposited to improve adhesion to the insulation layer. The metal layer was patterned by wet etching of Ti using buffered oxide etch (BOE) and Au using gold etchant (Gold Etchant TFA, Transene). Three insulating layers ($SiO_2$ / $Si_3N_4$ / $SiO_2$) were deposited by plasma enhanced chemical vapor deposition. Using the BOE solution, the electrode part and the contact pad were exposed by wet etching of the insulating layer and Ti. A PDMS cell culture layer was prepared by two-step PDMS casting method to obtain high aspect ratio capture structure (Width: 30 μm, height: 200 μm). First, a silicon master mold having a trapping structure was fabricated on a 4 inch silicon wafer by a deep reactive ion etching (DRIE) process. The PDMS replica with the inverse structure of the final PDMS layer was then cast molded from a silicon master by pouring 6 g of PDMS prepolymer and curing at 65 °C for 3 hours. The replicated PDMS master mold was then coated with trichlorosilane and rinsed with IPA for 5 minutes in a sonicator. The PDMS cell culture layer was then replicated from the PDMS master by pouring 40 g of PDMS prepolymer and curing overnight in a 65 °C oven. The PDMS culture layer was cut in a circle, and the inlet port was punched out using circular punch bits of 10 mm and 4 mm, respectively. Finally, four PDMS culture chambers and additional PDMS wall chambers were assembled on the MEA substrate after oxygen plasma treatment. Each PDMS

culture chamber was individually placed inside each large hole structure of the PDMS wall chamber (Figure 3). The assembled device was immersed in deionized water and autoclaved at 121 °C for 30 minutes.

## 2.4 Tissue Dissociation and Primary Cell Preparation

Primary neurons were prepared from cortical areas in the whole brain of ED (embryonic days) 16 Sprague-Dawley rat. Briefly, the meningeal-free forebrain was placed in an ice-cold dissection buffer (10 mM HEPES-containing $Ca^{2+}$ / $Mg^{2+}$ free Hank's balanced salt solution) containing L-cysteine activated papain (10 units/ml) in dissociation buffer at 37 °C and resuspended in a dissection medium containing trypsin inhibitor (10 mg/ml) for 3 minutes. After two more washes with trypsin inhibitor solution, the tissue was resuspended in NBB 27 / DMEM medium (Neurobasal+DMEM medium containing 2% B27, 1 mM pyruvic acid, 63 ng/mL N-acetyl cysteine, 0.75 mM GlutaMax, SATO, 10 nM d-Biotin, 5 μg/mL insulin, and 1% penicillin/streptomycin) and triturated with a fire-polished glass Pasteur pipette until all clumps disappeared. The cells were then passed through a 70 μm cell sieve, and viable cells were counted using a hemacytometer and trypan blue exclusion assay.

## 2.5 Uniform Size Aggregate Formation using Microwell Array

3D neuronal aggregates cultured in the microfluidics platform were prepared using microwell arrays. We utilize a substrate with an array of microwells to generate nerve aggregates of more controlled size with better aggregate capture efficiency and to develop *in vitro* myelinogenesis models with high reliability and reproducibility (Figure 6). Initially, an array of microwells was made by PDMS soft lithography from an SU-8™ patterned Si master mold with inverted replication (pillar structure) of microwells (diameter: 150 μm, depth: 150 μm). Second, PDMS replicas can be cut into discs by circular punch bits (9 mm diameter), and each PDMS microwell substrate can be placed in each well of a 48-well cell culture plate. The multiwell array discs were then treated with oxygen plasma, immersed in deionized water and subsequently autoclaved. After sterilization, the microwell disc was placed in a 48-well cell culture plate, and dissociated neurons were added at a concentration of 5 million cells per well. Finally, the cells were cultured for 3 days in a temperature and humidity controlled 5% $CO_2$ incubator, and then the aggregates formed were collected by rapidly stirring the PDMS disk in the medium bath.

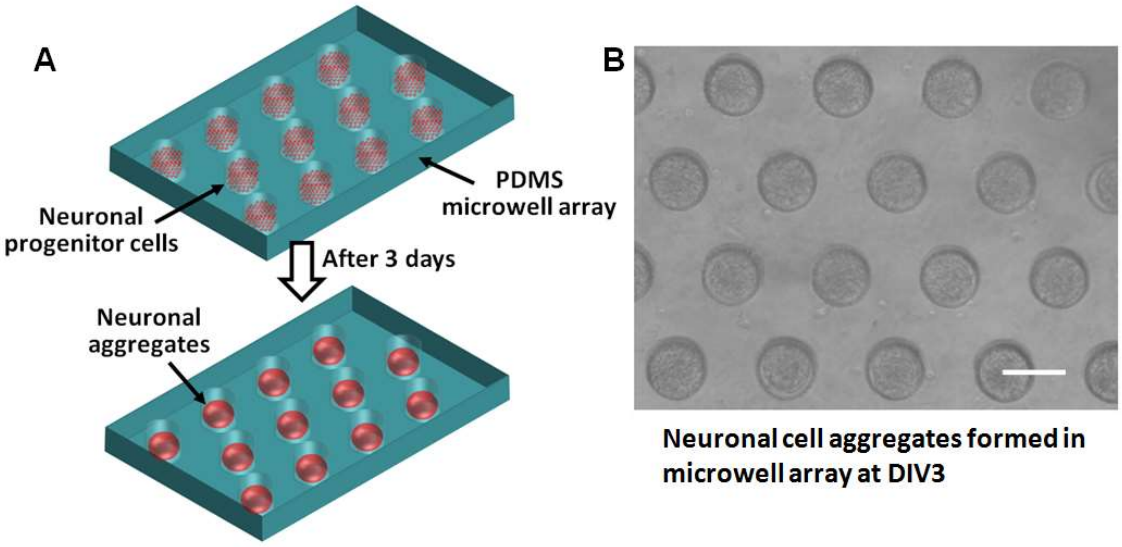


**Figure 6 Micro-well array.** (A) An illustration showing the generation of size-controlled neural aggregates using a micro-well array. (B) Microscopic images of neural aggregates with pre-determined size inside the micro-wells after 3 days. Scale bar: 150 μm.

### 2.6 Neural Aggregate Culture on Brain-organ-on-a-chip

3D neural aggregates were loaded into four culture chambers at the same time through the central collection opening of the device. These aggregates were captured at each capture site by a hydrodynamic pressure driven flow, and then the culture medium was replenished every 3 to 4 days and cultured for up to 4 weeks. For experiments involving biomolecular processing, aggregates were cultured for 2 weeks to establish the development of dense axon layer and glial cells, followed by biomolecular processing.

## 2.7 Electrical Stimulation for Myelination

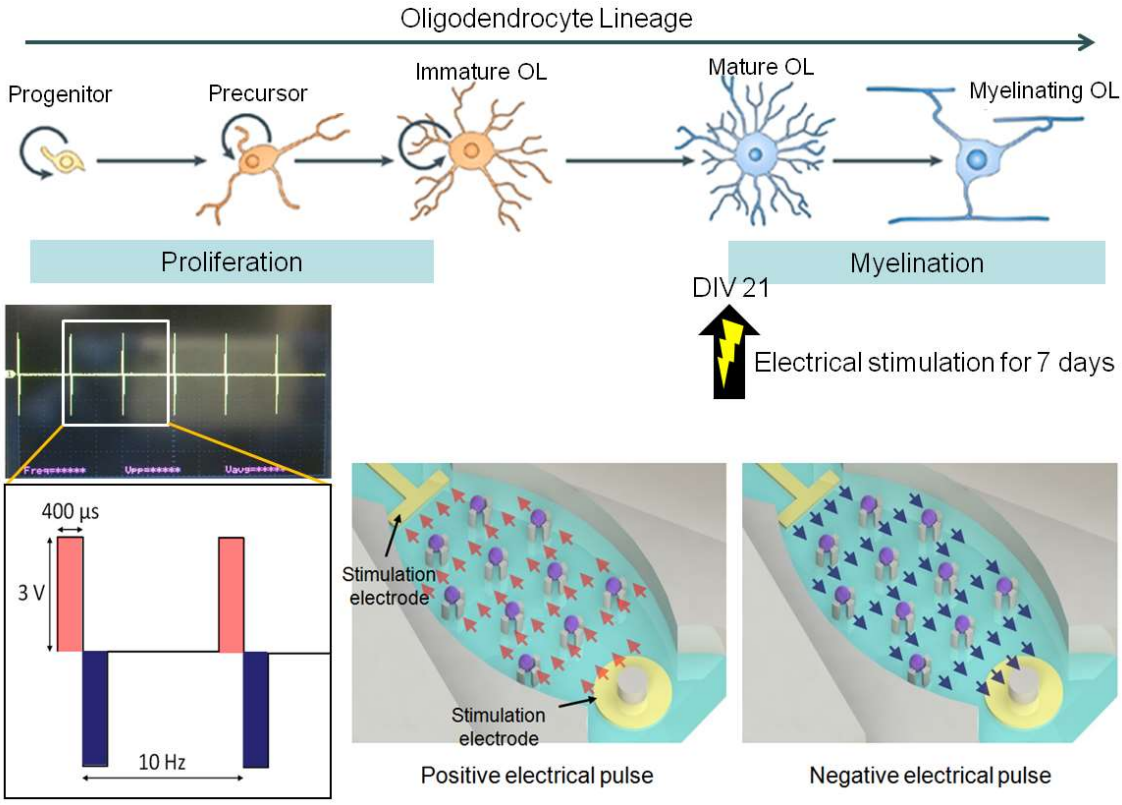


**Figure 7 Electrical Stimulation for Myelination.** An electrical signal applied to aggregates from DIV 21 for 7 days. Biphasic-voltage pulses (400 µs pulse-width, 10 Hz, ±3V).

Biphasic voltage pulses (400 µs pulse width, 10 Hz, 3 V) were applied to neural aggregates starting DIV 21 for 7 days (Figure 7). Each electrode was connected to an extracellular amplifier (Model 3600, A-M Systems, Inc., WA) equipped with a 2-channel function generator.

## 2.8 Pharmacological Treatment for Myelination

Retinoic acid (RA) is a metabolite of vitamin A (retinol) that mediates the functions of vitamin A for growth and development and promotes CNS remyelination [26]. To investigate the effect of RA on CNS myelination, 500 nM RA was applied to the aggregate culture via the central aggregate loading port at DIV 17 and incubated for another 10 days in supplemented RA-containing medium every 3-4 days.

## 2.9 Quantitation of Myelination

Quantitatively analyzing the formation of myelin sheath by inter-aggregate distance and measuring the average length of myelin segments per trapped nerve skeleton with a region of interest (ROI) 200 μm to 400 μm away from the center of the trapped aggregate (Figure 8). The reason for excluding the aggregate (about 200 μm from the center of the aggregate) is because the aggregate has a three-dimensional structure, and the myelin segment expressed in the aggregate was very difficult to quantify. Although the only way to quantify the myelin sheath formed in 3D in the aggregate was to reconstruct the Z-axis scan confocal image, image quality was not sufficient for accurate analysis. Thus, only the total myelin sheath formed outside of the aggregate was compared.

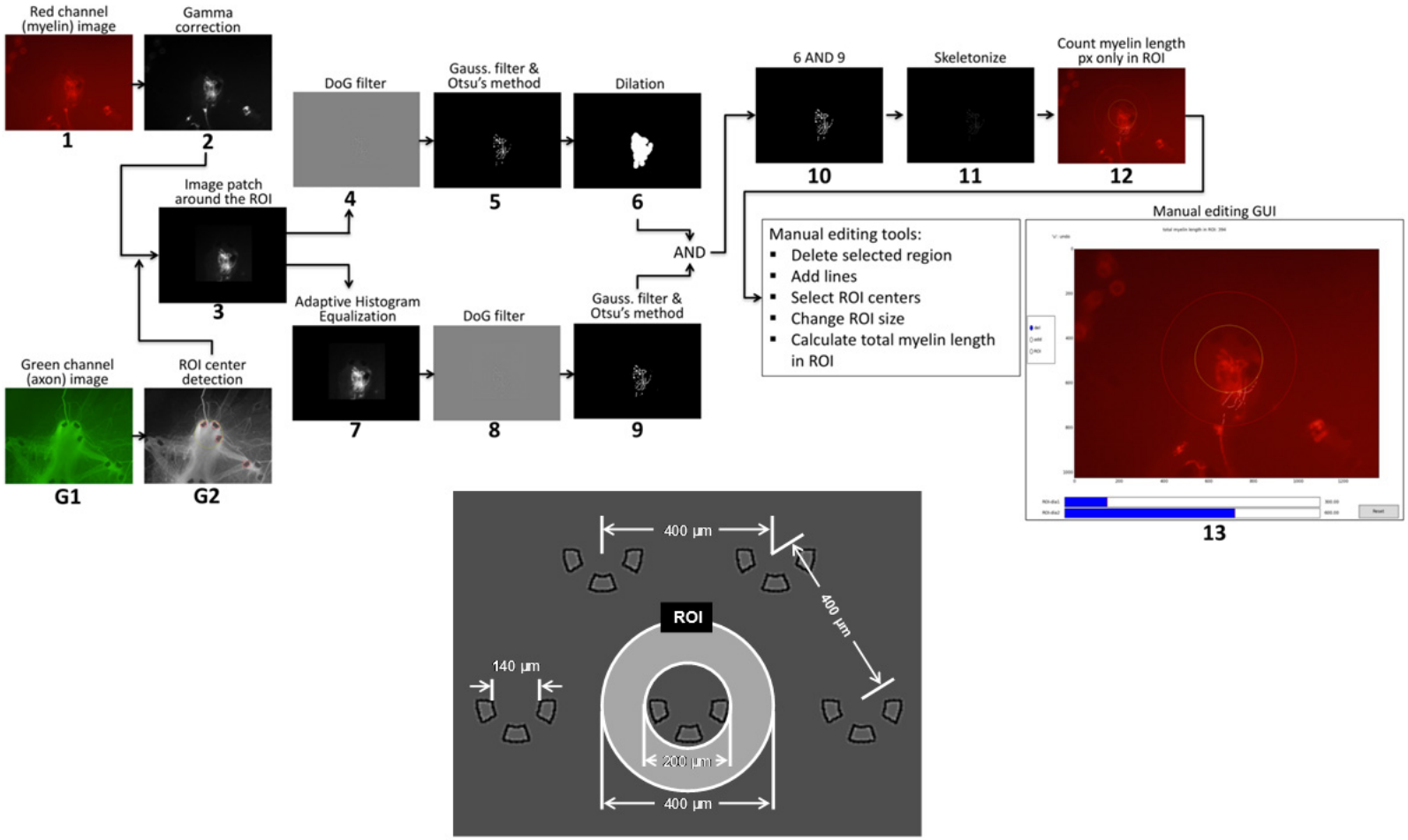


**Figure 8 Schematic of automatic image processing and myelin quantification process.** ROI for quantitative analysis of myelination.

### 2.10 Computational Automatic Analysis for Myelination Quantitation

Since many fluorescent images are taken, an automatic image processing method has been developed to quantify the extent of myelination. In the image processing of the data set, the first ROI in which the myelin segment is located is detected (steps 1-3 in Figure 8) by excluding the relatively bright and dotted part of the red channel, the remaining part is deleted (Step 4-6 in Figure 8). Second, processing is performed to find details of images by holding small segments that are relatively bright and even false positives (step 7-9 in Figure 8). Third, the ROI is detected in the green channel (axial channel) (step G1–G2), and the masked intensity value of the outer region of the rectangular image patch around the detected ROI becomes zero (step 3 in Figure 8). Fourth, executing an AND logical operation between images (steps 6 and 9) leaves details only in the region of interest (step 10 in Figure 8). Fifth, the centerline of the segment (innermost line with one-pixel width) is extracted by the skeletonization algorithm [27], and we counted only the myelin length of ROI (step 11 -12 in Figure 8). Finally, the manual editing GUI tool can be applied to perform false positives and false negatives, and to reset the ROI center and size if necessary.

## 2.11 Aggregate Formation and Growth in the Microfluidic Platform

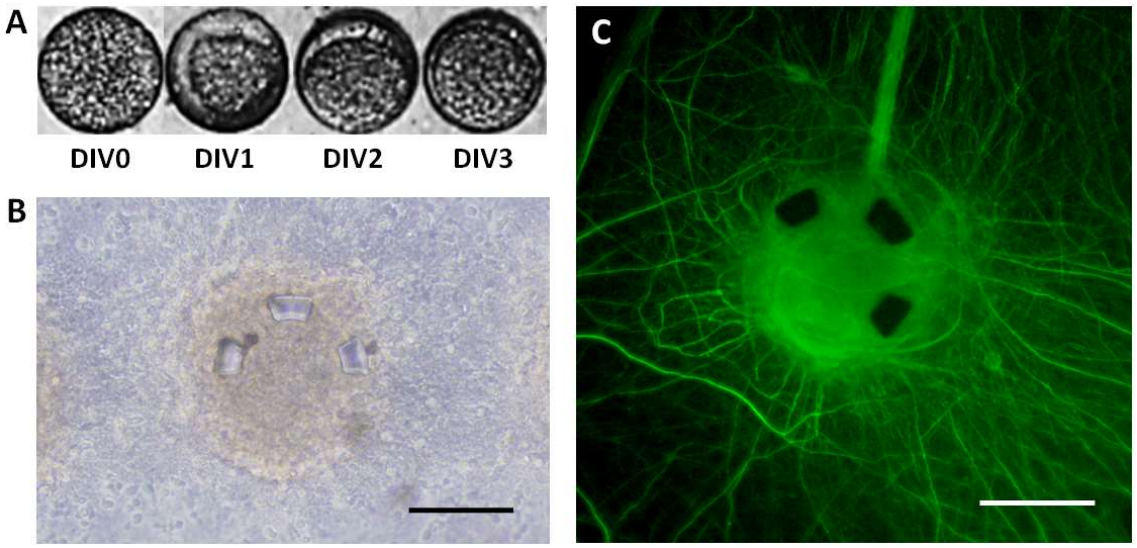


**Figure 9 Aggregate Formation and Growth in the Microfluidic Platform.** (A) Microscopic images of neural aggregates inside the microwells from DIV 0 to DIV 3. (B) The neural aggregates produced by the microwell array are cultured in a microfluidic platform and show a high density of axonal growth and migration of aggregates of glial precursor cells throughout the culture chamber. (C) Immuno-stained image of axons (NF – green) at DIV 28. Scale bar: 150 µm.

Neural aggregates showed a uniform size distribution when collected in the microwell at DIV 3 after culture (Figure 9A). Initially, the microwells were filled with dissociated neural aggregate cells, began to form aggregates and became slightly smaller than the size of the microwell of DIV 1. Over time, the aggregates in the microwell became larger and were the same size as the microwell (DIV 3), where they were collected and seeded on the culture platform. The culture platform was incubated in a cell culture incubator for 10 minutes to allow the neural aggregate cells to adhere to the

bottom and maintain its position during the culture medium exchange and allow controlled neural aggregate cells distance throughout the culture. After one day of loading on the aggregate, the nerve processes began to grow. The substrate area was covered with a dense layer of axons that migrated from the trapped aggregates (Figure 9B). Figure 9C shows the immunostaining axon of DIV 28 neuronal aggregates. As can be seen, a healthy dense layer of axons covering the entire cell culture chamber was observed. Thus, all subsequent aggregate culture experiments were performed on a microfluidic platform.

### 2.12 Myelination in the Brain-organ-on-a-chip

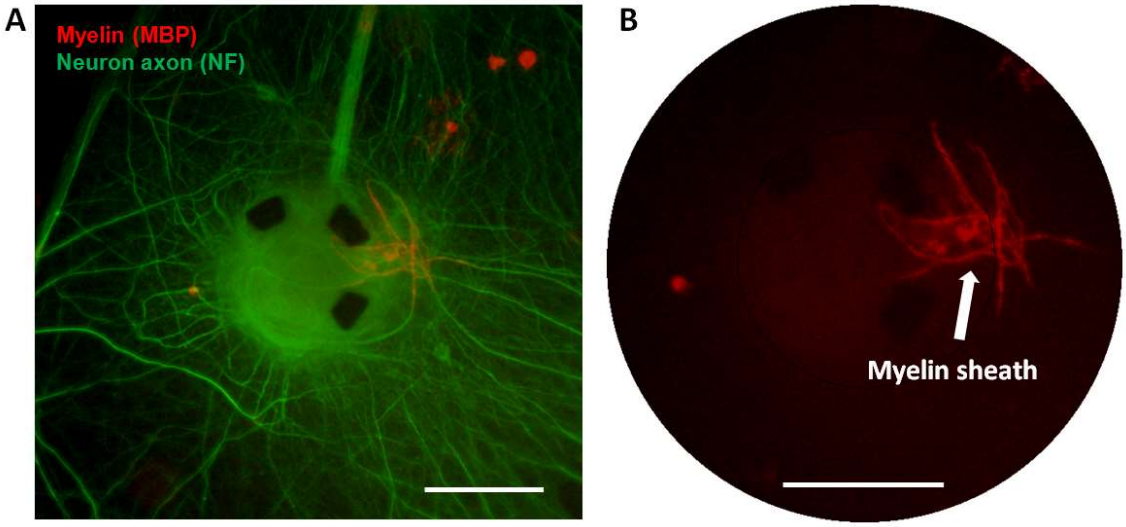


**Figure 10 Myelination in the Brain-organ-on-a-chip.** (A) Fluorescence image of myelin sheath formed in culture platform at DIV 31 (MBP – red, NF – green). (B) Enlarged fluorescent image. A white arrow indicates the axon of myelin sheaths. Scale bars = 150 μm.

After injecting the microwell-forming neural aggregates into the microfluidic culture platform, the aggregates were incubated for up to 4 weeks. In DIV 28, aggregates were fixed and stained with myelin basic protein (MBP) and nerve filaments (NF) to confirm the formation of the myelin sheath. Many oligodendrocyte progenitor cells migrate from neural aggregates and are successfully developed into mature oligodendrocyte expression MBP (Red) (Figure 10). More importantly, it is also evident that some oligodendrocyte processes are perfectly aligned with the underlying axon fibers and wrap around them to form a sturdy myelin sheath. So, the smooth and thick form of the $MPB^{+}$-oligodendrocyte process distinguishes them from other unmyelinated oligodendrocyte processes, with perfect alignment with axons. The immunostained image is clear evidence that a robust CNS myelin sheath was successfully formed *in vitro* in the microfluidic aggregate culture platform in which it was developed.

### 2.13 Effect of Retinoic Acid on Myelination

The effect of retinoic acid on the myelin sheath formation was investigated using the developed microfluidic platform. 500 nM retinoic acid contained media was added to the aggregate culture from DIV 14 to DIV 27. Figure 11 shows that the retinoic acid treatment resulted in more myelin sheath (193.54 ± 35.60%, n = 3) when the distance between the aggregates was 400 μm compared to the control.

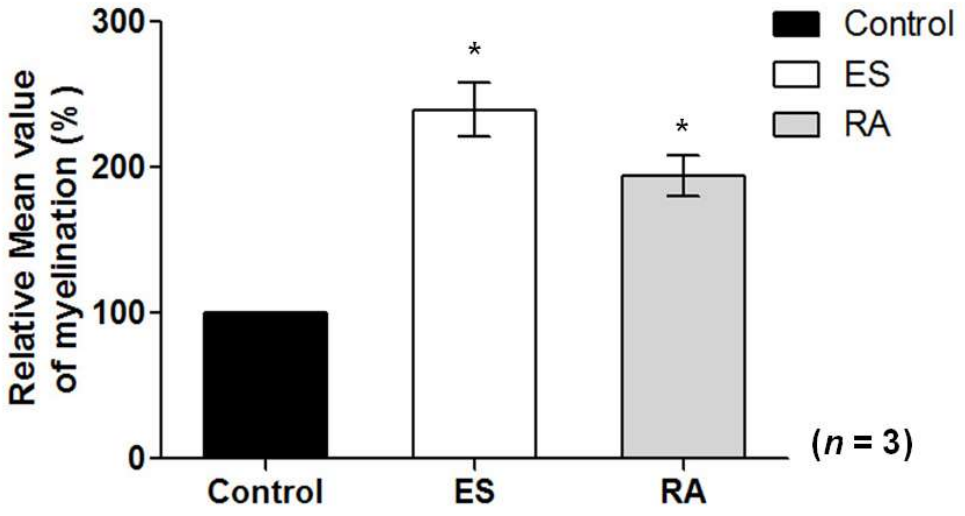


**Figure 11 Effect of retinoic acid (RA) and electrical stimulation (ES) on myelination.** All values are plotted as a mean ± standard error of the mean. * $p < 0.05$, $n = 3$ sets.

### 2.14 Effect of Electrical Stimulation on Myelination

Neurons evoke action potentials during development. Therefore, we also hypothesized that electrical stimulation during *in vitro* culture could influence neuronal myelination in a microfluidic platform, as acute electrical pulse induces a neuronal action potential. Much higher levels of myelin sheath formation were observed when electrical stimulation was used compared to control cultures without electrical stimulation (Figure 11). Quantitative analysis shows that the increase in myelin sheath formation is 239.46 ± 29.71% ($n = 3$) compared to control cultures without electrical stimulation. This result shows a new finding that electrical activity promotes myelination of CNS axons. The results of this study are consistent with some evidence that the

development of electrical activity in the form of action potentials according to axon plays an important role in oligodendrocyte development [28].

### 2.15 High-throughput Analysis with the Computational Automatic Quantitation

It is very difficult to manually quantify the degree of myelin sheath formation since about 100 fluorescence and bright field images are generated per microfluidic device in a typical experiment. Using automated image processing algorithms, myelin quantification results of automated methods were compared to those performed manually. Compared with automatic analysis of computed data and manual data analysis, using either manual image analysis or automatic analysis, myelin length shows the same tendency under any conditions and makes good use of automatic image analysis as shown in Figure 12. To compare between the manual image analysis and the automatic analysis, a total of 149 photographs and 196 photographs in three independent experiments were used for the control and electrical stimulation conditions, respectively.

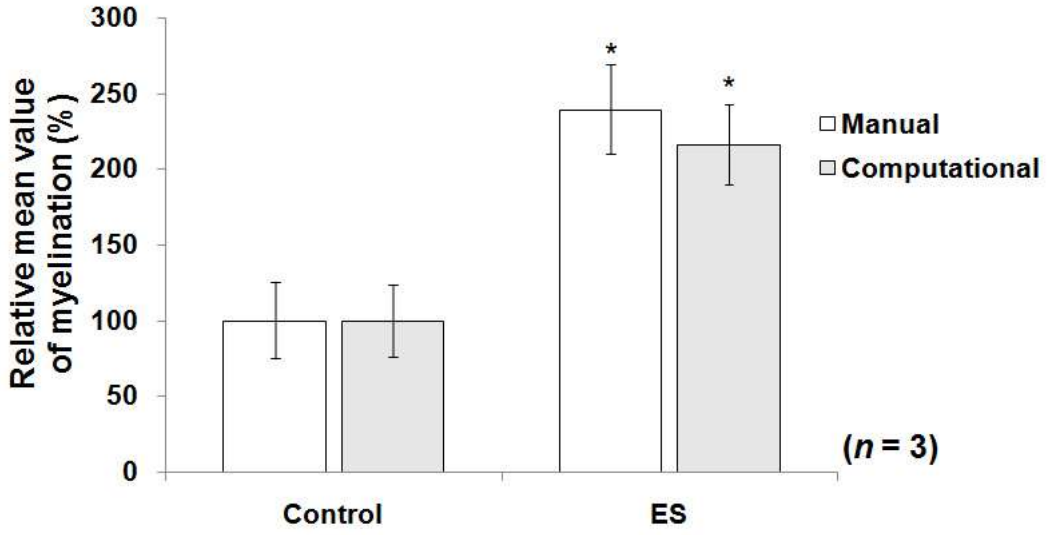


**Figure 12 Comparison of automatic quantification and manual quantification.**

All values are plotted as a mean ± standard error of the mean.* $p < 0.05$, $n = 3$ sets.

## 2.16 Conclusion

We have developed a microelectrode array-based 3D CNS neuronal aggregate culture system that can provide electrophysiological and biochemical manipulations to investigate neuron-glia interactions and neural progenitor cell development. This microsystem, which cultivates neural progenitor aggregates in a spatially controlled 3D environment, was developed for the study of CNS myelin formation. The dense axonal layer was formed, and the myelin sheath was formed around the differentiated oligodendrocyte axon. This is the first achievement of CNS myelin formation in the microfluidic device, and the electrical stimulation for the promotion of myelination was successfully confirmed using our device with retinoic acid treatment results.

# 3. 3D ARRAYED MICROFLUIDIC BLOOD-BRAIN BARRIER MODEL WITH THE INTEGRATED ELECTRICAL SENSOR ARRAY [*]

## 3.1 Motivation

This organ–on–a–chip is being developed to mimic the *in vivo* physiological conditions more accurately by creating three-dimensional (3D) multicellular tissue structures and combining them with microfluidic systems. Significant efforts have been made in developing systems that can better represent structural and functional units of organs, with the purpose of facilitating new *in vitro* testing approaches to enable cost-effective and accurate predictions of drug efficacy and toxicity [29, 30]. In the case of new drug developments for diseases in the central nervous system (CNS), only 7% of the drugs in clinical developments have reached marketplace despite increased investment in this area and increasing number of patients suffering from various brain diseases [31]. One of the major reasons for the low success rate of CNS drug development is the existence of the blood-brain barrier (BBB), a highly selective permeability barrier that protects the brain from most pathogens and potentially toxic chemical compounds while allowing the passage of molecules that are crucial to proper neural functions. While this unique barrier structure is essential for protecting CNS from potentially harmful chemicals and maintaining a stable brain environment [32], successful drug delivery

---

[*] Reprinted with permission from "A Three-Dimensional Arrayed Microfluidic Blood–Brain Barrier Model With Integrated Electrical Sensor Array" by Sehoon Jeong, Sunja Kim, John Buonocore, Jaewon Park, C Jane Welsh, Jianrong Li, Arum Han, 2018. IEEE Transactions on Biomedical Engineering, 65 (2), 431-439, Copyright © 2018 by IEEE.

through the BBB has become a major challenge for drug development against a broad range of neurological diseases, from acute brain infection to chronic neurodegenerative diseases [33]. Thus being able to conduct *in vitro* testing against BBB, which can be used to understand the barrier functions better and to develop new drugs against neurological diseases, is critically needed.

Conventional *in vitro* culture methods for BBB studies utilize transwell inserts that simply allow endothelial cells to be grown on a porous membrane in the upper chamber that is immersed in the growth media chamber as a vertical diffusion system, and thus partially mimicking the BBB and their environment [34, 35]. Although cells grown in such transwell systems do show some levels of barrier functions, the functions are still quite different from those seen *in vivo* and fail to generate organ–level functionalities, as they typically lack shear stress during culture. Physiological shear stress plays a key role in promoting neurovascular endothelial cell differentiation and BBB functions regarding expression, localization, and association of tight junction proteins [36-39]. In addition, even though transwell platforms allow co-culture of endothelial cells with other BBB cell types such as astrocytes and pericytes in the lower chamber, this results in large distance between the two cell types (from the top of the membrane to the bottom of the culture well), which is quite different from the *in vivo* environment where those two cell types are located close together within tens of micrometers. Alternatively, astrocytes and pericytes can be cultured on the backside of the porous membrane of the transwell insert, but achieving cell uniformity and batch-to-batch variations are extremely challenging during cell seeding on the backside of the

transwell inserts. Accordingly, the endothelial cells often lack the necessary factors needed for the proper development and maintenance of BBB properties. As a result, the measured transendothelial electrical resistance (TEER) levels, an indicator of barrier integrity, are typically lower and also often show irregular patterns due to cell adhesion or cell uniformity issues [35].

To overcome some of these limitations, *in vitro* BBB models that have flow chambers or capillary-like 3D configurations, where applying shear stress to endothelial cell culture is possible or culturing both endothelial cells and astrocytes on the inside and outside of hollow fibers for enabling co-culture conditions, have been developed [40, 41]. Nevertheless, there remains a large gap in physiological functions that can be achieved by these *in vitro* systems compared to *in vivo* systems. This is in part due to the significantly lower shear stress applied compared to *in vivo* conditions because of their relatively large inner chamber and lack of primary cells used in such systems to name a few [35, 42]. Also, these systems are not amenable to high-throughput screening applications, as each setup is complicated and takes a significant amount of cost and effort to set up.

In recent years, several microfluidic BBB models that mimic *in vivo* BBB have been emerging. There are largely two different configurations of microfluidic BBB–on–a–chip systems, the planar types and the vertical types. The planar microfluidic BBB models typically utilize arrays of micropillars or microchannels as a boundary between the blood and brain side of chambers. The gaps between these microstructures are small enough to trap cells on either side and thus allow endothelial cells and astrocytes to be

cultured on each side of the microstructures, functioning similarly as a vertically placed porous membrane [43, 44]. However, there are several limitations. The channel length of the interface connecting both the luminal and the abluminal sides were 50 μm, which is much longer than the distance between real vascular side and astrocytes in *in vivo* (≤1 μm), and even compared to those in transwell inserts (10 – 20 μm thick porous membrane). On the other hand, the vertical microfluidic BBB models typically utilize the same type of porous membranes used in transwell culture as a boundary between the blood and brain side of chambers. This porous membrane is sandwiched between two microfluidic structures, one side serving as the blood vessel side and the other side serving as the brain tissue side. As one example, the BBB chip by Achyuta et al. is made up of neuronal (neurons, astrocytes, and microglia) and vascular (endothelial cell line) sides to establish a more realistic cerebrovascular BBB structure by using primary rat neuronal cell co-cultures [45]. However, this BBB platform did not apply any shear stress to the culture because of the concern over leakage due to the weak bonding between the layers if a high level of fluidic pressure is applied, as stated by the authors. Moreover, the culture time in this system was limited to 2–3 days because of the inaccessibility to the neuronal side of the system. As another model, the micro blood-brain barrier–on–a–Chip (μBBB–chip) has integrated the aforementioned structural advantages from all the previous platforms [46]. The μBBB–chip is made up of luminal (endothelial cells) and abluminal (astrocytes) side microfluidic channels, which are separated by a 10 μm thick polycarbonate membrane having 0.4 μm pores. The model also provided real-time TEER measurements through the on-chip electrodes. This

system successfully demonstrated that TEER values in flow–based co-culture showed a 10–fold increase compared to static co-culture, both conditions using endothelial cells and astrocytes [46]. Yet, due to the inside chamber size (2 × 5 $mm^2$), the platform still has some limitations in the degree of shear stress that can be applied (max 0.0008 dyne/$cm^2$ applied), which is significantly lower than the condition in brain microcapillaries *in vivo* (5–25 dyne/$cm^2$) [47-49]. Another similar BBB chip reduced the channel width to 500 μm and increased the shear stress applied to about 5.8 dyne/$cm^2$ and the resulting increased TEER on this BBB chip provides a more realistic *in vitro* BBB model [50]. Nevertheless, there remains a large gap in physiological cellular interactions achieved by these *in vitro* systems compared to *in vivo*. This could be due to the use of cell lines instead of primary cells used and only mono-culturing with endothelial cells. To overcome these potential limitations, another BBB chip by Brown et al. used mostly primary cells made up of primary human endothelial cells and primary human pericytes, although the astrocytes used were cell lines and the neuronal cells were derived from human induced pluripotent stem cells (hiPSCs) [51]. The system was successful in incorporating all the cell types involved in the BBB formation. However, this platform still has the same limitation of significantly lower shear stress applied (0.02 dyne/$cm^2$) because of their relatively larger chamber size (3 × 6.2 × 1 $mm^3$) as with the previous *in vitro* BBB models, limiting the degree of shear stress that can be applied using the same flow rate [42]. Also, the astrocyte condition did not significantly enhance the tight junction formation, contrary to previous reports, and the effect of hiPSC neuron co-culture was not clear.

Here, we present a multi-compartment microfluidic BBB chip that recapitulates the critical functional astrocyte–capillary interface of the brain, while also allowing up to 16 different assays to be conducted in parallel using each of the 16 BBB units on a single chip. This bioinspired microsystem is a multicellular integrated organ level analytical platform that mimics the CNS brain–capillary interface by using only mouse primary endothelial cells and mouse primary astrocytes, co-cultured on each side of a porous membrane and connected through a microfluidic network that allows the physiologically relevant level of shear stress to be applied. Each of the BBB compartment is equipped with integrated electrical impedance sensors that can measure the permeability of the barrier function continuously and non–invasively. Our approach provides for the first time an *in vitro* BBB chip that satisfies most of the features needed to form an *in vivo*-like BBB chip that is also amenable for medium-throughput screening, namely: (i) controllable and reproducible formation of a realistic brain–capillary interface through co-culture of primary astrocytes and primary endothelial cells on each side of a porous membrane, (ii) optimized extracellular matrix (ECM) configuration that significantly increased the tight junction, (iii) an optimized *in vivo* level shear stress applied to the culture, and (iv) a versatile multichannel screening architecture that utilizes 4 rows of microfluidic channels that represents the brain side and 4 columns of microfluidic channels that represents the brain capillary side to create 16 semi-independent BBB compartments at their cross-sections, and (vi) integrated electrical impedance sensor array that can non–invasively measure barrier permeability in each of the BBB compartments in real time, continuously, and in parallel.

### 3.2 Design of Microfluidic Multichannel BBB Chip

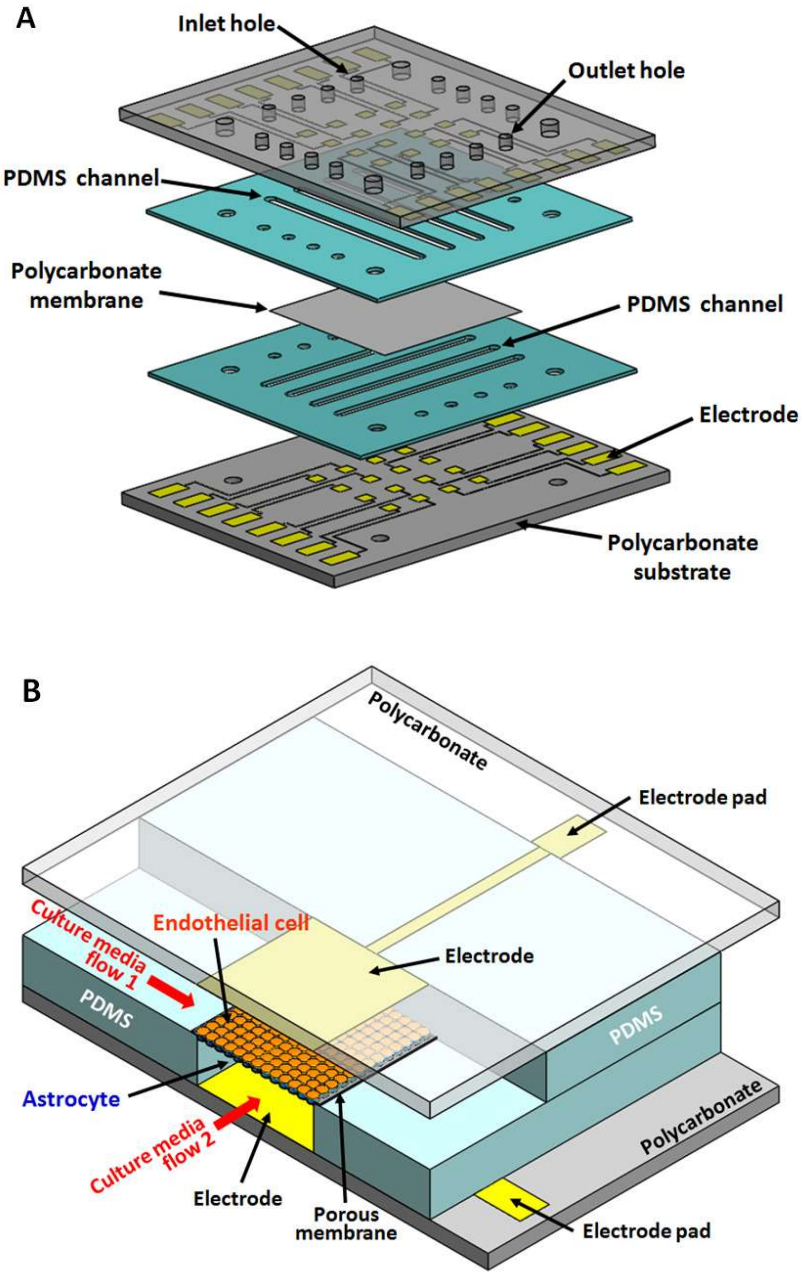


**Figure 13 A multi-channel multi-layer BBB chip with the integrated electrical impedance sensor array for TEER analysis.** (A) 3D illustration showing the multi-layer structure. (B) 3D structure of a single BBB unit of the 16-unit BBB chip.

The microfluidic multi-channel BBB chip is composed of two intersecting PDMS microfluidic channel arrays (4 channels each), a luminal channel array filled with endothelial cell culture media and an abluminal channel array filled with astrocyte cell culture media, placed on each side of a 10 μm thick porous polycarbonate membrane (Figure 13A). The area where these two microchannels intersect forms a single BBB unit, as illustrated in Figure. 13B, resulting in a total of 16 BBB units on a single chip. This configuration allows the intersecting channels to be connected to the porous membrane, which functions as a physical isolation barrier that separates the two cell types (luminal and abluminal compartments), while still allowing diffusion of molecules through the membrane pores. Thus neurovascular endothelial cells and astrocytes, grown in each of the two separate microenvironments, are still connected through the porous membrane to have localized interactions, especially between astrocyte endfeet and endothelial cells. The 4 top fluidic channels and four bottom fluidic channels respectively allow 16 different conditions to be tested in one experimental run through the multi-channel structure (4×4 intersecting channels) (Figure 14). However, as each channel fluidically connects 4 BBB units, the 16 units are not completely independent. The four units that are connected through the same channel can be used as technical replicates but not as biological replicates, while the units in a different channel can represent one biological replicate. Each BBB unit in the chip has their top and bottom electrodes to measure TEER for tight junction analysis, allowing all 16 BBB units to be monitored simultaneously throughout the culture. The TEER electrodes are designed so that

microscopic observation of both sides of the channels are still possible during the cell culture through a microscope (Figure 14B).

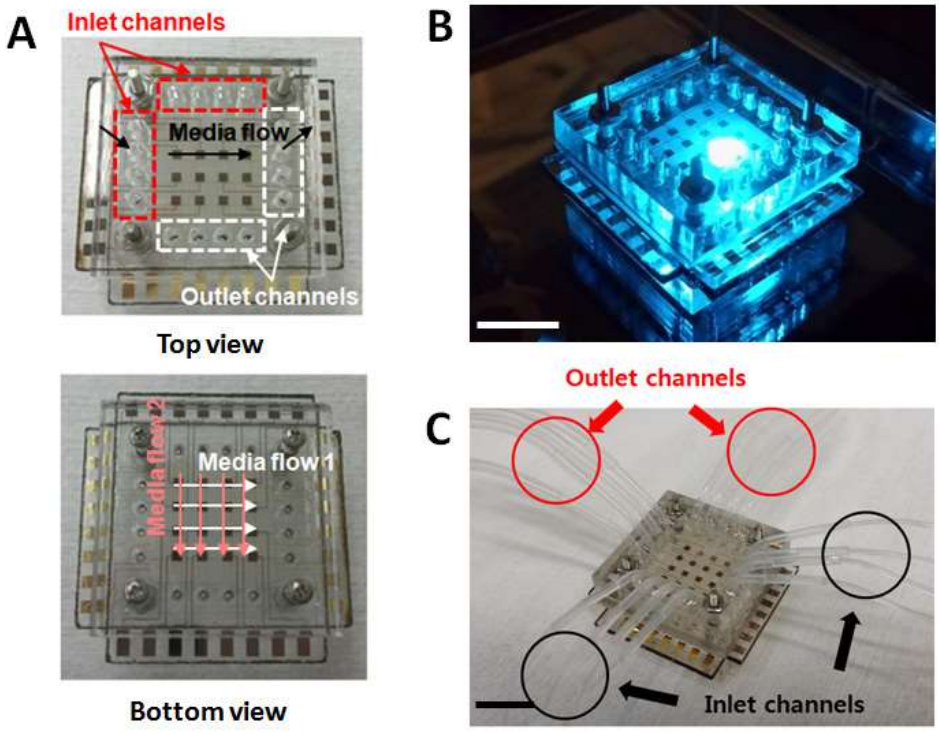


**Figure 14 The microfluidic multi-channel BBB chip.** (A) Intersecting PDMS microfluidic channel arrays, the luminal channel array for endothelial cell culture and the abluminal channel array for astrocyte culture. (B) Photograph of an assembled device on an inverted fluorescent microscope. (C) Fabricated microfluidic BBB chip connected with inlet and outlet tubings and ready for testing. Scale bar: 1 mm.

### 3.3 Chip fabrication

The BBB chip was fabricated by standard photolithography and assembling techniques. Multielectrode arrays (MEAs) were fabricated using a semiconductor process. Thin titanium adhesion layer (20 nm) and a gold layer (200 nm) were deposited on polycarbonate substrates (Lexan # 9034) and patterned using standard photolithography and metal etching. The MEAs were designed to have 16 electrodes (4×4 array) with 3 mm site-to-site spacing in between each electrode. The exposed area of each electrode site was 1 $cm^2$. The MEA-patterned polycarbonate substrates were then cut to 26 mm by 34 mm and the inlet/outlet holes and screw holes were made by a laser cutter (PLS6, Universal Laser Systems, AZ). Poly(dimethylsiloxane) (PDMS, 10:1 mixture) prepolymer was spin-coated (160 RPM) onto a Si wafer to form a 300 μm thick layer, and then cured for 4 hours at 65 °C. The cured PDMS layer was cut by a laser cutter to make the microfluidic channel array (W, L, H: 1 mm, 19 mm, 300 μm). The cut PDMS layers were attached to the MEA-patterned substrates and then released. After stamping each PDMS channel layer bonded on the MEA-patterned substrate onto a thin layer of PDMS prepolymer (spin-coated at 2100 RPM), a 0.4 μm pore membrane (10 μm thickness) (Corning, NY) was placed between these two layers still having uncured thin PDMS prepolymer layers. The two PDMS channel layers on the MEA-patterned substrate were placed perpendicularly to each other. The entire assembly was placed between two thick poly(methyl methacrylate) (PMMA) substrate (4 mm), and the four screws that are holding the two PMMA substrates together were uniformly tightened up to the same level using a gauged torque wrench. The device was then cured in an oven

for 4 hours at 65 °C to allow the prepolymer between the channels to cure with the porous membrane for sealing. After loosening the four screws to take out the top PMMA substrate, a PDMS gasket was placed between the top PMMA substrate and the top MEA-patterned substrate to ensure tight sealing between the two layers. Again, the four screws were uniformly tightened using a gauged torque wrench to ensure tight sealing (Figure 15). After autoclaving at 121 °C for 30 min, the screws were firmly tightened using the same torque wrench and the inlet/outlet tubings inserted into the top PMMA substrate and fixed with acryl glue.

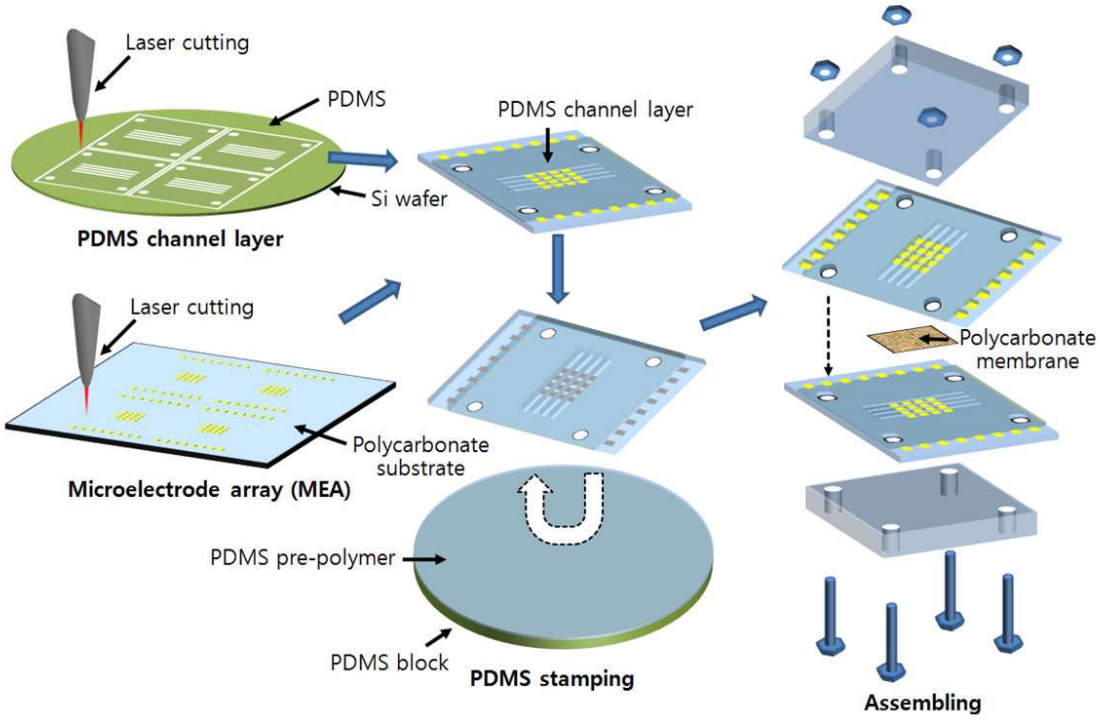


**Figure 15 Total chip fabrication procedure of 3D arrayed microfluidic BBB model with the integrated electrical sensor array.**

### 3.4 Tissue Dissociation and Primary Cell Preparation

Primary astrocytes were obtained as previously described [52]. In brief, brains were separated from the forebrains of 1–2 day old C57BL/6 mice. Cortices were dissected under a stereomicroscope and put in ice-cold HBSS ($Ca^{2+}$/$Mg^{2+}$–free Hank's Balanced Salt Solution, Invitrogen, CA). Tissues were digested with 0.25% trypsin (Sigma–Aldrich, MO) and DNase (Thermo Fisher Scientific, MA) for 15 min at 37 °C. After digestion, cortices were dissociated by triturating repeatedly using a 10 ml pipette until they became homogenous cells. Dissociated glial cultures were grown in poly–D–lysine coated culture flasks in 10% FBS supplemented DMEM (Thermo Fisher Scientific, MA) containing 1.0 mM Pyruvic acid (P2256, Sigma–Aldrich, MO) and 4.0 mM GlutaMAX (Invitrogen, CA). Astrocytes were purified from the glial layer in the flask that has been exposed to the specific microglia toxin L–leucine methyl ester (1 mM) for one hour, followed by 1–2 cycles of subculture and repeated exposure to L–leucine methyl ester. Purified astrocytes were maintained in growth medium for 3 days before use. Primary mouse brain microvascular endothelial cells derived from C57BL/6 mice (provided by Prof. Jane Welsh, Texas A&M University) were passaged as previously described [53]. The primary endothelial cells were maintained in 10% FBS supplemented with IMDM (Thermo Fisher Scientific, MA) containing 2.0 mM GlutaMAX (Invitrogen, CA). All animal procedures were approved by the Institutional Animal Care and Use Committee (IACUC) at Texas A&M University (Protocol # 2014–0252).

### 3.5 Microfluidic Perfusion Culture in the BBB Chip

For astrocyte and endothelial cell co-culture, primary astrocytes were first seeded at a density of 300 cells/mm$^2$ on ECM-coated BBB chips. Either fibronectin (10 μg/mL, Trevigen, MD) or 10% Matrigel (BD Biosciences, CA) was used as the ECM material. Astrocyte cultures were maintained in a static culture condition initially to allow the astrocytes to adhere to the microchannels of the chip. After 24 hours from cell seeding, astrocytes continued to be cultured in fresh growth media with extremely low flow rate (0.1 μL/min) provided by a syringe pump (Chemyx, TX) for 6 days. To seed endothelial cells, the chip was flipped over to make the bottom part of the chip the upper side. Primary endothelial cells were seeded at a density of 150 cells/mm$^2$ on the backside channels of the chip, which were also coated with the same ECM as the astrocyte side. The endothelial cell culture was maintained in static condition first to allow the cells to adhere to the channels of the chip. During this time the astrocyte culture was also in the static condition without any additional media supply. After 24 hours from seeding endothelial cells, endothelial cells continued to be cultured to proliferate at a growth media flow rate of 1.5 μL/min for 3 days. The shear stress value on the bottom wall ($\tau_{wall}$) of a microfluidic channel was derived from the Navier–Stokes equation describing the fluidic motion inside a rectangular shaped channel (Equation 1).

$$\tau_{wall} = \frac{6Q\mu}{wh^2} \qquad (1)$$

Where $\tau_{wall}$ is the shear stress, $Q$ is the volumetric flow rate, $\mu$ is the dynamic fluid viscosity, $w$ and $h$ indicate the width and height of the channel, respectively. In the

case of the monoculture experiment (endothelial cell only), only primary endothelial cells were cultured on one side of the BBB chip following the above endothelial cell culture procedure. All cell cultures were maintained at 37 °C in a humidified 5% $CO_2$ incubator.

### 3.6 Immunocytochemistry

Cells were fixed in 4% paraformaldehyde for 20 min at 25 °C and permeabilized with 1% Triton X–100 for 10 min at room temperature. After being treated in 5% goat–serum for 1 hour at room temperature, samples were agitated overnight at 4 °C in primary antibodies: anti–zonula occludens–1 (ZO–1, mouse monoclonal, 1:100, Life Technologies, NY) and anti–GFAP (glial fibrillary acidic protein, rabbit, 1:1000, Sigma–Aldrich, MO). Samples were then agitated in secondary antibodies of Alexa 594 goat antimouse (1:1000, Life Technologies, NY) and Alexa 488 goat anti-rabbit (1:1000, Life Technologies, NY) for 1 hour at room temperature. Samples were rinsed with PBS after each step. ZO–1 was used for identification of tight junction proteins among endothelial cells. Positive GFAP labeling identified astrocytes. Nuclei and actin were respectively stained with Hoechst 33342 (1 mg/mL, Life Technologies, NY) and Alexa 594 phalloidin (1:40, Life Technologies, NY) to observe cell morphology on the porous membrane. Fluorescently labeled cells were imaged using an inverted microscope (Olympus, Japan).

### 3.7 TEER Measurement for Non–invasive Permeability Assessment

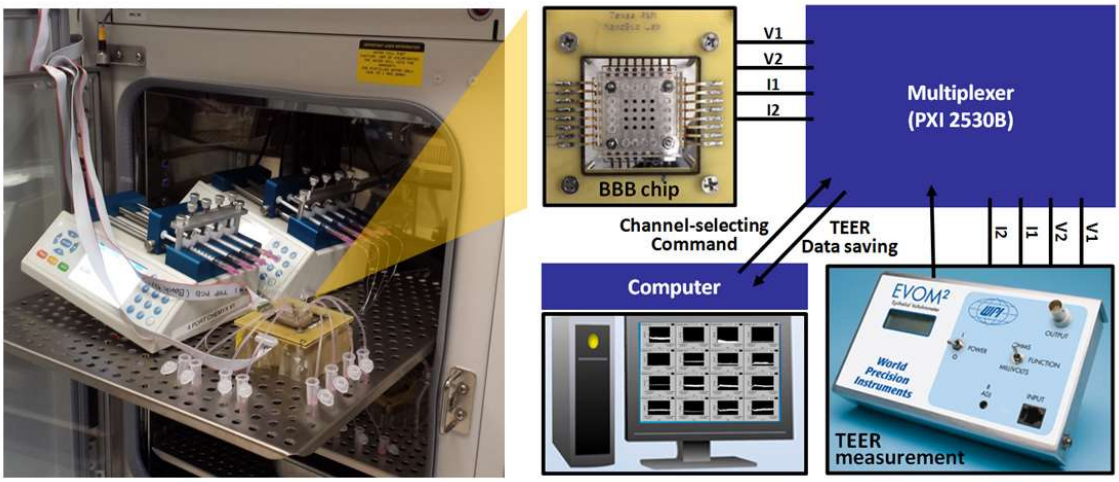


**Figure 16 Real–time multi-site TEER recording setup.** The BBB chip is connected to an epithelial voltohmmeter through a multiplexer. A Labview program is used to monitor the TEER value from all 16 sites.

To quantitatively assess the barrier permeability non–invasively, TEER was measured using an alternating current (AC) square wave with a frequency of 12.5 Hz using the EVOM2 epithelial volt/ohm meter (WPI, FL). To allow TEER measurements from all 16 BBB units on the chip continuously, a system consisting of a multiplexer (PXI–2530, National Instruments, TX) and a data acquisition board (DMM–4065 (National Instruments, TX) was used. Each of the 16 pairs of TEER measurement electrodes was connected to the multiplexer, which was then connected to the EVOM2 instrument. A LabView$^{TM}$ (National Instruments, TX) program controlled the multiplexer to switch the four wires used by the EVOM2 in a 4×16 configuration to each

of the electrical contact pads of the electrode array in each of the BBB compartments. The analog TEER values from the EVOM2 were sent to the data acquisition board and graphically displayed on the monitor while recording the values (Figure 16).

### 3.8 Permeability Assessment using Fluorescent Tracer Molecule

In another method for barrier permeability assessment, fluorescent tracer molecules having different molecular sizes were used. A mixture of red–fluorescent dextran 3,000 Da (Texas Red dextran, Life Technologies, NY), blue–fluorescent dextran 10,000 Da (Alexa 546 dextran, Life Technologies, NY), and green–fluorescent dextran 70,000 Da (FITC dextran, Sigma–Aldrich, MO), each at a concentration of 500 μg/mL in culture media, was loaded into the luminal channel of the BBB chip so that dextran could be diffused through the exposed porous membrane into the abluminal channel of the chip. After 6 hours in no flow condition, samples were collected from the abluminal channel and the fluorescent intensities measured using a multichannel fluorescent plate reader (Cytation 5, BioTek Instruments, VT). Fick's laws of diffusion was used to calculate the permeability coefficient (ratio between the original dextran concentration and the diffused dextran concentration). All permeability assays were conducted at days *in vitro* (DIV 4) of endothelial culture.

### 3.9 The growth of Primary Neurovascular Endothelial Cells and Formation of Tight Junction in the Microfluidic BBB Chip

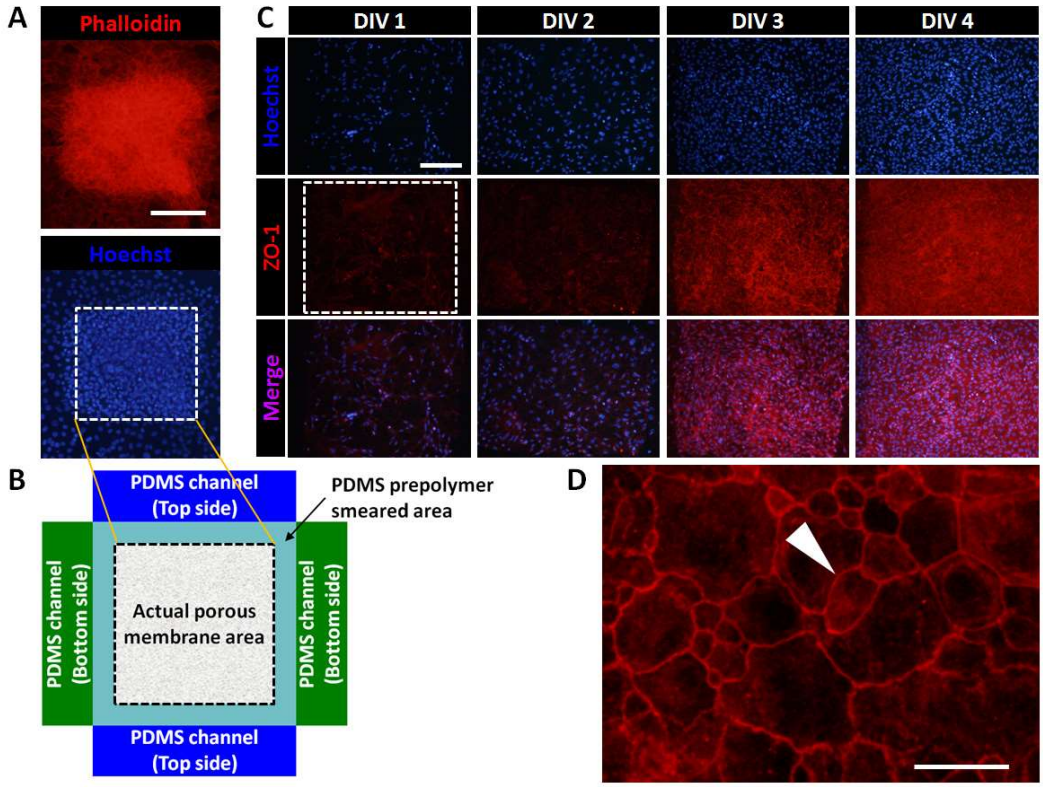


**Figure 17 The growth of primary neurovascular endothelial cells and formation of tight junction in the microfluidic BBB chip.** (A) Fluorescent images showing primary neurovascular endothelial cells (C57BL/6) cultured on top of the porous membrane in the BBB chip (red: phalloidin stain for actin, blue: Hoechst stain for nuclei). Dotted box indicates the area of the exposed porous membrane. (B) A drawing showing the actual exposed area of the porous membrane not smeared by PDMS prepolymer during the chip assembling process. (C) Immunocytochemistry showing endothelial cell growth and formation of tight junctions using tight junction protein ZO–1 (blue: Hoechst stain for nuclei, red: ZO–1 stain for tight junction).

Although the use of cell lines are convenient, endothelial cell lines have shown critical differences in their ability to respond to cytokines and in various functional markers as compared to primary endothelial cells [54, 55]. In this study, primary neurovascular endothelial cells were used in the microfluidic BBB chip. Primary neurovascular endothelial cells grew and proliferated in the device without any observable cell death. The number of endothelial cells growing on the porous membrane area increased gradually and were confluent by DIV 3 as evaluated by actin filament and nuclei staining, respectively (Figure 17A). Interestingly, a higher density cell population was observed inside the porous membrane area not smeared by the PDMS prepolymer during the assembling process and thus exposed to the backside microfluidic channel, as compared to the vicinity of the exposed area of the membrane (Figure 17B). This significant endothelial cell coverage feature may reinforce BBB properties by reducing the net loss of endothelial cells over the porous membrane, as in transwell culture net loss of cells in culture commonly resulted in lower levels of TEER [35].

To investigate whether the primary neurovascular endothelial cells cultured in the microdevice form proper tight junctions, cells were immunostained with an antibody to the tight junction protein ZO–1. Figure 17C shows that as the number of endothelial cells increases from DIV 1 to DIV 4, the expression of ZO–1 also simultaneously increases, indicating the time-dependent formation of tight junctions among the endothelial cells. Importantly, a drastic increase in tight junction formations is observed between DIV2 and DIV 3. By DIV 4, tight junctions were densely formed throughout the endothelial cell culture, covering the entire area of the exposed porous membrane.

Figure 17D clearly shows an enlarged view of tight junction formation among endothelial cells.

## 3.10 Optimizing BBB Chip Configuration

### *3.10.1 Extracellular matrix (ECM) configuration*

The basement membrane plays a critical role in cellular interaction and regulation of cell behaviors. The ECM can form an interstitial basement membrane that provides the framework for cell attachment, and thus a reliable ECM is required for *in vitro* BBB models. To investigate how different ECM affect the degree of tight junction formation, the effects of fibronectin and Matrigel (composed of a mixture of ECM proteins laminin, collagen IV, nidogen/entactin and proteoglycan) on the formation of tight junction were compared by coating each ECM on the porous membrane in the BBB chip. As shown in Figure 18, in the case of the fibronectin-coated device, the TEER values increased considerably by 2.5 times over the course of 4 days, from 663 ± 162 Ω at DIV 0 to 1674 ± 427 Ω at DIV 4 ($n$ = 10, $p < 0.05$), consistent with the time-dependent increases in ZO–1 expression. Similarly, the TEER values in the Matrigel-coated device also increased considerably by 5.5 times, from 615 ± 122 Ω at DIV 0 to 3368 ± 441 Ω at DIV 4 ($n$ = 12, $p < 0.001$). Importantly, the Matrigel-coated device showed a significantly higher TEER value (2.0 times higher) than that of the fibronectin-coated device ($p < 0.05$). This finding shows that the use of Matrigel as the basement

membrane results in tighter barrier formation with high TEER value, and is thus used throughout the subsequent experiments.

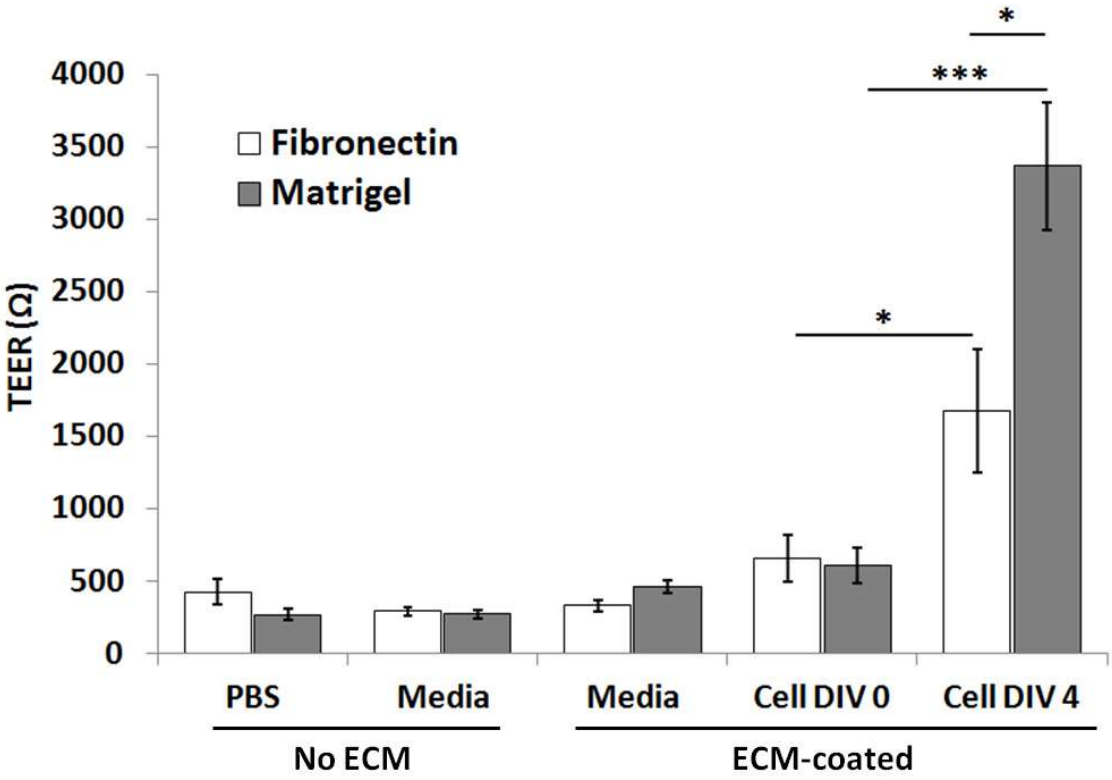


**Figure 18 Effect of fibronectin and Matrigel coating of the porous membrane on tight junction formation.** PBS, media, and media ECM-coated have no cells loaded in the device. TEER measurements were taken 12 hours after cell seeding (DIV 0), and then again after 4 days (DIV 4). All values are plotted as a mean ± standard error of the mean. * $p < 0.05$, *** $p < 0.001$.

*3.10.2 Optimization of shear stress stimulation*

Shear stress plays an important role in cell culture, and although shear stress was applied in previously developed BBB chips, the levels of shear stress applied (0.0008 –

0.15 dyne/cm$^2$) were significantly lower compared to *in vivo* level shear stress (5 – 25 dyne/cm$^2$) [46-49, 56]. We hypothesized that applying shear stress similar to *in vivo* shear stress range may lead to higher degree of tight junction formation. Fig. 4 shows the degree of ZO–1 expression in endothelial cells cultured under eight different shear stress conditions (0, 1, 5, 10, 15, 20, 25 and 30 dyne/cm$^2$) applied in the BBB chip by adjusting the luminal side of the culture media flow rate. Compared to the static culture case, ZO–1 expression showed a significant increase when shear stress ranges from 1 to 25 dyne/cm$^2$ were applied. Shear stress levels of 20 dyne/cm$^2$ and 25 dyne/cm$^2$ showed the highest degree of ZO–1 expression ($n$ = 16). On the other hand, when too high of shear stress was applied (30 dyne/cm$^2$), no statistically significant increase was observed compared to the static culture case (Figure 19). Thus for all subsequent experiments, the optimized shear stress level of 20 dyne/cm$^2$ was used.

A

*In vivo* shear stress level

| Shear stress $\tau_{wall}$ (dyne/cm²) | Flow rate $Q$ (μL/min) |
|---|---|
| 0 | Static |
| 1 | 0.075 |
| 5 | 0.375 |
| 10 | 0.750 |
| 15 | 1.125 |
| 20 | 1.500 |
| 25 | 1.875 |
| 30 | 2.250 |

B

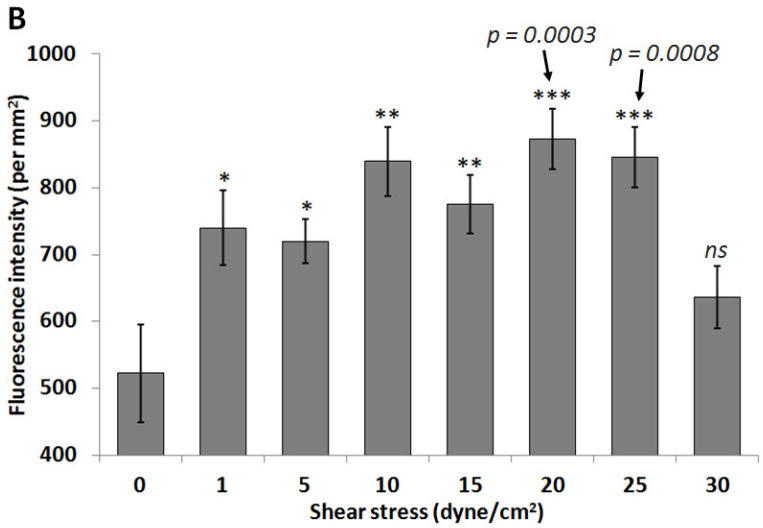


**Figure 19 The effect of shear stress on the tight junction.** (A) Culture media flow rates ($Q$, μL/min) corresponding to the various shear stress ($\tau_{wall}$, dyne/cm$^2$) tested. Gray highlights indicate *in vivo* level shear stress in the brain blood vessels. (B) Fluorescent intensity per mm$^2$ displaying ZO–1 expression in endothelial cells inside the BBB chip (static culture for 1 day, followed by perfusion culture for 3 days). All values are plotted as a mean ± standard error of the mean ($n$ = 16). * $p < 0.05$, ** $p < 0.01$, *** $p < 0.001$.

*3.10.3 Astrocyte–endothelial interactions in the 3D cellular network through co-culture*

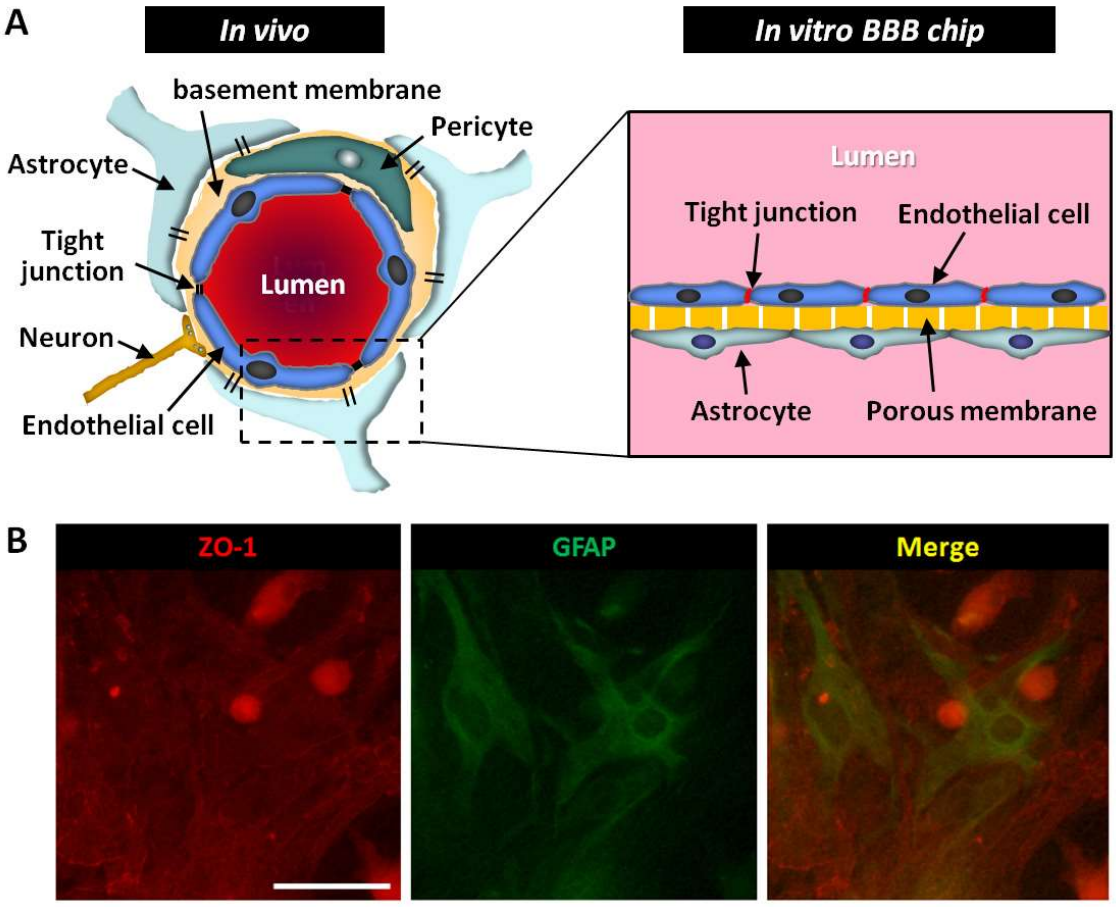


**Figure 20 Astrocyte–endothelial interactions in the 3D cellular network through co-culture.** (A) Schematic cross section of an *in vivo* neurovascular unit compared to the structure of the *in vitro* BBB chip developed here. (B) Immunocytochemistry images of astrocyte-endothelial cell co-culture on the same porous membrane interface (endothelial cells on the front side and astrocytes on the back side) of the BBB chip. Tight junction: ZO–1 staining (red), astrocyte: GFAP staining (green). Scale bar: 100 μm.

Astrocytes promote BBB formation as well as neurovascular endothelial cell maturation, contributing to tighter junction formation [57]. The main reason is because various molecules that astrocytes produce can induce aspects of BBB phenotypes in endothelial cells, such as the glial-derived neurotrophic factor (GDNF), basic fibroblast growth factor (bFGF), transforming growth factor–β (TGF–β), and angiopoietin 1 (ANG1) acting on the TIE2 endothelium-specific receptor tyrosine kinase 2. Also, astrocytes can affect the expression and polarized localization of P–glycoprotein (a gatekeeper) and GLUT1 (transport barrier) as well as enzyme modulation of γ–glutamyl transpeptidase (γ–GTP) (metabolic barrier).

To investigate the effect of astrocytes on the BBB properties, primary mouse astrocytes were co-cultured with primary endothelial cells in the BBB chip. Following the *in vivo* structure of the neurovascular unit (Figure 20A), endothelial cells were cultured on the top side and astrocytes on the back side of a porous membrane in the microfluidic BBB chip. Immunocytochemistry images show that astrocytes were properly cultured on the porous membrane, with the endothelial cells cultured on the opposite side of the porous membrane, leading to cellular interactions through the 10 μm porous structure (Figure 20B). To examine the effect of astrocyte–endothelial interactions, the barrier permeability between co-culture (astrocyte + endothelial cell) and monoculture (endothelial cell only) were compared by using two methods, TEER analysis and dextran permeability assay. As shown in Figure 21, the permeabilities of both cases were selective according to the Stokes size of dextran having different molecular sizes (3kDa, 10kDa, and 70kDa). Dextran with smaller Stokes size showed

higher permeability as expected, demonstrating that smaller compounds can pass through the barrier with ease. The difference between the co-culture condition and the monoculture condition was greatest with the smallest molecule (3kDa dextran), where co-culture with astrocytes showed 2.48 times lower permeability coefficient compared to that of the monoculture case ($n$ = 8). This permeability result demonstrates that the microfluidic BBB chip developed here enables size–dependent molecular transport from the luminal channels to the abluminal channels through the established tight junctions. More importantly, the lower permeability of 3kDa dextran in the co-culture condition quantitatively showed that astrocyte interactions with endothelial cells led to tighter barrier formation.

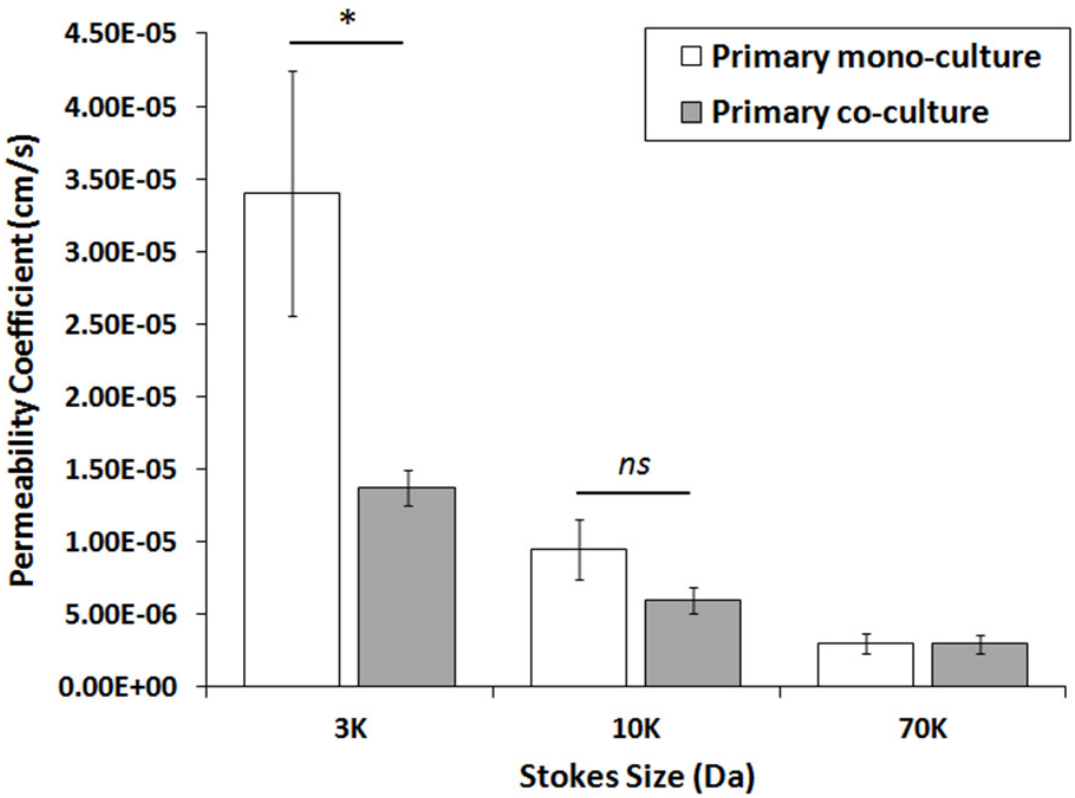


**Figure 21 Effect of astrocyte–endothelial co-culture on barrier permeability.** Fluorescent dextran permeability depending on different dextran sizes. Only the smallest dextran size (3kDa) showed a significant difference between monoculture and co-culture ($p$ = 0.0168,). All values are plotted as a mean ± standard error of the mean. * $p < 0.05$, *ns* (no significant difference).

### 3.11 Conclusion

A microfluidic multi-channel BBB chip model with integrated electrical impedance sensor array for label-free barrier function analysis has been successfully developed. The developed system includes features that closely mimic the *in vivo* structures of the BBB and a multitude of physiological functions, including i) more effective selection of ECM, ii) optimized *in vivo* level shear stress applied, and iii) using primary endothelial cells co-cultured with primary astrocytes, all contributing to increased level of tight junction formation. The barrier function was confirmed using three different methods, immunofluorescent staining, TEER measurement, and fluorescent molecular permeability assay. The system also provided preliminary evidence of a more realistic drug response of brain tissue protection when exposed to histamine treatment, as is the case in *in vivo* BBB. The 16 BBB units on a single chip can also open up the possibility of medium-throughput drug screening. In these regards, the developed *in vitro* BBB system has the potential to replace or minimize the use of animal studies by effectively predicting the BBB permeability against various drug candidates that are in preclinical stages.

# 4. BRAIN INFLAMMATION-ON-A CHIP: MONOCYTE INFILTRATION INTO THE CENTRAL NERVOUS SYSTEM

## 4.1 Motivation

The immune system plays an important role in protecting organisms from an invasion of viruses, bacteria, and parasites. It further distinguishes between diseased and healthy tissues. Leukocytes are important blood components that play a major role in innate and adaptive immune responses including pathogen infection, allergic reactions, and malignancies. Leukocytes are heterogeneous mixtures of multiple cell subsets, such as granulocytes, lymphocytes, and monocytes. These cell subsets are defined by their morphology, surface antigen expression, and production of cytokines [58-60].

In the central nervous system (CNS), the presence of the blood-brain barrier (BBB) limits the migration of soluble mediators and leukocytes from entering the periphery of the CNS. Despite the presence of this tightly regulated BBB, invasion of leukocytes into the CNS is an early event of multiple sclerosis (MS). Inflammation initiates MS lesions, and CNS paresthesis is accompanied by accumulation of blood-derived inflammatory cells. The inflammatory molecule cascade leading to CNS tissue infiltration by blood-derived leukocytes has been gradually elucidated. This study has led to the hypothesis that leukocytes migrate first through the blood-brain barrier (BBB) via pial vessels located on the surface of the brain and spinal cord [61]. Chemokines and adhesion molecules regulate transendothelial migration of leukocytes across the BBB and are attractive targets for the development of drugs that manage MS [62-64].

Blockade of leukocyte trafficking to the CNS has been shown to be therapeutically effective, thus confirming the role of blood-derived white blood cells in MS etiology. The therapies that inhibit leukocyte trafficking by blocking adhesion molecules affect the entire spectrum of the white blood cell population [65]. This has a negative effect on a person's overall immune system. More selective means are needed to prevent leukocyte entry into the CNS of patients with neuroinflammatory diseases such as MS. To achieve this goal, clear insights into the mechanism by which blood-derived leukocytes enter the CNS in both healthy and diseased patients is necessary. However, the complexity of leukocyte transmigration and chemokine receptor regulation is a challenge in identifying the mechanism behind neuroinflammatory diseases (Figure 22).

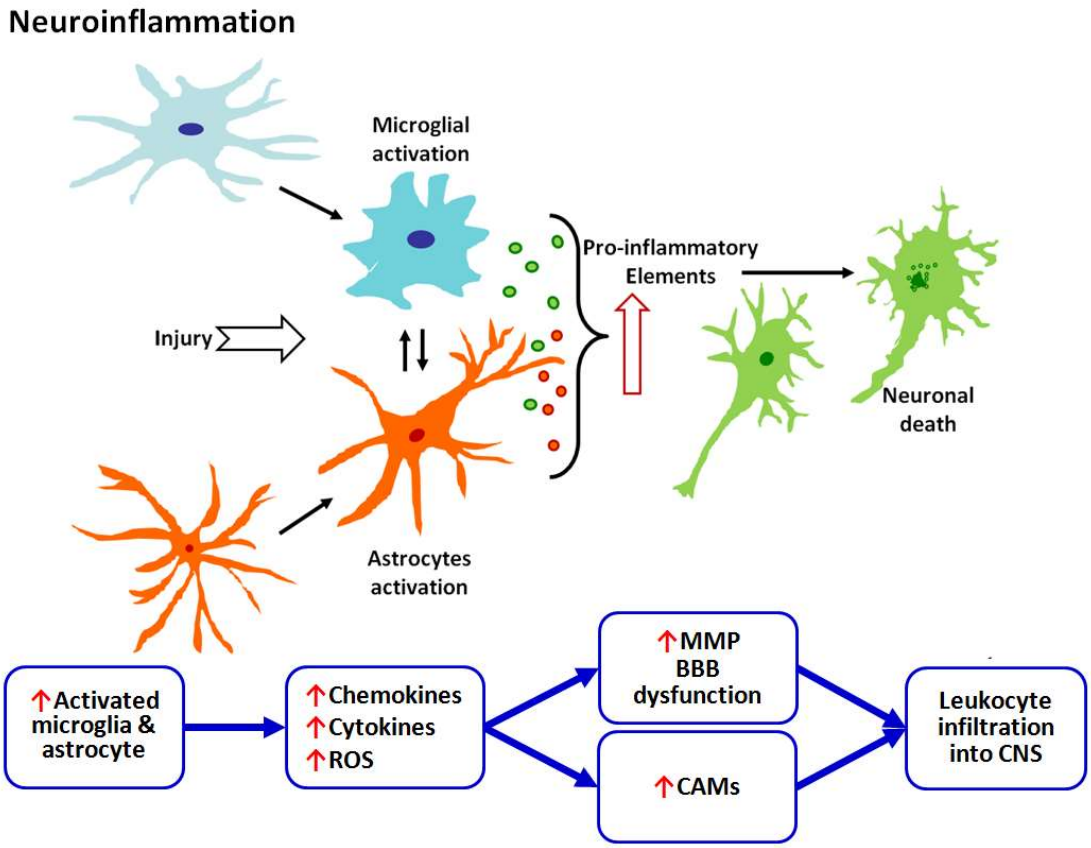


**Figure 22 Schematic design of CNS brain inflammation-on-a Chip.** Monocytes can invade through the endothelial cell culture layer by stimulating the vascular endothelium with monocyte chemotactic protein, CCL2. ROS: reactive oxygen species, MMP: matrix metalloproteinases, CAMs: cell adhesion molecules.

An organ-on-a-chip is a microfluidic device for culturing live cells in a continuously perfused micrometer-sized chamber to model the physiological functions of tissues and organs. The goal is not to build the whole living organism but rather to synthesize the smallest functional unit that requires organizational and organ level functions. Two or more microchannels are connected by porous membranes by different

cell types to reproduce the interface between the different tissues for the blood-brain barrier. These systems can incorporate physical forces, including physiologically relevant levels of shear stress, periodic strain, and mechanical compression. Moreover, they analyze the organ-specific responses including recruitment of circulating immune cells, in response to drugs or toxins. Organs-on-chips mimic physiological interactions between different organs directly from the one stromal tissue compartment to another or through a second channel lined with the vascular endothelium directly or through the hydrodynamic coupling. To mimic physiological interactions between different organs or to study drug distribution, similar analysis can be performed with the chip lined by cells from different organs that are fluidically coupled, either directly from one stromal tissue compartment to another, or via a second channel lined potentially with vascular endothelium.

It has been found very useful to control the flow of fluid within such chips. Since viscous forces are dominant over the inertial forces on a small length scale, the flow is laminar when the microfluidic channel diameter is less than about 1 mm. This allows the generation of physical and chemical gradients that are utilized for cell migration, metabolic response, and cell-cell junction integrity [66-68]. Shear stress can be controlled by changing the flow rate or channel size, and by separating cells from the flow path with a porous membrane or microtechnological posts that limit the passage of cells. The ability to integrate porous substrates to separate the two microchannels allowed for tissue barrier function and analysis of transcytosis, absorption, and secretion. By culturing two different cell types on the opposite side of the substrate, it is possible to

create a tissue-tissue interface that mimics the interaction of the vascular endothelium with the parenchymal tissue defining the organ [29, 46, 69].

To be able to reproduce complex mechanical microenvironments of living tissues *in vitro*, organ-on-chips have great potential for the study of fundamental mechanisms of organ physiology and diseases. They are particularly well suited to studies of biological phenomena that rely on the microstructure and perfusion of tissues and involve relatively acute pathophysiological processes. The BBB-on-chip was developed by lining a porous matrigel-coated polycarbonate membrane with brain microvascular endothelium on one side and astrocyte on the other. The device contained embedded microelectrodes to measure transepithelial electrical resistance (TEER) across the barrier. Remarkably, the TEER level was much higher in this chip than in the same cells grown on the opposite sides of the polycarbonate membrane in a conventional static Transwell culture system. Coculture on the chip was also impermeable to larger molecules than the single cell culture of endothelial cells. This device is superior to conventional culture models for measuring the barrier permeability of the central nervous system and has great value in studying how biomolecules pass through the blood-brain barrier [70].

Cell recruitment activated via BBB endothelial cells is thought to be an essential step to inducing CNS inflammation and brain injury. The explosion of inflammation observed in brain diseases is regulated by circulating monocytes. This same kind of inflammation appears in monocyte invasive perivascular brain disease [16-18]. Thus, in this study, using this realistic BBB system, we can see how monocytes can invade through the endothelial cell culture layer by stimulating the vascular endothelium with

monocyte chemotactic protein 1 (MCP1), CCL2. We are working on the development of a novel inflammation on a BBB chip to study this, similar to what occurs *in vivo* in situations such as nerve infections. We observed that primary mouse monocytes migrated with CCL2 treatment and TEER shows how the barrier properties changed before and after monocyte infiltration. In this regard, this study showed that inflammation on BBB chips could be a novel way to quantify the mechanisms behind neuroinflammatory diseases.

## 4.2 Design of the Microfluidic BBB Chip

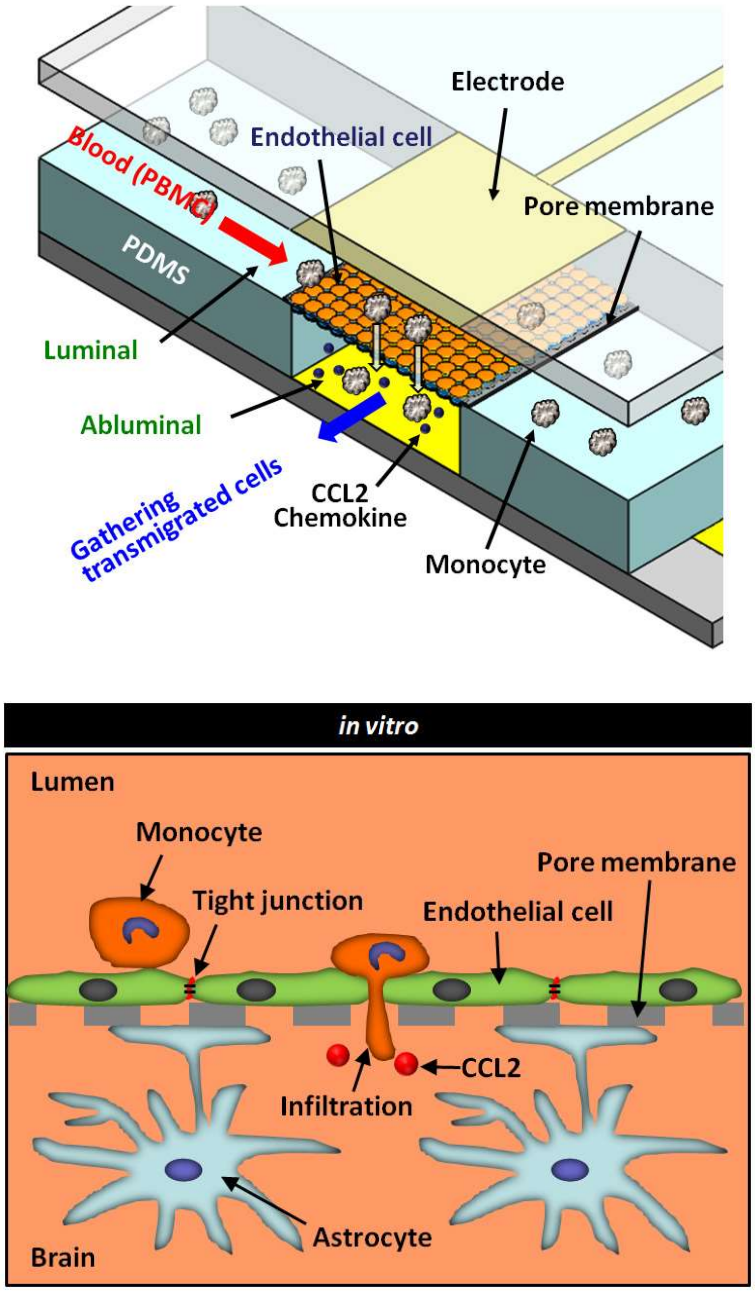


**Figure 23 Schematic design of CNS brain inflammation-on-a Chip.** Monocytes can invade through the endothelial cell culture layer by stimulating the vascular endothelium with monocyte chemotactic protein, CCL2.

The microfluidic BBB chip consists of two intersecting PDMS microfluidic channel arrays (4 channels each), a luminal channel array filled with endothelial cell culture medium, and an abluminal channel array filled with astrocyte culture medium, placed on an 8 μm pore polycarbonate membrane having a thickness of 10 μm. The region where these two microchannels intersect forms a single BBB unit so that a total of 4 × 4 BBB units are obtained on one chip. This configuration allows connecting the crossing channels via a porous membrane that serves as a physical isolation barrier separating the two cell types (the lumen and the luminal organ compartment), while the membrane pore allows diffusion of molecules to pass through (Figure 23). Each BBB unit in the chip has its upper electrode and the lower electrode for measuring TEER for tight junction analysis, and all 16 BBB units can be monitored simultaneously throughout the culture (Figure 24). The TEER electrode is designed to enable microscopic observation of both sides of the channel through the microscope during cell culture. Polycarbonate membranes were also verified using optical profiler scanning (NT9100, Veeco, NY).

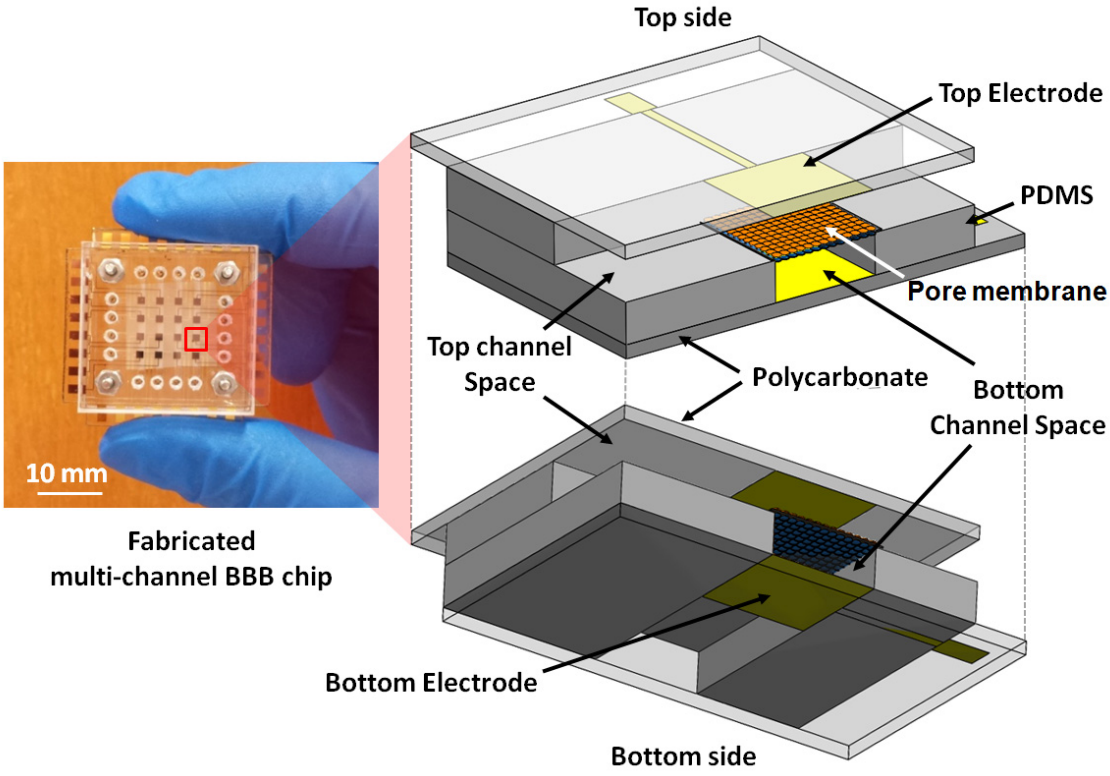


**Figure 24 3D illustration showing the multi-channel multi-layer BBB chip with integrated electrical impedance sensor array for CNS inflammation studies.** 3D structure of a single BBB unit of the 16-unit BBB chip. Intersecting PDMS microfluidic channel arrays, the luminal channel array for endothelial cell culture and the abluminal channel array for brain tissue culture. Photograph of an assembled device. Scale bar: 10 mm.

### 4.3 Tissue Dissociation and Primary Cell Preparation

Primary mouse brain microvascular endothelial cells derived from C57BL/6 mice were passaged as described above [25]. Primary endothelial cells were maintained in 10% FBS supplemented with IMDM (Thermo Fisher Scientific, MA) containing 2.0 mM GlutaMAX (Invitrogen, CA). Spleen and drainage lymph nodes of C57BL/6 mice were disrupted with 3 ml syringe plunger and passed through a 70 μm cell strainer. Splenocytes were centrifuged and resuspended in 3 ml RBC lysis buffer (R7757, Sigma-Aldrich, MO), incubated for 2 minutes at room temperature and then washed with complete RPMI 1640 medium. 200 μl of blood collected from mice was mixed with 100 μl of heparin (10 usp/ml; H3393; Sigma-Aldrich, MO). One ml of RBC lysis buffer was added, and the sample was incubated at room temperature for 15 minutes. The cells were then centrifuged and resuspended in PBS containing 2% FBS. If clear white pellets were not observed after centrifugation, the lysis procedure was repeated once. Single cell suspensions of splenocytes prepared from mice were resuspended in BD iMAG buffer (552362, BD Biosciences, CA) at a density of $2.0 \times 10^7$ cells/ml in 15 ml conical tubes and 20 μg/ml α-CD11b-biotin (13-0112, eBioscience, CA) for 15 minutes on ice. Cells were then washed twice and resuspended in iMAG buffer at a density of $4.0 \times 10^7$ cells/mL. Streptavidin (557812, BD Biosciences, CA) was added (10 μl per $1.0 \times 10^7$ cells) and incubated at 8 °C for 30 minutes. The volume was then brought to $2.0 \times 10^7$ cells/ml, and the tube was placed on a cell separation magnet (# 552311; BD Biosciences, CA) and incubated for 8 minutes at room temperature. The negative part was removed while the tube was on the magnet and the positive part was resuspended in iMAG buffer

at $2.0 \times 10^7$ cells/ml. Separation was repeated more than once with 4 min incubation at room temperature each time. After the last separation, the positive part was resuspended in complete IMDM medium. All animal procedures were approved by the Institutional Animal Care and Use Committee (IACUC) at Texas A&M University (Protocol # 2014–0252).

### 4.4 Microfluidic Perfusion Culture in the BBB Chip

For endothelial cell culture, 10% Matrigel (BD Biosciences, CA) was used as the ECM material. Primary endothelial cells were seeded at a density of 150 cells/$mm^2$ on the upper channel of the chip. Endothelial cell cultures were first kept quiescent and the cells adhered onto the channels of the chip. The endothelial cell culture was kept static so that the cells could be attached to the channel of the chip. Endothelial cells were cultured 24 hours after seeding of the endothelial cells and proliferated for 3 days at a growth culture media flow rate of 1.5 μl/min. All cell cultures were maintained at 37 °C in a humidified 5% $CO_2$ incubator.

### 4.5 Cell Viability and Tight Junction Expression

For direct observation of cell viability, live/dead cell staining was performed using the live/dead viability/cytotoxicity kit (Invitrogen, CA). After rinsing the culture once with Dulbecco's phosphate buffered saline (D-PBS), 2 μM calcein AM and 4 μM ethidium homodimer (EthD)-1 working solution is added to the culture. While Calcein AM induces green fluorescence by reacting with the esterase of the inner cell membrane

of viable cells, EthD-1 shows red fluorescence when it penetrated the damaged cell membrane of dead cells.

To observe the tight junction of endothelial cells, cells were fixed with 4% paraformaldehyde at 25 °C for 20 minutes and infiltrated with 1% Triton X-100 for 10 minutes at room temperature. After treatment with 5% goat serum for 1 hour at room temperature, it was agitated overnight at 4 °C with primary antibody: anti-zonula occludens-1 (ZO-1, mouse monoclonal, 1:100, Life Technologies, NY). The sample was agitated with a secondary antibody of Alexa 594 goat anti-mouse (1: 1000, Life Technologies, NY) for 1 hour at room temperature. Samples were rinsed with PBS after each step. ZO-1 was used to identify tight junction proteins between endothelial cells. Fluorescently labeled cells were imaged using an inverted microscope (Olympus, Japan).

### 4.6 TEER Measurement

The barrier permeability is quantitatively evaluated noninvasively using an alternating current (AC) square wave with a frequency of 12.5 Hz using an EVOM2 epithelial volt/ohm meter (WPI, FL). A system consisting of a multiplexer (PXI-2530, Texas Instruments) and a data acquisition board (National Instruments, National Instruments, DMM-4065) was used to enable continuous TEER measurements on all 16 BBB units on the chip. After connecting each of the 16 pairs of TEER measurement electrodes to the multiplexer, the multiplexer was connected to the EVOM2 device. The LabView™ (National Instruments, TX) program controlled the multiplexer to switch the four wires used in EVOM2 in the 4×16 configuration to each electrical contact pad in

the electrode array of each BBB compartment. The EVOM2 analog TEER value is sent to the data acquisition board and is graphically displayed on the monitor while recording the value.

### 4.7 Infiltration of Chemokine-associated Monocyte

To confirm that monocytes can be infiltrated by chemokine treatment, 20 ng/ml recombinant mouse CCL2/JE/MCP-1 protein (R&D Systems, MN) in culture medium was applied to the lower channel at a continuous 0.3 μl/min flow rate before monocyte injection at DIV 4. For infiltration testing, $CD11b^+$ monocytes were stained with CellTracker™ Green CMFDA (5-chloromethyl fluorescein diacetate, Thermo Fisher Scientific, MA) to identify monocytes and fluorescent dyes were used to monitor cell migration and location. Green fluorescence monocyte cells were injected into individual top channels cultured by endothelial cell culture at a monocyte cell seeding density of 1200 cells/$mm^2$. After 24 hours (top channel: static, bottom channel: 0.15 μl/min flow rate), the effluent from each outlet of the bottom channel was centrifuged at 1000 RPM for 5 minutes for the cell downing in each e-tube. Cells were counted using a hemocyte counter or a flow cytometer (BD Accuri™ C6 Plus, CA) after removing the redundant media.

### 4.8 Optimization of Matrigel-coating Conditions for Pore Membrane Structures

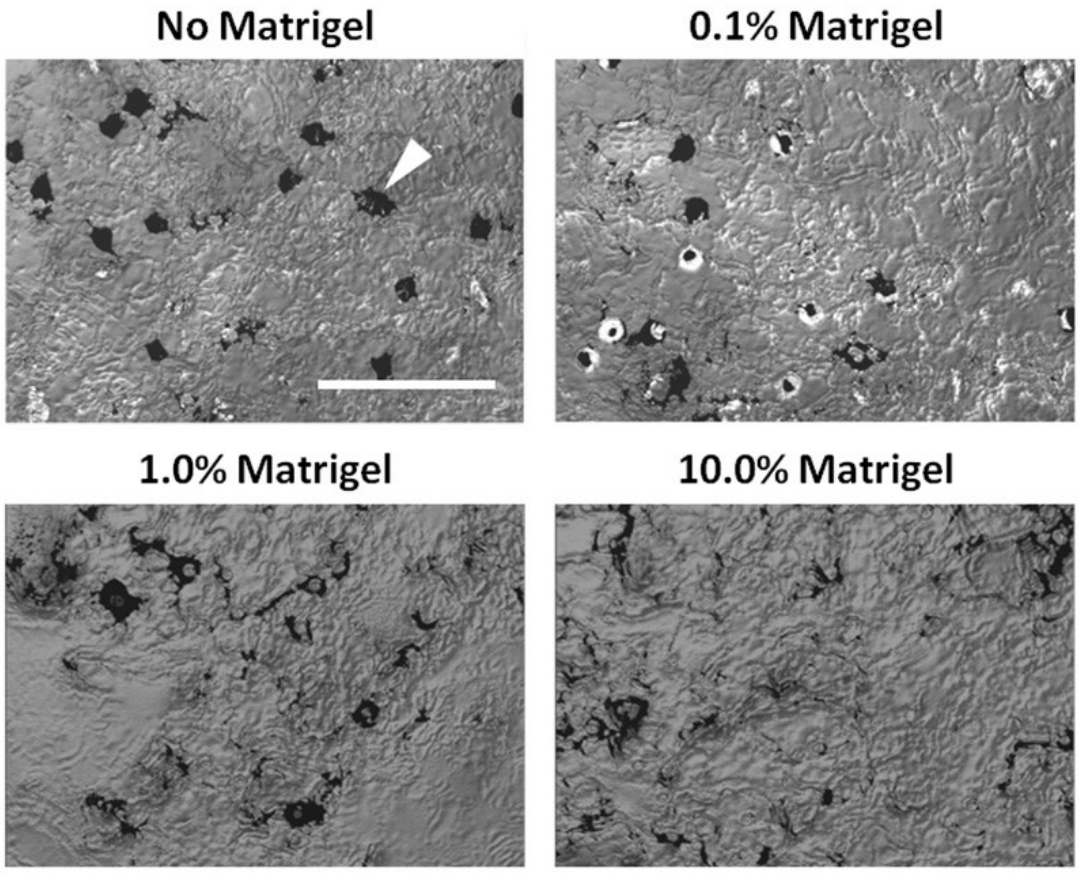


**Figure 25 Optimization of Matrigel coating conditions for pore membrane structures.** Optical surface image of a polycarbonate membrane coated with no Matrigel, 0.1% Matrigel, 1.0% Matrigel and 10% Matrigel. There are no actual pores on the membrane in the condition of 10% Matrigel. Scale bar: 50 μm.

Since the pore size of the polycarbonate membrane is 8 μm, many monocytes can probably pass through the perforated membrane considering the monocyte cell size range (5 to 10 μm). To prevent unrelated infiltration of monocytes by specific

chemokine treatment, we optimized the concentration of Matrigel coating to physically cover the pore structure on the membrane. Figure 25 shows a surface image of a polycarbonate membrane coated with no Matrigel, 0.1% Matrigel, 1.0% Matrigel and 10% Matrigel. The luminance intensity shows the vertical profile of the sample and the dark area is the pore. Pores are visible as small distinct dark areas on the image. An increase in Matrigel concentration causes a decrease in the number of pores in the membrane. And in the state coated with 10% Matrigel, there are no actual pores on the membrane. However, because they are covered with gelated matrigel, either the chemical solution or the culture medium can pass through the membrane and cell migration can also occur with chemokines [71].

### 4.9 Cell Growth of Primary Neurovascular Endothelial Cells in the BBB Chip

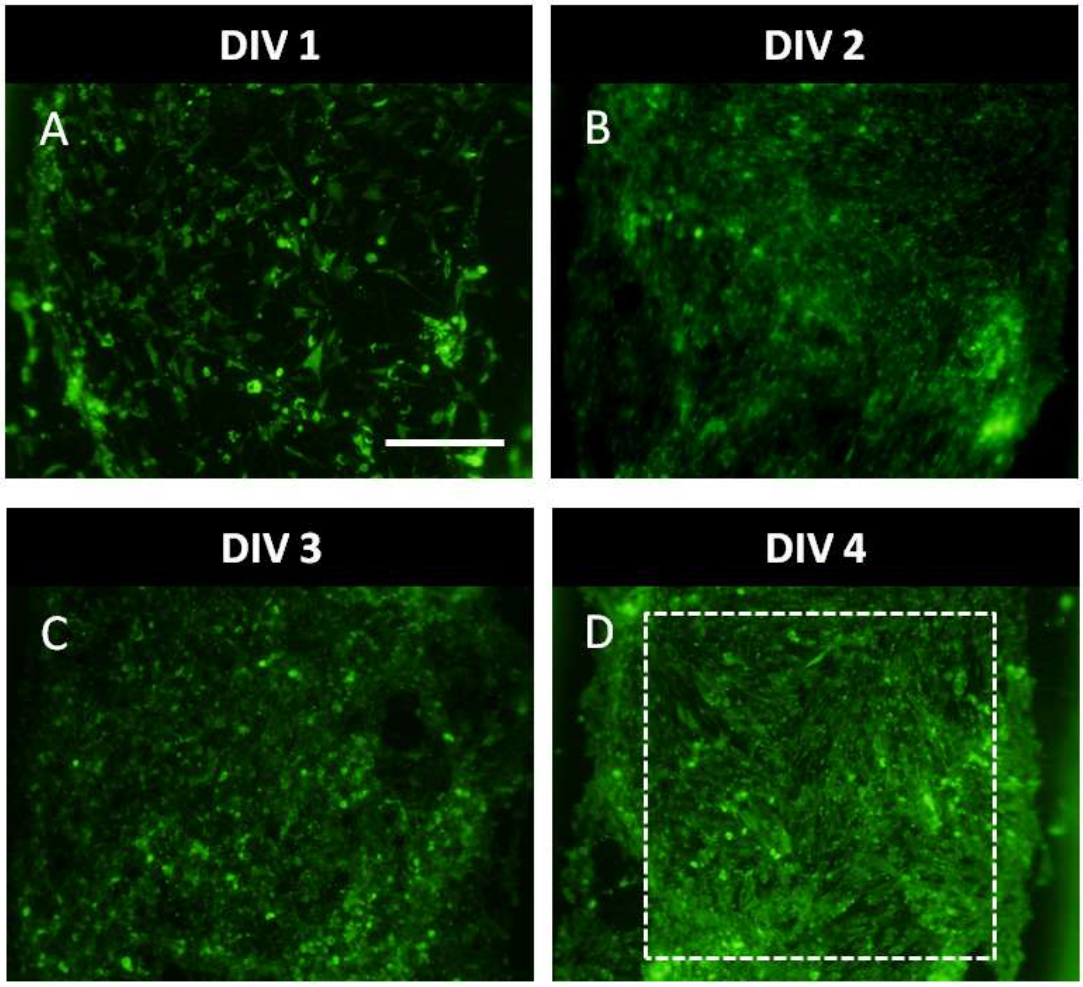


**Figure 26 Cell growth of primary neurovascular endothelial cells in the BBB chip.** The number of endothelial cells growing on the porous membrane area (inside of the dotted line) covered with 10% matrigel gradually increased and was confirmed by live cell staining from DIV 1 to DIV 4. Scale bar: 200 μm.

Primary neurovascular endothelial cells were used for microfluidic BBB chips to establish a condition that is more similar to the *in vivo* condition. This is because

endothelial cell lines showed decisive differences in their ability to respond to cytokines and various functional markers compared to primary endothelial cells [54, 55]. Primary neurovascular endothelial cells proliferated in the device without observable cell death as shown in Figure 26. The number of endothelial cells proliferating on the porous membrane area coated with 10% Matrigel gradually increased, confirmed by live/dead cell staining from DIV 1 to DIV 4. At DIV 4, we previously confirmed that tight junctions are formed densely through endothelial cell cultures covering the entire area of the exposed porous membrane [70]. Figure 27A shows an enlarged view of distinct tight junction formation between endothelial cells. This significant endothelial cell coverage feature reduces the net loss between endothelial cells on the porous membrane, as in the transwell culture, such that a net loss of cells in the culture results in a decrease in TEER levels, thereby enhancing the BBB characteristics [35].

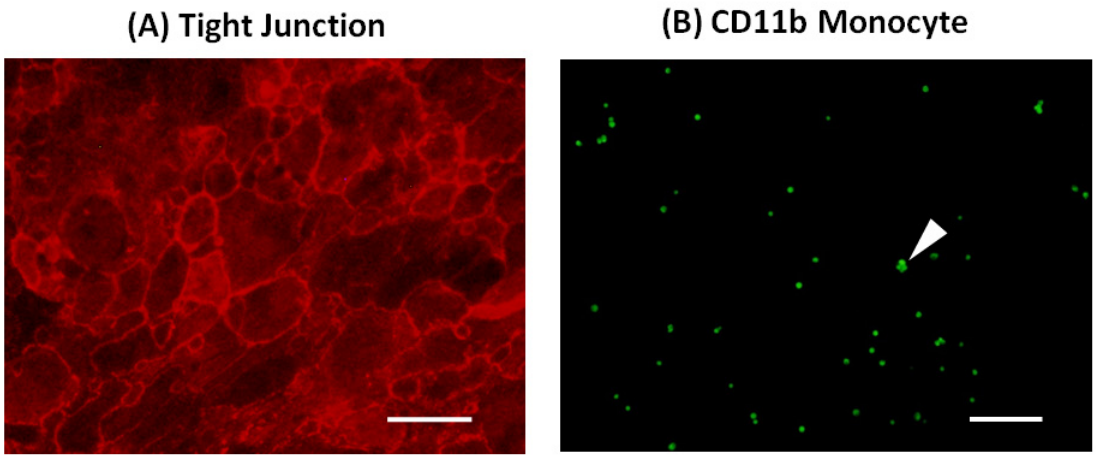


**Figure 27 Immunocytochemistry images.** (A) The tight junction between endothelial cells on the porous membrane in the BBB chip. Tight junction: ZO–1 staining (red). (B) For infiltration testing, $CD11b^{+}$ monocytes were stained with CellTracker™ to identify monocytes to monitor cell migration and location. Monocyte: CMFDA staining (green). Scale bar: 100 µm.

### 4.10 Monocyte Infiltration against the BBB

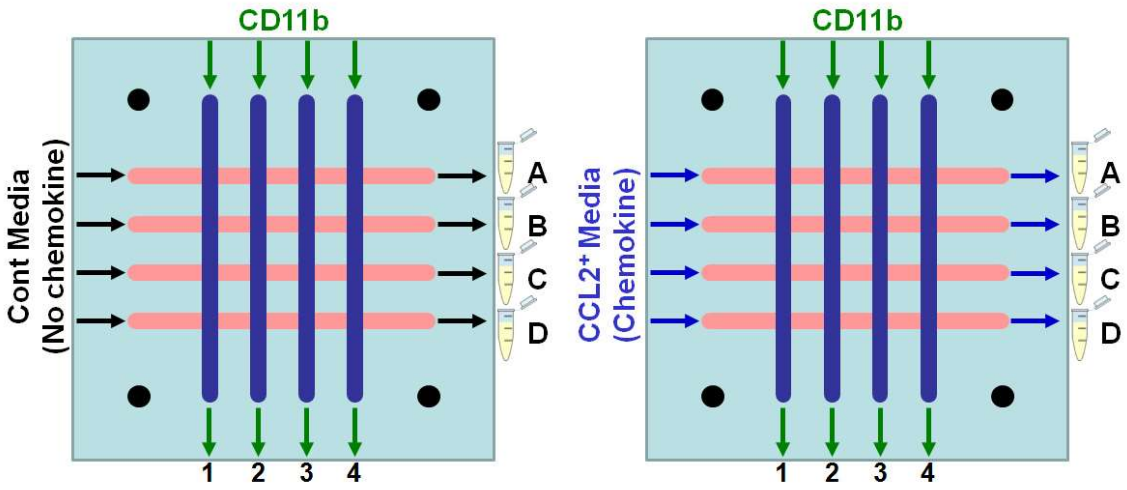


**Figure 28 CD11b$^{+}$ monocyte infiltration test against the BBB.** Two chips for control conditions (no CCL2) and CCL2 treatment conditions were prepared. A-D effluents for infiltrated monocyte quantitation analysis. Monocytes were stained to monitor cell migration or location with CellTracker™ Green CMFDA.

Two chips for control conditions and CCL2 treatment conditions were prepared (Figure 28). Figure 27B shows that monocytes were stained to monitor cell migration or location with CellTracker™ Green CMFDA. In DIV 4, since tight junctions were formed densely throughout the primary neurovascular endothelial cell culture by covering the entire area of the exposed porous membrane, CD11b$^{+}$ monocytes were treated with both BBB chips in the control and CCL2 treated condition.

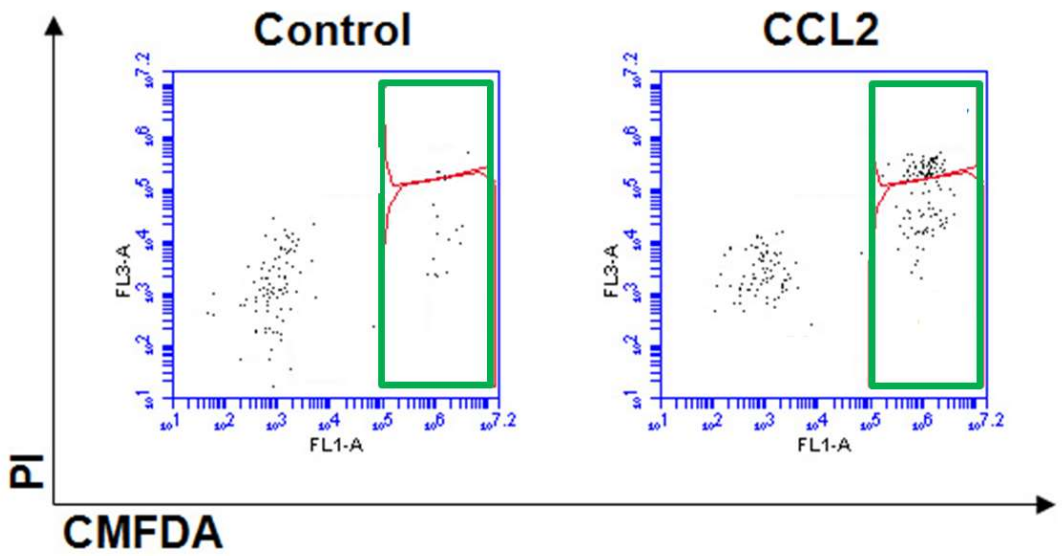


**Figure 29 Monocyte quantitation with cell cytometry.** Monocyte chemotactic protein-1, CCL2 is the important chemokine regulating migration and infiltration of monocytes to BBB in the CNS.

Quantitative data on the number of infiltrating monocytes showed a difference between control and CCL2 conditions. Figure 29 shows that 18 monocytes were obtained from the control effluent while 120 monocytes were counted from the effluent as CCL2 treated by cell cytometry. Mean 94.67 ± 42.23 monocytic cells (infiltrated ratio: 0.11% per a chip) were obtained from the control effluent, whereas the CCL2 treated condition showed mean 2940 ± 260.3 monocytic cells (infiltrated ratio: 3.40% per a chip) as shown in Figure 30.

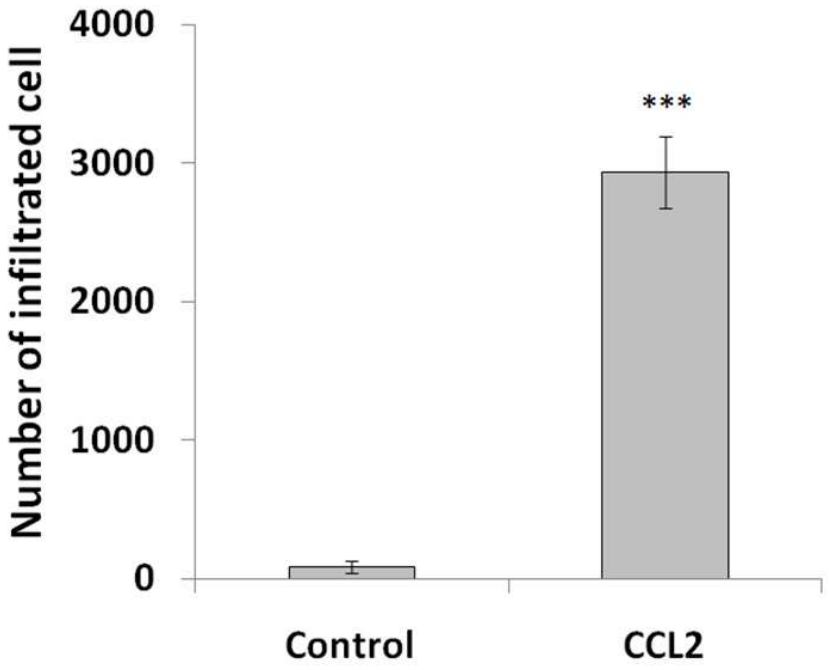


**Figure 30 The CCL2 effect for monocyte infiltration against the endothelial cell layer in the BBB chip.** All values are plotted as a mean ± standard error of the mean ($n$ = 3 sets). *** $p < 0.001$.

This result demonstrated that monocyte chemotactic protein-1 (MCP-1) CCL2 is one of the important chemokines regulating migration and infiltration of monocytes to BBB in the CNS. Also, we investigate whether monocyte infusion and CCL2 can affect BBB characteristics during testing. Therefore, we measured TEER values before and after both conditions. The mean TEER value before injection of $CD11b^+$ monocytes was higher than the mean TEER value after injection of $CD11b^+$ monocytes. Comparing the two cases of control and CCL2 treatment during $CD11b^+$ monocyte injection, the % TEER was 94.56 ± 4.54% in the control condition and 73.26 ± 2.27% in the CCL2

treated condition (Figure 31). Based on the results it is clear that the CCL2 effect can change the significantly reduced TEER value compared to the control without CCL2. More importantly, comparing the control and CCL2 conditions after monocyte infusion, cell-cell interaction with monocytes CCL2 resulted in a dramatic TEER reduction, whereas only monocytes not containing CCL2 did not significantly affect the TEER change indicating the BBB properties (Figure 31). Monocyte infiltration by CCL2 treatment may be associated with the role of glycosaminoglycan (GAG) and Duffy antigen receptor for chemokines (DARC) for monocyte recruitment *in vivo*. CCL2 associates with GAGs in specific tissues and establishes gradients that guide monocytes towards sites of inflammation. In support of this model, recruitment of monocytes is impaired by amino acid substitution of CCL2 which prevents dimerization or association with GAG [72, 73]. It has been suggested that CCL2 circulates through lymph nodes and binds to the endothelial blood vessels of lymph nodes, thereby inducing monocytes into the lymph nodes [74]. On the other hand, DARC, a non-signaling chemokine receptor that binds to CCL2 and transports endothelial cells to the luminal side, is important for the recruitment of monocytes from blood flow to inflamed tissue [75].

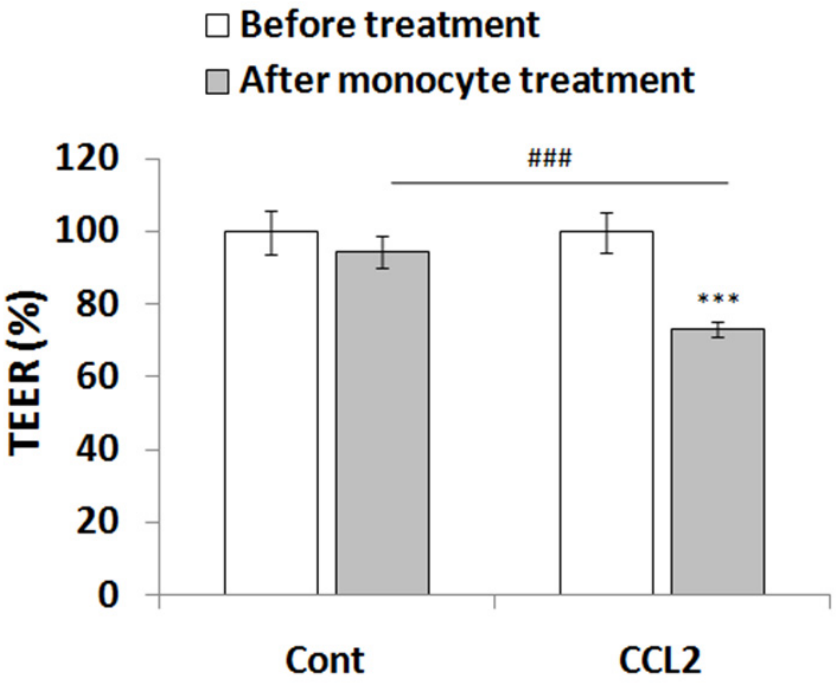


**Figure 31 TEER change in the BBB chip before and after monocyte injection on the luminal channel cultured with the endothelial cells in control and CCL2 treatment.** Percentage changes in normalized TEER ($TEER_{after}$ / $TEER_{before}$ × 100) after $CD11b^{+}$ monocyte treatment. All values are plotted as a mean ± standard error of the mean ($n \geq 15$). *** $p < 0.001$, ### $p < 0.001$.

## 4.11 Conclusion

A microfluidic brain inflammation analysis platform has been developed that allows for the initial investigation of monocyte infiltration into the CNS. Primary monocyte cell recruitment was characterized by CCL2 treatment through the BBB among the primary endothelial cells that allowed them to monitor their behavior during brain inflammation for the BBB, as well as mimic the actual organ level physiological immune response. Primary monocyte infiltration in chips was monitored by CMFDA with monocyte green fluorescent cells and quantified by the cell counting process using effluent from the subsequently developed platform. The physiological response in the organ-chip of the monocyte infiltration phenomenon was successfully confirmed in CCL2 against the BBB of the CNS. Moreover, successful analysis and comparison of TEER, which shows the BBB characteristics of brain inflammation by monocytes and CCL2, demonstrated the potential screening capacity of the platform. This system is expected to serve as a powerful brain inflammation analysis and screening tool to investigate various neurodegenerative diseases and find actual cures by studying the correlation between inflammation and numerous drug candidates.

# 5. MULTIPLE DRUG TESTING-ON-A-CHIP: DRUG EFFICACY AND PERMEABILITY TEST ON THE NEW BBB MODEL*

## 5.1 Motivation

Development of new drugs for brain diseases is a significant task, and there is few effective treatments for the majority of brain diseases. In the US, annual socioeconomic costs of brain diseases are now estimated to be over 250 billion dollars, and it is expected to increase significantly in the next 30 years [76]. Recently, the range of improvement of the drug has increased considerably. However there has been little approval of a drug with a new mechanism of action for brain disorders. The development of new drugs is inherently difficult as only 11% of the drugs entering clinical trials are entering the market in all therapeutic areas. Also, the CNS drug discovery-related medical statistical data show an 8% chance of being significantly lower than the total industry average (15%) in the other treatment areas, especially when CNS drugs enter clinical development (Figure 32) [77].

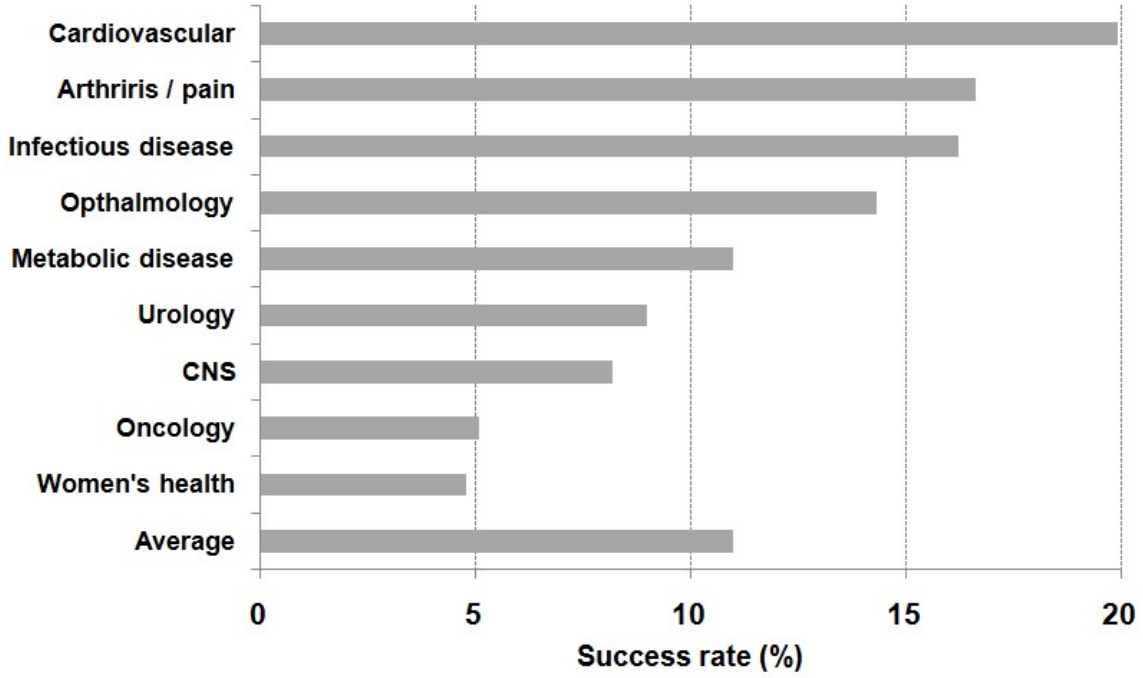


**Figure 32 Success rates from first-in-man to registration.** The overall clinical success rate is about 11%. CNS success rate is about 8% [77].

There are several reasons for the complexity of the brain when the success rate of CNS drug development is lower than the average. First, the blood-brain barrier where most therapeutic agents are not able to penetrate pharmacokinetically exists in the brain. Second, CNS drugs tend to cause side effects mediated by CNS. Nausea, dizziness, and seizures are examples. Third, there is a lack of verified biomarkers indicating whether a given neurotherapeutic reaches the brain at a concentration sufficient to regulate the required CNS target [76]. To solve this problem, we need to develop a technique for how each drug works in the brain blood vessels, what kind of action it has in the brain tissue, and how well the drug moves from the brain blood vessels to the brain tissue. Most of all,

it is crucial that these experimental assays are physiologically very similar to animals to be an effective test.

Therefore, we investigated how the BBB chip developed by us could show i) the pharmacological function of the cerebral blood vessels, and investigated ii) how the brain tissue cells react with the vascular cells. After the BBB chip was pharmacologically and physiologically verified, we examined iii) how much of the drug passed through the brain blood vessels (luminal) and into the brain tissue (abluminal).

### 5.2 Pharmacological test in the neurovascular region on the BBB chip

Histamine is known to increase endothelial permeability by disrupting junction barriers in the blood vessel [57, 78]. To observe the neurovascular response by confirming that the tight junction barrier formed with endothelial cells can be disrupted by pharmacological treatments, histamine (EMD Millipore, Germany) in the culture media was applied at DIV 4 while continuously measuring the TEER value to monitor the change in barrier permeability in real time.

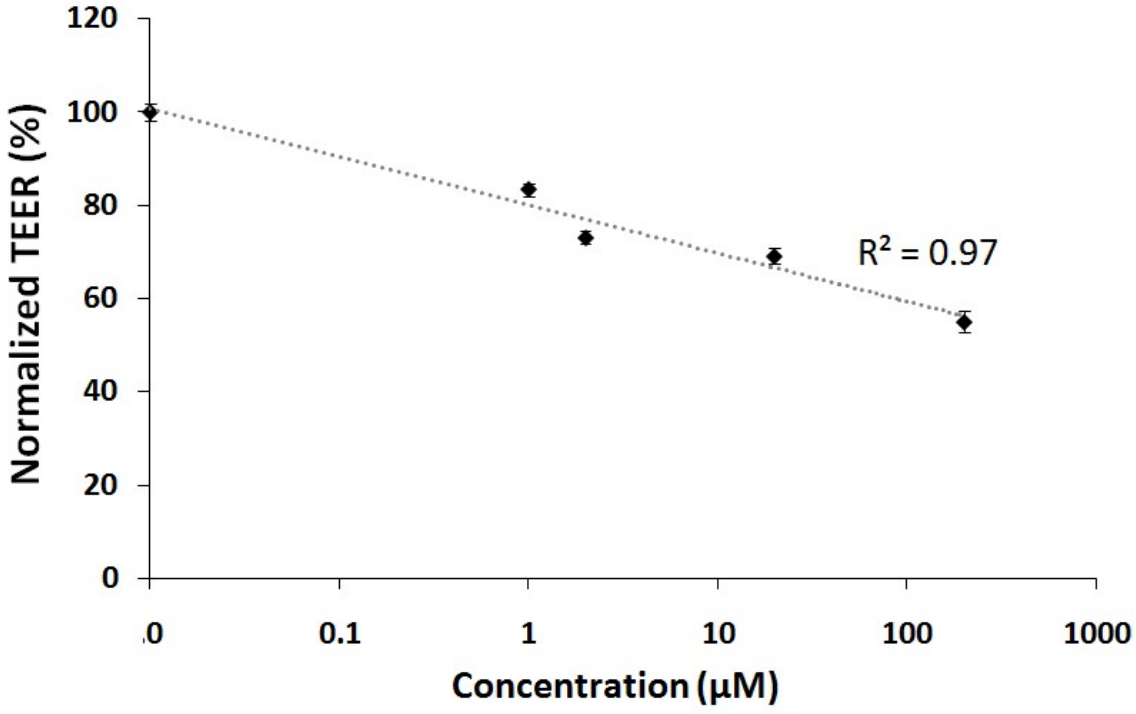


**Figure 33 The trend of normalized TEER value in the BBB chip according to histamine drug concentration.** As the concentration of histamine increases, the TEER value decreases in monoculture. All values are plotted as a mean ± standard error of the mean.

To find the optimal concentration condition showing the histamine effect, the initial drug treatment was carried out at various concentrations from 1 μM to 200 μM. After culturing endothelial cells on BBB chip, TEER values were measured at individual concentrations and normalized to control TEER values not treated with histamine. Figure 33 shows that as the concentration of histamine increases the normalized TEER value decreases on the BBB chip ($n$ = 10).

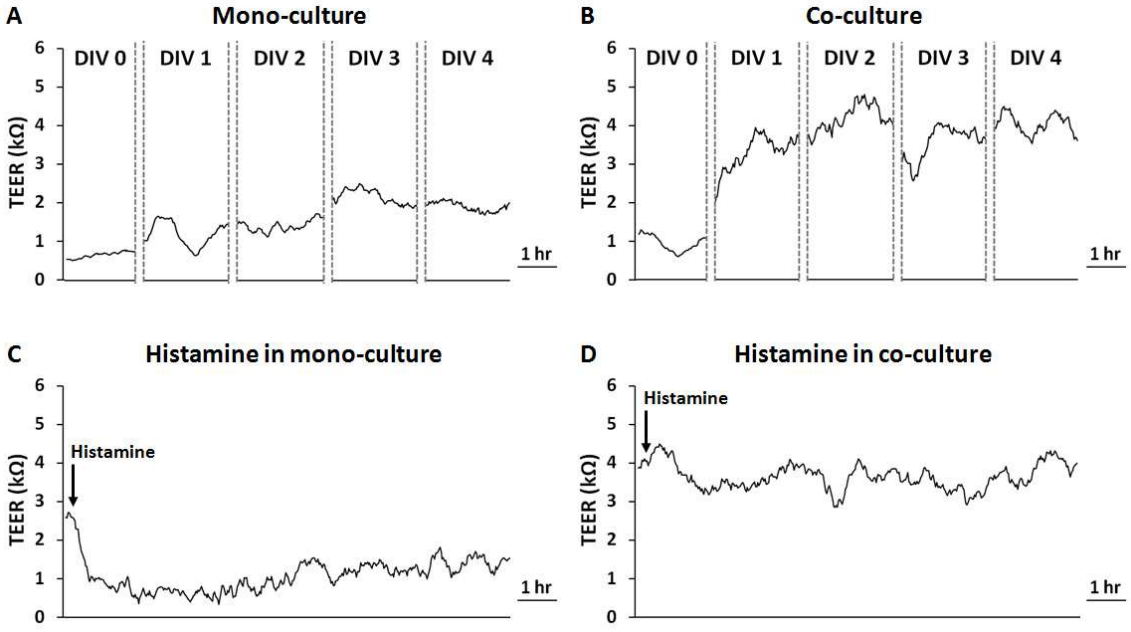


**Figure 34 Real–time TEER measurement in the BBB chip during drug treatment.** (A) TEER values during monoculture (endothelial cell only, DIV 0 – DIV 4) (B) TEER values during co-culture (endothelial cell and astrocyte, DIV 0 – DIV 4) (C) TEER values in response to 100 μM histamine treatment in the monoculture case. (D) TEER values in response to 100 μM histamine treatment in the co-culture case.

TEER values were monitored in real time while 100 μM of histamine was applied to both the monoculture (endothelial cell only) BBB chip and the co-culture (astrocyte + endothelial cell) BBB chip. After culturing endothelial cells for 4 days, real-time TEER recording was conducted to investigate the change in BBB permeability upon histamine treatment. Figure 34A shows TEER values in monoculture condition from DIV 0 to DIV 4, which increased from around 0.5 kΩ to around 2.5 kΩ. In the

astrocyte co-culture condition, the TEER values increased from around 0.6 kΩ and then saturated in the range of 3.6 – 4.5 kΩ (Figure 34B). When 100 μM histamine–containing media was injected only into the luminal channel where endothelial cells reside, an immediate decrease in TEER value was observed in monoculture condition, where it decreased to around 0.5 kΩ (81% lower than the DIV 4 TEER value) within 4 hours. The TEER value then showed a slow recovery over time, eventually saturating to about 1.6 kΩ (62% of the DIV 4 TEER level) in about 4 hours (Figure 34C). On the other hand, astrocyte co-culture condition did not show any drastic decrease in the TEER value under 100 μM histamine treatment (Figure 34D).

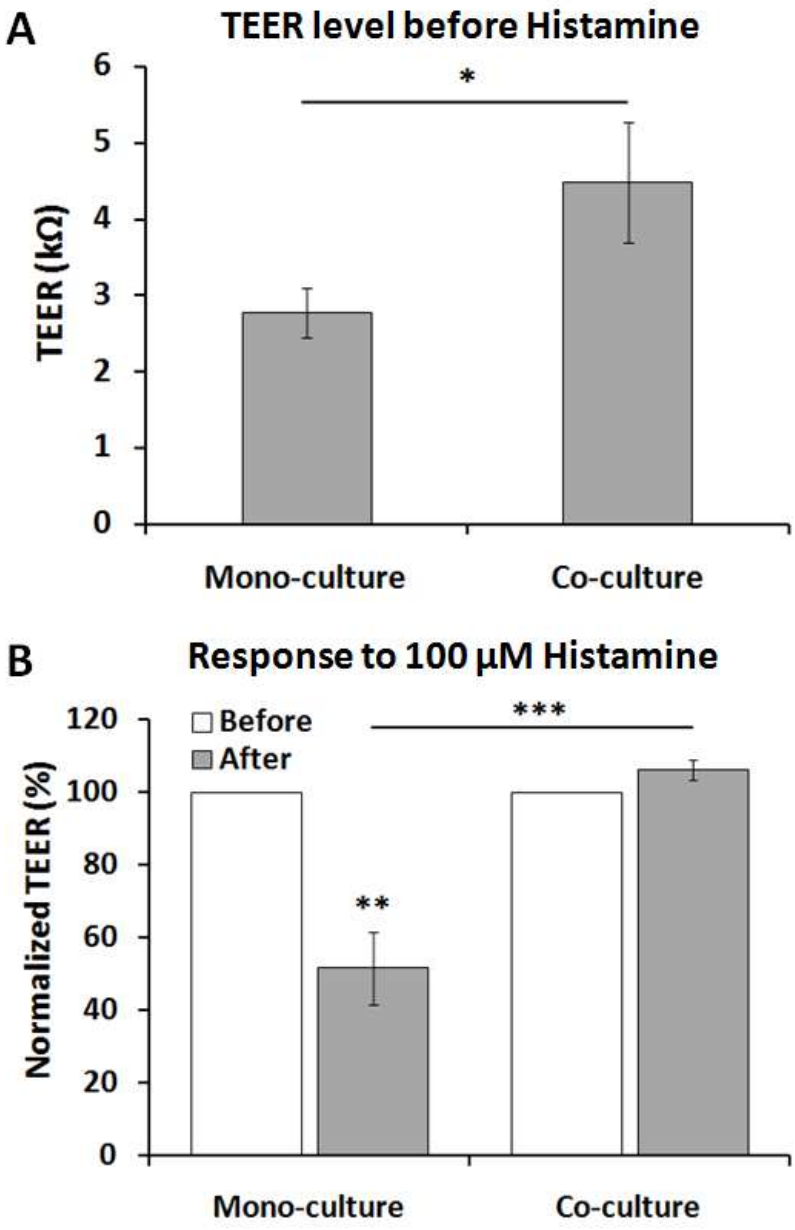


**Figure 35 Comparison of TEER change in the BBB chip during drug treatment.** (A) Comparing TEER values from monoculture vs. co-culture at DIV 4. (B) Percentage changes in normalized TEER ($TEER_{after}$ / $TEER_{before}$ × 100) after 100 µM histamine treatment. All values are plotted as a mean ± standard error of the mean. * $p < 0.05$, ** $p < 0.01$, *** $p < 0.001$.

Initially, the average TEER value of the co-culture condition was higher than that of the monoculture condition (2.77 ± 0.32 kΩ vs. 4.48 ± 0.79 kΩ, $n \geq 12$) (Figure 35A). Comparing the two cases during histamine treatment (Figure 35B), it is clear that the BBB formed through astrocyte-endothelial cell co-culture (106.37 ± 2.80%, $n = 12$) showed much higher resilient in its barrier function compared to the monoculture case (51.67 ± 9.97%, $n = 4$). As can be seen in Figure 35A, TEER value before histamine treatment shows a much higher value in the co-culture compared to the case of monoculture, as also indicated in Figure 21 where the barrier permeability for the co-culture case was significantly lower as measured by the dextran permeability assay. Moreover, in the case of co-culture, the TEER value did not drop even after histamine treatment, contrary to the case for monoculture. This stable BBB permeability with co-culture against histamine treatment could be related to the role of astrocytes in regulating histamine clearance or inactivation to avoid histaminergic neuronal activity by plasma membrane monoamine transporter (PMAT), organic cation transporter 3 (OCT3), and histamine N–methyltransferase (HNMT) [79-81].

### 5.3 Pharmacological test in the neuronal cell region on BBB chip

In recent studies, the physiology and pharmacology of signal transduction between brain endothelial cells that form the BBB and astrocyte that is involved in the regulation of BBB have been attracting attention in this module [57, 82]. Astrocytes are cells that support neurons and are also closely related to the function of neurons. However, there is little known relationship among neurons, astrocytes, and the BBB

because there is little information on the relationship between neuronal activity and the BBB formation in the brain.

Here, our microfluidic multi-channel BBB chip model has powerful features that closely mimic the *in vivo* structures of the BBB and a multitude of physiological functions. So we can investigate how neuronal activity can affect to tight junction formation between endothelial cells by separately culturing neuronal cells on the one side of the exposed membrane and endothelial cells on the other back side, still sharing the same interface to keep the realistic cell-cell interactions.

### *5.3.1 Neuronal activity-dependent BBB formation*

Two methods can be used to control neuronal activity. The first is an electrical stimulation to increase neuronal activity and the second is tetrodotoxin (TTX) drug treatment method to eliminate the neuronal activity. The electrical stimulation is a technique to stimulate the neural network of the brain through the cell membrane excitation by using high frequency of the electrical current. Thus, neuronal activity can be increased during the controlled electrical stimulation. On the other hand, TTX is known to decrease the neuronal activity in the neuronal network effectively. Since TTX is a sodium channel blocker, it binds to the voltage-gated sodium channel of the cell membrane and prevents the sodium ions from passing through the neurons, thereby suppressing the ignition of the action potential.

For multiple cultures, while primary endothelial cells are cultured on the pore membrane on the top channel side of the chip in Figure 36A, primary neurons and

astrocytes are cultured on the surface just below the pore membrane. Accordingly, the individual culture medium injected into each channel is used for different kinds of cultures optimized for each cell culture. While primary endothelial cells were maintained in IMDM containing 10% FBS, primary neurons and primary astrocytes were cultured in Neurobasal and DMEM (1:1) mixed medium containing 2% B27, 1 mM pyruvic acid, 63 ng/mL N-acetyl cysteine, 0.75 mM GlutaMax, SATO, 10 nM d-Biotin, 5 μg/mL insulin on the BBB chip.

To be specific for the procedure of multiple cultures (neurons, astrocytes, and endothelial cells), primary neurons and astrocytes were first seeded at a density of 300 cells/mm$^2$ on a 10% Matrigel-coated BBB chip. Both neuron and astrocyte cultures were first maintained in static culture conditions to allow the initial cells to attach to the pore membrane region in the microchannels of the chip. 24 hours after cell seeding, the neurons and astrocytes continued to culture in fresh growth medium for 6 days at a flow rate of 0.1 μL/min provided by the syringe pump. To seed the endothelial cells, the chip was turned over, and the bottom of the chip was placed on the upper side. Similar to ECM-coating conditions on the neuronal side, it was coated with 10% Matrigel, and primary endothelial cells were sown at the density of 150 cells/mm$^2$ on the backside channel of the chip. Endothelial cell cultures were kept static so that the cells could initially adhere to the pore membrane in the channel of the chip and during this time the neuronal culture was maintained in a static condition. After seeding endothelial cells, endothelial cells were cultured for 24 hours in a static condition, and every cell was grown for 3 days at a growth medium flow rate of 1.5 μL/min.

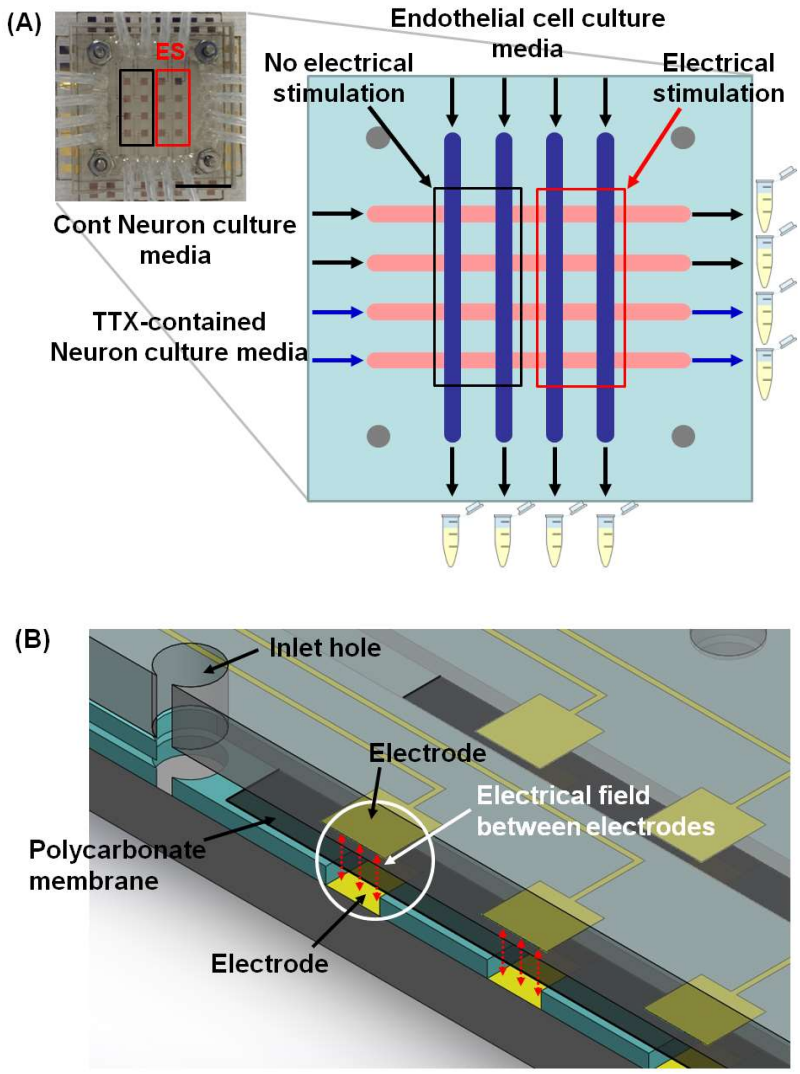


**Figure 36 Pharmacological combination test in the neuronal cell region on the co-culture BBB chip.** (A) Neuron and astrocyte are cultured on the backside of the membrane. And endothelial cells are cultured on the top side of the membrane. Pharmacological combination conditions with electrical stimulation (ES) and TTX in a multiple cultured BBB chip (Control, ES only, TTX only, and ES+TTX) (B) An illustration of the biphasic electrical field between two electrodes (top and bottom) in a chip.

Figure 36A shows that there are four possible combination tests in one chip. Each condition is a control, electrical stimulation (ES) condition to increase neural activity (400 μs pulse width, 20 Hz, ±3 V), TTX drug treatment condition to reduce neural activity, and both ES and TTX drug treatment. Figure 36B shows a biphasic electric field between the top and bottom electrodes placed at each site under ES conditions in the BBB chip. Under these four conditions, each cell is cultured in continuous perfusion culture (1.5 μL/min).

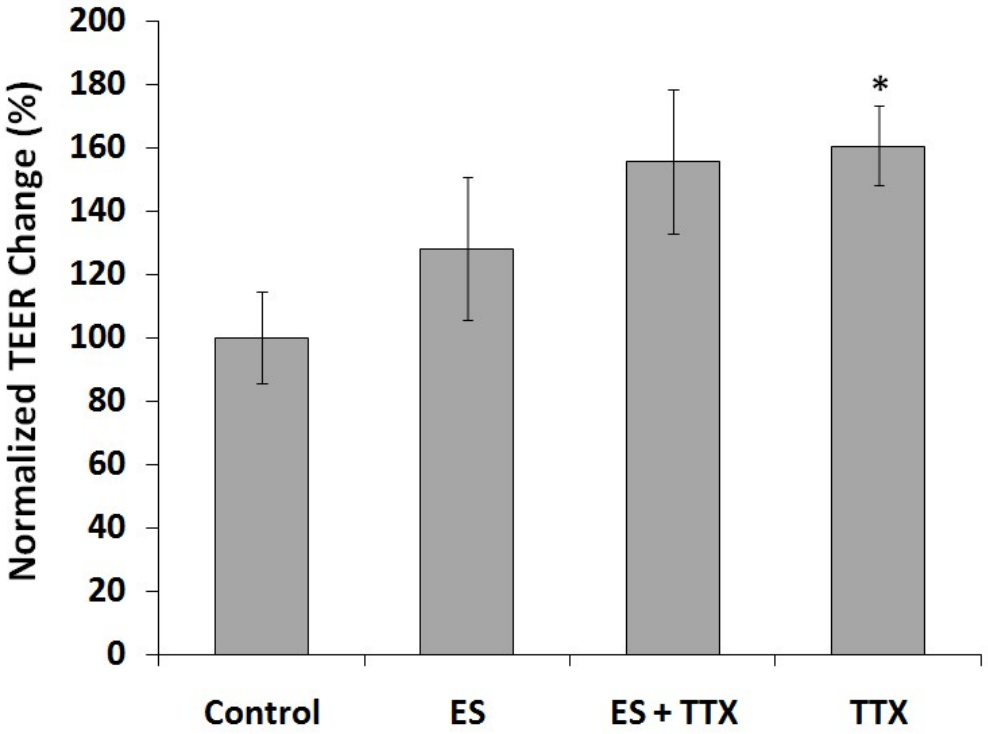


**Figure 37 Normalized TEER % change in four conditions of control, ES only, ES+TTX, and TTX only.** Pharmacological combination tests in the neuronal cell region were performed on the multiple cultured BBB chip. Percentage changes in normalized TEER ($TEER_{after}$ / $TEER_{before}$ × 100) after each treatment. All values are plotted as a mean ± standard error of the mean. * $p < 0.05$.

Figure 37 shows each normalized TEER change in four conditions of control, ES only, TTX only, and ES+TTX. The mean values of ES (128.27 ± 30.32 %, $n = 5$), ES + TTX (155.61 ± 36.39 %, $n = 4$), and TTX treatment conditions (160.59 ± 20.21 %, $n = 5$) were increased compared to the control group, but statistical significance was shown only in the TTX condition (* $p < 0.05$). This result demonstrates that the tight junction of endothelial cells was strengthened when the activity of neurons was decreased by TTX

under the condition of multiple cultures with neurons and astrocytes. As shown in Figure 35A, the tight junction of the endothelial cell was strengthened under the condition that only the astrocytes were co-cultured. However, in Figure 37, astrocyte is simultaneously cultured on the pore membrane in all the bottom channels where neurons are cultured. Although astrocytes are co-cultured with neurons in the control condition, astrocyte enhances tight junction formation only when neuron activity is weakened by TTX drug treatment as much as possible.

### *5.3.2 The BBB property in neuronal cellular interaction*

To quantitatively compare these differences, the TEER absolute values at each of these conditions are compared in Figure 38. In the endothelial monoculture, the TEER value was 2.77 ± 0.32 kΩ ($n$ = 15), while the barrier property of BBB was enhanced at 4.48 ± 0.79 kΩ ($n$ = 12) in co-culture with astrocyte. However, in the multiple culture condition including the neurons, the TEER value was 2.63 ± 0.24 kΩ ($n$ = 18), which showed a statistically significantly lower barrier property than the astrocyte co-cultured condition (# $p < 0.05$). In addition, it can be seen that this value is considerably similar to the TEER value in the endothelial monoculture condition.

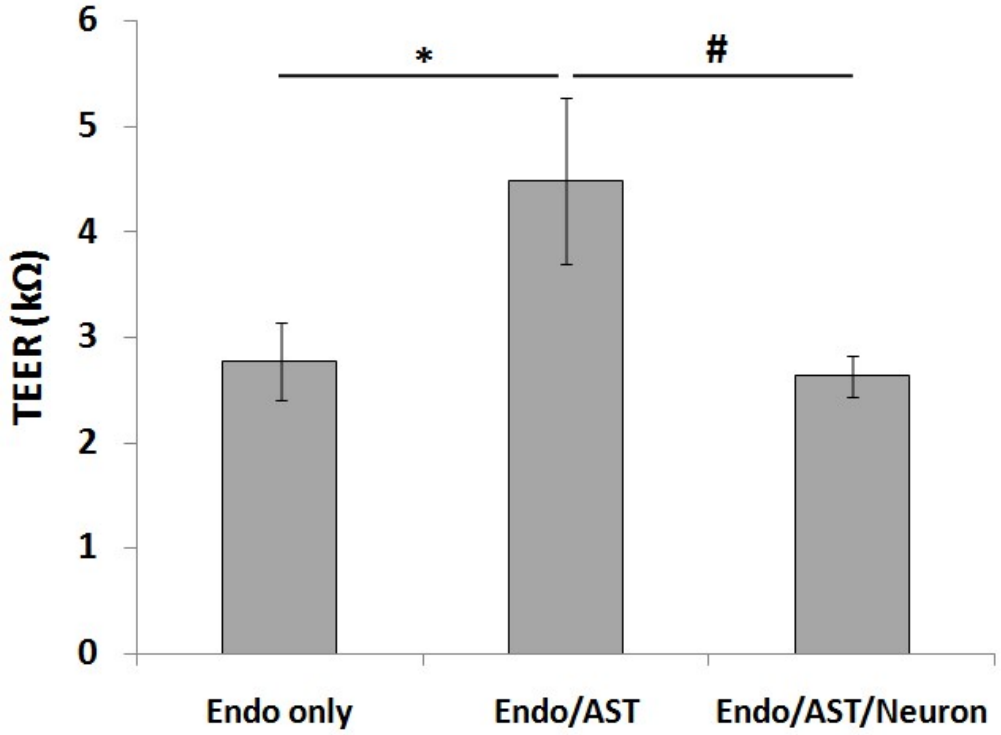


**Figure 38 Comparison of TEER change in the BBB chip among monoculture, astrocyte co-culture, and neuron & astrocyte multiple culture.** All values are plotted as a mean ± standard error of the mean. * $p < 0.05$, # $p < 0.05$.

## 5.4 Drug permeability test from brain blood vessel to brain tissue

So far, we have examined the drug response in the vascular channel on the BBB chip, the drug response in the brain tissue channel and the neurophysiological response. The next step is to investigate the extent to which the drug passes through the blood vessels and into the brain cells. We investigated the drug permeability of BBB chips by selecting three drugs with very low permeability (Atenolol, Sigma-Aldrich, MO), very high permeability (Propranolol, Sigma-Aldrich, MO) and medium permeability (Verapamil, Sigma-Aldrich, MO) among the drugs investigated by Nakagawa [83].

### *5.4.1 Toxicological screening*

Before the actual test chip, a cell viability test of the concentration of each drug was carried out using a typical well culture plate to examine the appropriate drug concentration. The same primary endothelial cells were cultured in a 96-well plate coated with Matrigel, and the concentration of the treated drug was diluted 10 times from 1 mM to 1 nM and 0 nM (control). For each cell viability, the fluorescent intensity in each well was measured with a plate reader after 4 hours of treatment with alamarBlue cell viability assay (Invitrogen, CA). As shown in Figure 39, three drugs of atenolol, verapamil, and propranolol were treated for 1 hour, 12 hours, and 24 hours, showing cell viability of 83% or more up to 100 μM in all three drugs. However, while atenolol treatment condition still showed cell viability of more than 89.62% at 1 mM ($n$ = 4), cell viability of verapamil and propranolol was very low at 6.40 % (1 hour), 2.38 % (12 hour), and 2.30 % (24 hour) in verapamil treatment condition ($n$ = 4) and 31.63 % (1

hour), 2.24 % (12 hour), and 2.21 % (24 hour) in propranolol treatment condition ($n$ = 4), respectively. Based on these results, it was found that the maximum stable concentration of each drug on the endothelial cells was 100 μM.

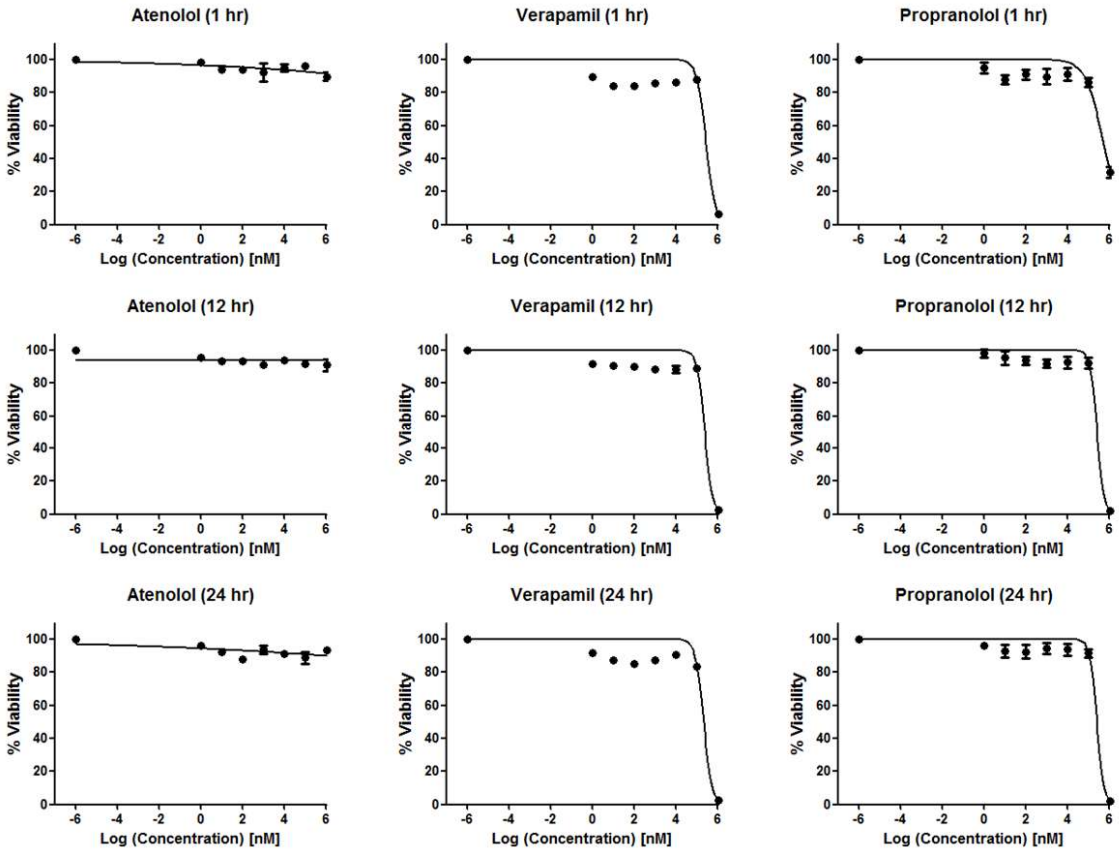


**Figure 39 Toxicological screening test of atenolol, verapamil, and propranolol.** Each cell viability tests under three individual drug treatment were carried out using with alamarBlue cell viability assay.

*5.4.2 Drug absorption testing in the microfluidic chip system*

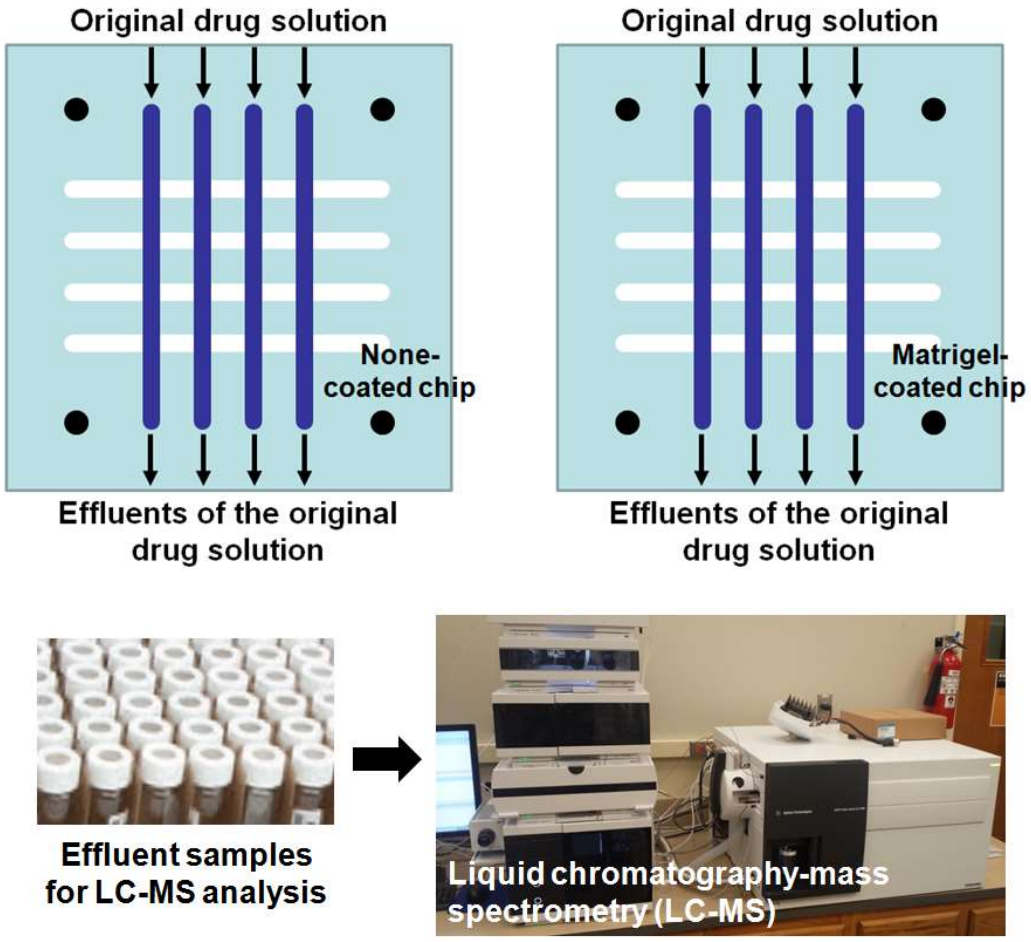


**Figure 40 The experimental procedure of drug absorption on the chip.** Each drug is passed from the inlet to the cell-free chip, and the effluent is collected from the outlet channel. All individual effluent samples collected from bare chips and Matrigel-coated chips are analyzed by a liquid chromatography-mass spectrometry to measure the concentration of each drug compound.

As a next step, an experiment was conducted to verify the extent to which each drug was absorbed into the chip, to ensure that each drug was capable of stable drug testing on the chip. As shown in Figure 40, each drug was passed from the inlet to the cell-free chip, and then the effluent was collected from the outlet channel and compared to the initial drug concentration. 1 μM of atenolol, verapamil, and propranolol was injected into bare chips and Matrigel-coated chips at a flow rate of 1.5 μL/min for 60 min, respectively. Each effluent collected was analyzed by liquid chromatography-mass spectrometry (LC-MS/MS, 6470 Triple Quad LC/MS, Agilent Technologies, CA).

In the drug absorption test, we measured the concentration of the original drug solution, the effluents passing through the none-coated chip and the Matrigel-coated chip to show the absorption ratio by calculating the remained drug concentration come from each chip compared to the concentration of each original drug solution.

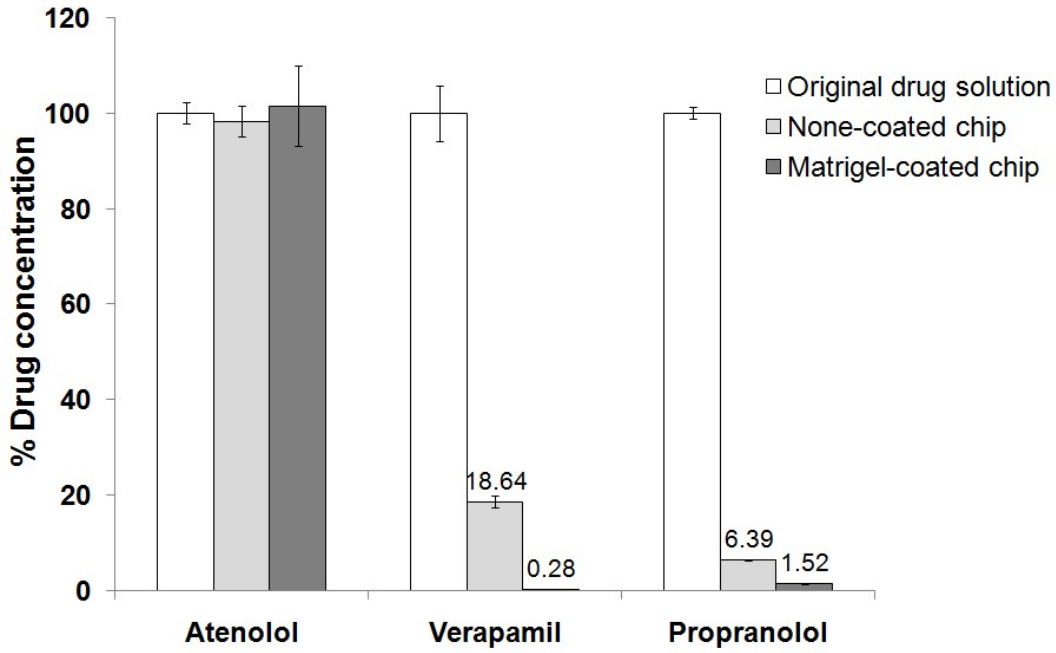


**Figure 41 Comparison of drug concentration change caused by drug absorption for 60 min in the BBB chip.** All values of drug concentrations are normalized compared to the original concentrations (1 μM of atenolol, verapamil, and propranolol). Each value is plotted as a mean ± standard error of the mean.

Figure 41 shows how the drug changes relative to the original concentration of each drug. In the case of atenolol, both the bare chip and the Matrigel-coated chip showed a level that was not different from the original drug concentration. However, propranolol showed 6.39 % in the bare chip and 1.52 % in the matrigel-coated chip, showing significantly severe drug absorption in the chip. In the case of verapamil, the remained concentration was 18.64 % in the bare chip, which was absorbed relatively less than verapamil but still significant amount of drug was absorbed into the chip. In addition, only 0.28 % of verapamil remained in the Matrigel-coated chip condition,

indicating that the drug was mostly absorbed by Matrigel and the fabricated chip. Thus, only atenolol, which has little drug absorption, is applicable to drug permeability test.

*5.4.3 Practical drug permeability test in co-culture BBB chip.*

| Purpose | Item | Day 0 | Day 1 | Day 2 | Day 3 | Day 4 | Day 5 | Day 6 | Day 7 | Day 8 | Day 9 | Day 10 |
|---|---|---|---|---|---|---|---|---|---|---|---|---|
| Preparation | ECM coating | X | | | | | | | | | | |
| Preparation | Washing | | X | | | | | | | | | |
| Process | Astrocyte loading into the bottom side of the BBB chip | | X | | | | | | | | | |
| Process | Astrocyte culture media flow 0.1 µL/min | | | X DIV1 | X DIV2 | X DIV3 | | | | | | |
| Process | Chip upside down | | | | | X | | | | | | |
| Process | Endothelial cell loading into the top side of the BBB chip | | | | | X | | | | | | |
| Process | Endothelial culture media flow 1.5 µL/min | | | | | | X DIV1 | X DIV2 | X DIV3 | X DIV4 | | |
| Process | Astrocyte culture media flow 1.5 µL/min | | | | | | X DIV4 | X DIV5 | X DIV6 | X DIV7 | | |
| Process | Change the effluent collection vial | | | | | | | | | X | | |
| Treatment | Drug<br>Flow: 1.5 µL/min for 60 min | | | | | | | | | X | | |
| Treatment | Change the effluent collection vial | | | | | | | | | X | | |
| Treatment | Washing | | | | | | | | | X | | |
| Measurement | Effluent<br>LC-MS analysis | | | | | | | | | | X | X |

**Figure 42 The procedure of drug permeability test with the astrocyte co-culture BBB chip.**

Finally, the drug permeability of atenolol was tested in astrocyte-endothelial co-culture conditions which showed the highest TEER level of the BBB chip. Figure 42 shows the detailed procedure of drug permeability test using the co-culture BBB chip.

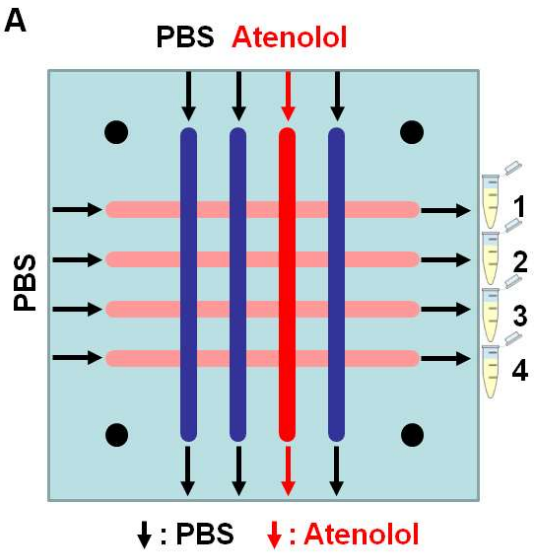


B

| | |
|---|---|
| $C_A$ | 2.49 μM |
| $V$ | 90 μL |
| $t$ | 3600 s |
| $A$ | 0.0081 $cm^2$ |
| $C_L$ | 100 μM |

C

| Drug type | Permeability $P_e$ ($\times 10^{-6}$ cm/s) | Test method |
|---|---|---|
| Atenolol | 0.25 | *In vivo* |
| | 2.49 | Transwell |
| | 2.33 | Co-cultured BBB chip |

**Figure 43 Drug permeability test of atenolol in the astrocyte co-culture BBB chip.** (A) An illustration of the drug permeability test of atenolol in the co-culture BBB chip. (B) Each experimental value for the calculation of permeability coefficient value. (C) Comparison of the calculated permeability coefficient average value of *in vivo* and *in vitro* conditions of transwell and our BBB chip.

As shown in Figure 43A, 100 μM of atenolol drug was injected at a rate of 1.5 μL/min for 60 min in the top channel and phosphate-buffered saline (PBS) solution was injected at the same rate in the bottom channel, which effluents were gathered to measure the concentration of the drug diffused from the top channel. The concentration of the collected effluent solution was determined by the liquid chromatography-mass spectrometry. The permeability coefficient was calculated by applying each concentration to Equation 2-4.

$$J_S = \frac{C_A V}{t} \quad (2)$$

$$P = \frac{J_S}{A C_L} \quad (3)$$

$$\frac{1}{P_e} = \frac{1}{P} - \frac{1}{P_b} \quad (4)$$

Where $J_s$ is the solute flux, $t$ is the assay time, $V$ is the volume of substance, $C_A$ is the concentration of drug solution in abluminal side, $P$ is the permeability coefficient, $A$ is the membrane area, $C_L$ is the concentration on the luminal (source) side, $P_b$ is the coefficient from a blank membrane, $P_e$ is the endothelial coefficient, respectively.

Figure 43B shows each value for the calculation using Equation 2-4. Figure 43C shows the calculated permeability coefficient average value ($P_e = 1.22 \pm 0.76 \times 10^{-6}$ cm/s, $n = 8$), which is higher than the permeability coefficient *in vivo* and lower than half of the average value ($2.49 \times 10^{-6}$ cm/s) in the transwell shown by Nakagawa [83].

## 5.5 Conclusion

In this chapter, we applied the BBB chip to confirm various pharmacological changes in vascular channels and brain tissue channels with various kinds of drugs, and also conducted experiments to verify how much a specific drug passes through the BBB.

First, our BBB chip showed that the permeability did not change due to the existence of astrocyte in the cerebral blood vessels, unlike the high permeability pattern of histamine in other blood vessels. This BBB chip has a very important physiological significance in that histamine administration showed very similar results to the *in vivo* environment where the BBB of the brain does not open. Secondly, we found that astrocyte does not play a sufficient role in the formation of the BBB under the condition of high activity of neurons through the experiment of treating TTX drug in the channel where brain tissue is cultured. Finally, when additional drugs were injected onto the BBB chip for the permeability test, verapamil and propranolol were found to be drugs absorbed into the chip itself, and atenolol, which is not absorbed into the chip, showed a considerably low permeability value against the BBB.

# 6. CONCLUSIONS AND FUTURE WORK

## 6.1 Conclusions

The advanced microfabricated organ-on-a-chip platforms developed in this study provided the capability to investigate neurophysiological phenomena under different neuronal stimulating conditions including various chemical, physical and drug candidate stimuli.

As a brain organ-on-a chip platform, the microelectrode array-based 3D CNS neural aggregate culture system was developed and successfully utilized to investigate how to promote myelin sheath formation with acute neural electrical stimulation, chemical stimulation with retinoic acid. Through primary neuron and astrocyte cultures, the platform allows for the formation of a large number of uniformly sized aggregates which are loaded into the array of culture chambers and the aggregate distance and number of aggregates in each culture chamber is measured at predetermined dimensions as well as it can be accurately controlled. Also, high-throughput screening for the myelin quantitation was achieved with our automated image analysis program.

As a neurovascular unit organ-on-a-chip platform, the 3D arrayed microfluidic blood-brain barrier chip with an integrated electrical sensor array platform was developed. It is capable of organ-level cell culturing and real-time electrical analysis with TEER measurement, followed by an investigation of drug permeability with various existing drug candidates for further study. We can measure TEER independently from 16 locations using a multi-electrode array, and enable continuous analysis of

barrier permeability, an important indicator of tight junction formation. The effect of endothelial-astrocyte co-culture, extracellular matrix, and shear stress on barrier permeability was successfully characterized by TEER measurements and dextran permeability assays.

A microfluidic brain inflammation analysis platform has been developed that allows for the initial investigation of monocyte infiltration into the CNS. Primary monocyte recruitment is characterized by CCL2 treatment by BBB in primary endothelial cells and not only monitors its behavior during inflammation of the brain to the BBB but also regulates the physiological immune response at the actual organ level. Primary monocyte infiltration in chips was monitored by CMFDA with monocyte green fluorescent cells and quantified by the cell counting process using the effluent from the subsequently developed platform. The physiological response in the organ chip of the monocyte infiltration phenomenon was successfully confirmed in CCL2 against the BBB of the CNS, demonstrating the capability of the platform as a medium-throughput screening tool.

As a drug screening platform, our microfluidic blood-brain barrier chip was verified by applying various drug compounds; histamine, tetrodotoxin, atenolol, verapamil, and propranolol. The developed BBB chip showed high biomimicry of *in vivo* environment when applying histamine on the neurovascular channels of the chip as the permeability is not changed due to the existence of astrocyte in the cerebral blood vessels similar to the *in vivo* environment where the BBB of the brain does not open. When administrating tetrodotoxin on the neuronal side channels on the chip, we

observed a biological phenomenon that astrocyte can sufficiently play a critical role in the tight junction formation of the BBB in the only case of that neuronal activity is suppressed when neurons, astrocytes, and endothelial cells are simultaneously cultured in the BBB chip. In the drug permeability test on the BBB chip, moreover, although applying verapamil and propranolol to the BBB chip shows drug absorption into the chip itself not suitable for drug test, we showed that atenolol has a very low drug permeability value against the BBB as shown in *in vivo* environment, which is relatively lower than the permeability value of the transwell system.

Our developed microfluidic platforms better mimic *in vivo* brain environment conditions and provide powerful high throughput examination of drug candidates and their toxicity by more accurately predicting modulation of drug candidates to find a cure against various brain disorders. Such platforms are to be used as an analysis and screening tool during preclinical drug development stages.

## 6.2 Future Work

Although we have verified how certain drugs exhibit pharmacological and physiological phenomena in the BBB environment and we have successfully investigated how much of the drug has passed through the BBB, some drugs have still been unable to investigate this drug permeability. Therefore, it is necessary not only to study the characteristics of the drug itself, which is difficult to investigate the drug permeability but also to modify the experimental condition to conduct the permeability test in accordance with the organ-on-chip environmental condition.

Ultimately, however, as an alternative to conventional cell culture and animal models, organ-on-chips may alter many areas of basic research and drug development. They can be applied to the study of molecular mechanisms concerning the interaction of stimuli with the body, such as organ development and diseases, organ-organ coupling and drugs, environmental factors, consumer products and medical devices. The basic questions to address include how microenvironmental cues regulate cell differentiation, tissue development, disease progression and how different types of immune cells and cytokines contribute to toxicity, inflammation, infection and multiple organ dysfunctions. Using our organ-on-chip technology, when combined with patient-specific primary cells, iPS cells, or when using gene-editing techniques to introduce disease-causing mutations, a personalized medicine model can be developed.

REFERENCES

[1] D. E. Goodkin, D. Hertsgaard, and R. A. Rudick, "Exacerbation rates and adherence to disease type in a prospectively followed-up population with multiple sclerosis. Implications for clinical trials," (in eng), *Arch Neurol,* vol. 46, no. 10, pp. 1107-12, Oct 1989.

[2] R. P. Kinkel and D. E. Goodkin, "Immunotherapy for Multiple Sclerosis," *Clinical Immunotherapeutics,* vol. 1, no. 2, pp. 117-134, 1994/02/01 1994.

[3] B. W. van Oosten, L. Truyen, F. Barkhof, and C. H. Polman, "Multiple sclerosis therapy. A practical guide," (in eng), *Drugs,* vol. 49, no. 2, pp. 200-12, Feb 1995.

[4] R. Martin and H. F. McFarland, "Immunological aspects of experimental allergic encephalomyelitis and multiple sclerosis," (in eng), *Crit Rev Clin Lab Sci,* vol. 32, no. 2, pp. 121-82, 1995.

[5] A. Huntley and E. Ernst, "Complementary and alternative therapies for treating multiple sclerosis symptoms: a systematic review," (in eng), *Complement Ther Med,* vol. 8, no. 2, pp. 97-105, Jun 2000.

[6] D. Barnes, P. M. Munro, B. D. Youl, J. W. Prineas, and W. I. McDonald, "The longstanding MS lesion. A quantitative MRI and electron microscopic study," (in eng), *Brain,* vol. 114 ( Pt 3), pp. 1271-80, Jun 1991.

[7] N. A. Losseff *et al.*, "Spinal cord atrophy and disability in multiple sclerosis. A new reproducible and sensitive MRI method with potential to monitor disease progression," (in eng), *Brain,* vol. 119 ( Pt 3), pp. 701-8, Jun 1996.

[8] W. Bruck *et al.*, "Monocyte/macrophage differentiation in early multiple sclerosis lesions," (in eng), *Ann Neurol,* vol. 38, no. 5, pp. 788-96, Nov 1995.

[9] M. A. van Walderveen *et al.*, "Histopathologic correlate of hypointense lesions on T1-weighted spin-echo MRI in multiple sclerosis," (in eng), *Neurology,* vol. 50, no. 5, pp. 1282-8, May 1998.

[10] B. Ferguson, M. K. Matyszak, M. M. Esiri, and V. H. Perry, "Axonal damage in acute multiple sclerosis lesions," (in eng), *Brain,* vol. 120 ( Pt 3), pp. 393-9, Mar 1997.

[11] B. D. Trapp, J. Peterson, R. M. Ransohoff, R. Rudick, S. Mork, and L. Bo, "Axonal transection in the lesions of multiple sclerosis," (in eng), *N Engl J Med,* vol. 338, no. 5, pp. 278-85, Jan 29 1998.

[12] C. A. Davie, G. J. Barker, A. J. Thompson, P. S. Tofts, W. I. McDonald, and D. H. Miller, "1H magnetic resonance spectroscopy of chronic cerebral white matter lesions and normal appearing white matter in multiple sclerosis," (in eng), *J Neurol Neurosurg Psychiatry,* vol. 63, no. 6, pp. 736-42, Dec 1997.

[13] D. J. Begley, "9 - Efflux Mechanisms in the Central Nervous System: A Powerful Influence on Drug Distribution within the Brain," in *Blood-Spinal Cord and Brain Barriers in Health and Disease*San Diego: Academic Press, 2004, pp. 83-97.

[14] J. Correale and A. Villa, "The blood–brain-barrier in multiple sclerosis: Functional roles and therapeutic targeting," *Autoimmunity,* vol. 40, no. 2, pp. 148-160, 2007/01/01 2007.

[15] A. Chakraborty, N. M. de Wit, W. M. van der Flier, and H. E. de Vries, "The blood brain barrier in Alzheimer's disease," *Vascular Pharmacology,* vol. 89, no. Supplement C, pp. 12-18, 2017/02/01/ 2017.

[16] R. A. Rudick and R. M. Ransohoff, "Cytokine secretion by multiple sclerosis monocytes. Relationship to disease activity," (in eng), *Arch Neurol,* vol. 49, no. 3, pp. 265-70, Mar 1992.

[17] S. L. Hauser, A. K. Bhan, F. Gilles, M. Kemp, C. Kerr, and H. L. Weiner, "Immunohistochemical analysis of the cellular infiltrate in multiple sclerosis lesions," (in eng), *Ann Neurol,* vol. 19, no. 6, pp. 578-87, Jun 1986.

[18] C. W. Adams, R. N. Poston, and S. J. Buk, "Pathology, histochemistry and immunocytochemistry of lesions in acute multiple sclerosis," (in eng), *J Neurol Sci,* vol. 92, no. 2-3, pp. 291-306, Sep 1989.

[19] E. A. Lidington, A. M. McCormack, M. H. Yacoub, and M. L. Rose, "The effects of monocytes on the transendothelial migration of T lymphocytes," (in eng), *Immunology,* vol. 94, no. 2, pp. 221-7, Jun 1998.

[20] L. A. Low and D. A. Tagle, "Tissue chips - innovative tools for drug development and disease modeling," (in eng), *Lab Chip,* vol. 17, no. 18, pp. 3026-3036, Sep 12 2017.

[21] E. W. Esch, A. Bahinski, and D. Huh, "Organs-on-chips at the frontiers of drug discovery," (in eng), *Nat Rev Drug Discov,* vol. 14, no. 4, pp. 248-60, Apr 2015.

[22] H. Olson *et al.*, "Concordance of the toxicity of pharmaceuticals in humans and in animals," (in eng), *Regul Toxicol Pharmacol,* vol. 32, no. 1, pp. 56-67, Aug 2000.

[23] B. A. Barres and M. C. Raff, "Proliferation of oligodendrocyte precursor cells depends on electrical activity in axons," (in eng), *Nature,* vol. 361, no. 6409, pp. 258-60, Jan 21 1993.

[24] L. Gyllensten and T. Malmfors, "Myelinization of the optic nerve and its dependence on visual function--a quantitative investigation in mice," *J Embryol Exp Morphol,* vol. 11, pp. 255-66, Mar 1963.

[25] I. H. Yang *et al.*, "Axon Myelination and Electrical Stimulation in a Microfluidic, Compartmentalized Cell Culture Platform," *NeuroMolecular Medicine,* journal article vol. 14, no. 2, pp. 112-118, 2012.

[26] R. J. M. Franklin *et al.*, "Retinoid X receptor gamma signaling accelerates CNS remyelination," *Nature Neuroscience,* 2011.

[27] T. Y. Zhang and C. Y. Suen, "A fast parallel algorithm for thinning digital patterns," *Commun. ACM,* vol. 27, no. 3, pp. 236-239, 1984.

[28] S. H. Jeong, S. B. Jun, J. K. Song, and S. J. Kim, "Activity-dependent neuronal cell migration induced by electrical stimulation," (in eng), *Med Biol Eng Comput,* vol. 47, no. 1, pp. 93-9, Jan 2009.

[29] D. Huh, B. D. Matthews, A. Mammoto, M. Montoya-Zavala, H. Y. Hsin, and D. E. Ingber, "Reconstituting Organ-Level Lung Functions on a Chip," *Science,* vol. 328, no. 5986, pp. 1662-1668, 2010.

[30] E. W. Esch, A. Bahinski, and D. Huh, "Organs-on-chips at the frontiers of drug discovery," *Nat Rev Drug Discov,* Perspectives vol. 14, no. 4, pp. 248-260, 04//print 2015.

[31] M. N. Pangalos, L. E. Schechter, and O. Hurko, "Drug development for CNS disorders: strategies for balancing risk and reducing attrition," *Nat Rev Drug Discov,* 10.1038/nrd2094 vol. 6, no. 7, pp. 521-532, 07//print 2007.

[32] S. M. Stamatovic, R. F. Keep, and A. V. Andjelkovic, "Brain Endothelial Cell-Cell Junctions: How to “Open” the Blood Brain Barrier," *Current Neuropharmacology,* vol. 6, no. 3, pp. 179-192, 10/05/received

[33] W. Loscher and H. Potschka, "Drug resistance in brain diseases and the role of drug efflux transporters," (in eng), *Nat Rev Neurosci,* vol. 6, no. 8, pp. 591-602, Aug 2005.

[34] V. Berezowski *et al.*, "Transport screening of drug cocktails through an in vitro blood-brain barrier: is it a good strategy for increasing the throughput of the discovery pipeline?," (in eng), *Pharm Res,* vol. 21, no. 5, pp. 756-60, May 2004.

[35] C. A. Palmiotti *et al.*, "In vitro cerebrovascular modeling in the 21st century: current and prospective technologies," (in eng), *Pharm Res,* vol. 31, no. 12, pp. 3229-50, Dec 2014.

[36] L. Cucullo, M. Hossain, V. Puvenna, N. Marchi, and D. Janigro, "The role of shear stress in Blood-Brain Barrier endothelial physiology," *BMC neuroscience,* vol. 12, no. 1, p. 40, 2011.

[37] N. Resnick *et al.*, "Fluid shear stress and the vascular endothelium: for better and for worse," *Progress in Biophysics and Molecular Biology,* vol. 81, no. 3, pp. 177-199, 4// 2003.

[38] O. C. Colgan *et al.*, "Regulation of bovine brain microvascular endothelial tight junction assembly and barrier function by laminar shear stress," (in eng), *Am J Physiol Heart Circ Physiol,* vol. 292, no. 6, pp. H3190-7, Jun 2007.

[39] S. Santaguida, D. Janigro, M. Hossain, E. Oby, E. Rapp, and L. Cucullo, "Side by side comparison between dynamic versus static models of blood–brain barrier in vitro: a permeability study," *Brain research,* vol. 1109, no. 1, pp. 1-13, 2006.

[40] L. Cucullo *et al.*, "A new dynamic in vitro model for the multidimensional study of astrocyte–endothelial cell interactions at the blood–brain barrier," *Brain Research,* vol. 951, no. 2, pp. 243-254, 10/4/ 2002.

[41] L. Cucullo, M. Hossain, W. Tierney, and D. Janigro, "A new dynamic in vitro modular capillaries-venules modular system: Cerebrovascular physiology in a box," *BMC Neuroscience,* journal article vol. 14, no. 1, p. 18, 2013.

[42] M. W. van der Helm, A. D. van der Meer, J. C. T. Eijkel, A. van den Berg, and L. I. Segerink, "Microfluidic organ-on-chip technology for blood-brain barrier research," *Tissue Barriers,* vol. 4, no. 1, p. e1142493, 2016/01/02 2016.

[43] B. Prabhakarpandian *et al.*, "SyM-BBB: a microfluidic blood brain barrier model," *Lab on a Chip,* 10.1039/C2LC41208J vol. 13, no. 6, pp. 1093-1101, 2013.

[44] J. Yeon, D. Na, K. Choi, S.-W. Ryu, C. Choi, and J.-K. Park, "Reliable permeability assay system in a microfluidic device mimicking cerebral vasculatures," (in English), *Biomedical Microdevices,* vol. 14, no. 6, pp. 1141-1148, 2012/12/01 2012.

[45] A. K. H. Achyuta *et al.*, "A modular approach to create a neurovascular unit-on-a-chip," *Lab on a Chip,* 10.1039/C2LC41033H vol. 13, no. 4, pp. 542-553, 2013.

[46] R. Booth and H. Kim, "Characterization of a microfluidic in vitro model of the blood-brain barrier (muBBB)," (in eng), *Lab Chip,* vol. 12, no. 10, pp. 1784-92, Apr 24 2012.

[47] A. G. Koutsiaris *et al.*, "Volume flow and wall shear stress quantification in the human conjunctival capillaries and post-capillary venules in vivo," (in eng), *Biorheology,* vol. 44, no. 5-6, pp. 375-86, 2007.

[48] S. Y. Desai *et al.*, "Mechanisms of endothelial survival under shear stress," (in eng), *Endothelium,* vol. 9, no. 2, pp. 89-102, 2002.

[49] L. Cucullo, N. Marchi, M. Hossain, and D. Janigro, "A dynamic in vitro BBB model for the study of immune cell trafficking into the central nervous system," (in eng), *J Cereb Blood Flow Metab,* vol. 31, no. 2, pp. 767-77, Feb 2011.

[50] L. Griep *et al.*, "BBB on chip: microfluidic platform to mechanically and biochemically modulate blood-brain barrier function," *Biomedical microdevices,* vol. 15, no. 1, pp. 145-150, 2013.

[51] J. A. Brown *et al.*, "Recreating blood-brain barrier physiology and structure on chip: A novel neurovascular microfluidic bioreactor," *Biomicrofluidics,* vol. 9, no. 5, p. 054124, 10/26

[52] S. Kim, A. J. Steelman, H. Koito, and J. Li, "Astrocytes promote TNF-mediated toxicity to oligodendrocyte precursors," (in Eng), *J Neurochem,* vol. 116, no. 1, pp. 53-66, Jan 2011.

[53] B. V. Sapatino, C. J. Welsh, C. A. Smith, B. F. Bebo, and D. S. Linthicum, "Cloned mouse cerebrovascular endothelial cells that maintain their differentiation markers for factor VIII, low density lipoprotein, and angiotensin-converting enzyme," (in Eng), *In Vitro Cell Dev Biol Anim,* vol. 29A, no. 12, pp. 923-8, Dec 1993.

[54] C. Pan, C. Kumar, S. Bohl, U. Klingmueller, and M. Mann, "Comparative proteomic phenotyping of cell lines and primary cells to assess preservation of cell type-specific functions," (in eng), *Mol Cell Proteomics,* vol. 8, no. 3, pp. 443-50, Mar 2009.

[55] E. A. Lidington, D. L. Moyes, A. M. McCormack, and M. L. Rose, "A comparison of primary endothelial cells and endothelial cell lines for studies of immune interactions," (in eng), *Transpl Immunol,* vol. 7, no. 4, pp. 239-46, Dec 1999.

[56] F. R. Walter *et al.*, "A versatile lab-on-a-chip tool for modeling biological barriers," *Sensors and Actuators B: Chemical,* vol. 222, pp. 1209-1219, 1// 2016.

[57] N. J. Abbott, L. Ronnback, and E. Hansson, "Astrocyte-endothelial interactions at the blood-brain barrier," *Nat Rev Neurosci,* 10.1038/nrn1824 vol. 7, no. 1, pp. 41-53, 01//print 2006.

[58] G. Pantaleo and A. Harari, "Functional signatures in antiviral T-cell immunity for monitoring virus-associated diseases," (in eng), *Nat Rev Immunol,* vol. 6, no. 5, pp. 417-23, May 2006.

[59] C. Auffray *et al.*, "Monitoring of blood vessels and tissues by a population of monocytes with patrolling behavior," (in eng), *Science,* vol. 317, no. 5838, pp. 666-70, Aug 03 2007.

[60] J. J. O'Shea, C. A. Hunter, and R. N. Germain, "T cell heterogeneity: firmly fixed, predominantly plastic or merely malleable?," (in eng), *Nat Immunol,* vol. 9, no. 5, pp. 450-3, May 2008.

[61] R. M. Ransohoff, "Immunology: In the beginning," (in eng), *Nature,* vol. 462, no. 7269, pp. 41-2, Nov 05 2009.

[62] S. Man, B. Tucky, N. Bagheri, X. Li, R. Kochar, and R. M. Ransohoff, "alpha4 Integrin/FN-CS1 mediated leukocyte adhesion to brain microvascular endothelial cells under flow conditions," (in eng), *J Neuroimmunol,* vol. 210, no. 1-2, pp. 92-9, May 29 2009.

[63] R. Chui and K. Dorovini-Zis, "Regulation of CCL2 and CCL3 expression in human brain endothelial cells by cytokines and lipopolysaccharide," (in eng), *J Neuroinflammation,* vol. 7, p. 1, Jan 04 2010.

[64] R. J. Fox *et al.*, "Chemokine receptors as biomarkers in multiple sclerosis," (in eng), *Dis Markers,* vol. 22, no. 4, pp. 227-33, 2006.

[65] I. F. Charo and R. M. Ransohoff, "The many roles of chemokines and chemokine receptors in inflammation," (in eng), *N Engl J Med,* vol. 354, no. 6, pp. 610-21, Feb 09 2006.

[66] N. Li Jeon, H. Baskaran, S. K. Dertinger, G. M. Whitesides, L. Van de Water, and M. Toner, "Neutrophil chemotaxis in linear and complex gradients of interleukin-8 formed in a microfabricated device," (in eng), *Nat Biotechnol,* vol. 20, no. 8, pp. 826-30, Aug 2002.

[67] C. C. Peng, W. H. Liao, Y. H. Chen, C. Y. Wu, and Y. C. Tung, "A microfluidic cell culture array with various oxygen tensions," (in eng), *Lab Chip,* vol. 13, no. 16, pp. 3239-45, Aug 21 2013.

[68] S. Chen and L. P. Lee, "Non-invasive microfluidic gap junction assay," (in eng), *Integr Biol (Camb),* vol. 2, no. 2-3, pp. 130-8, Mar 2010.

[69] H. J. Kim, D. Huh, G. Hamilton, and D. E. Ingber, "Human gut-on-a-chip inhabited by microbial flora that experiences intestinal peristalsis-like motions and flow," (in eng), *Lab Chip,* vol. 12, no. 12, pp. 2165-74, Jun 21 2012.

[70] S. Jeong, Kim, S., Buonocore, J., Park, J., Welsh, C. J., Li, J., Han, A., "A three–dimensional (3D) arrayed microfluidic blood–brain barrier model with integrated electrical sensor array," *IEEE Trans Biomed Eng,* 2018.

[71] M. Anguiano *et al.*, "Characterization of three-dimensional cancer cell migration in mixed collagen-Matrigel scaffolds using microfluidics and image analysis," (in eng), *PLoS One,* vol. 12, no. 2, p. e0171417, 2017.

[72] A. E. Proudfoot *et al.*, "Glycosaminoglycan binding and oligomerization are essential for the in vivo activity of certain chemokines," (in eng), *Proc Natl Acad Sci U S A,* vol. 100, no. 4, pp. 1885-90, Feb 18 2003.

[73] S. J. Allen, S. E. Crown, and T. M. Handel, "Chemokine: receptor structure, interactions, and antagonism," (in eng), *Annu Rev Immunol,* vol. 25, pp. 787-820, 2007.

[74] R. T. Palframan *et al.*, "Inflammatory chemokine transport and presentation in HEV: a remote control mechanism for monocyte recruitment to lymph nodes in inflamed tissues," (in eng), *J Exp Med,* vol. 194, no. 9, pp. 1361-73, Nov 05 2001.

[75] M. Pruenster *et al.*, "The Duffy antigen receptor for chemokines transports chemokines and supports their promigratory activity," (in eng), *Nat Immunol,* vol. 10, no. 1, pp. 101-8, Jan 2009.

[76] M. N. Pangalos, L. E. Schechter, and O. Hurko, "Drug development for CNS disorders: strategies for balancing risk and reducing attrition," (in eng), *Nat Rev Drug Discov,* vol. 6, no. 7, pp. 521-32, Jul 2007.

[77] I. Kola and J. Landis, "Can the pharmaceutical industry reduce attrition rates?," (in eng), *Nat Rev Drug Discov,* vol. 3, no. 8, pp. 711-5, Aug 2004.

[78] E. Dejana, "Endothelial cell-cell junctions: happy together," *Nat Rev Mol Cell Biol,* 10.1038/nrm1357 vol. 5, no. 4, pp. 261-270, 04//print 2004.

[79] T. Yoshikawa *et al.*, "Molecular mechanism of histamine clearance by primary human astrocytes," (in eng), *Glia,* vol. 61, no. 6, pp. 905-16, Jun 2013.

[80] J. C. Schwartz, J. M. Arrang, M. Garbarg, H. Pollard, and M. Ruat, "Histaminergic transmission in the mammalian brain," (in eng), *Physiol Rev,* vol. 71, no. 1, pp. 1-51, Jan 1991.

[81] K. Perdan-Pirkmajer, S. Pirkmajer, A. Raztresen, and M. Krzan, "Regional characteristics of histamine uptake into neonatal rat astrocytes," (in eng), *Neurochem Res,* vol. 38, no. 7, pp. 1348-59, Jul 2013.

[82] R. Cabezas *et al.*, "Astrocytic modulation of blood brain barrier: perspectives on Parkinson's disease," *Frontiers in Cellular Neuroscience,* vol. 8, p. 211, 08/04

[83] S. Nakagawa *et al.*, "A new blood-brain barrier model using primary rat brain endothelial cells, pericytes and astrocytes," (in eng), *Neurochem Int,* vol. 54, no. 3-4, pp. 253-63, Mar-Apr 2009.

APPENDIX A

MASK DESIGN

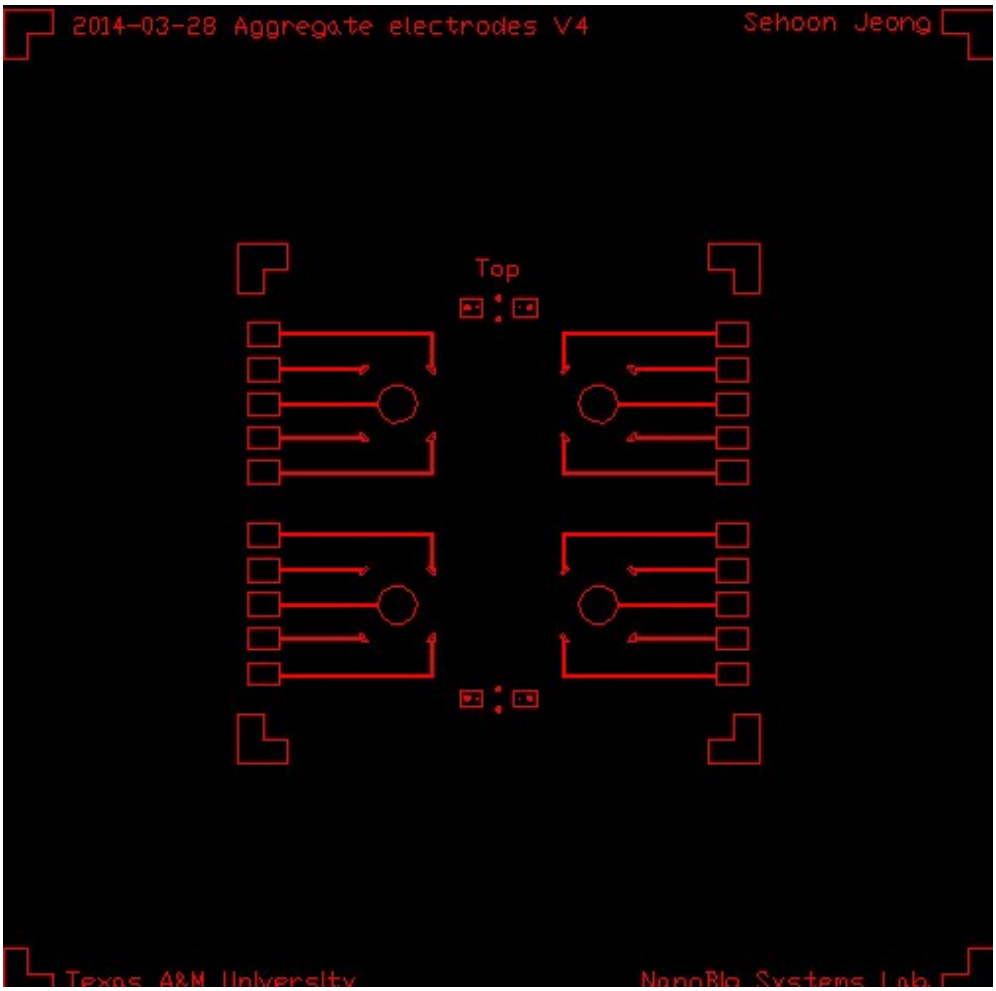


**Figure 44 Electrical stimulation-microelectrode array for 3D neuron aggregate culture system**

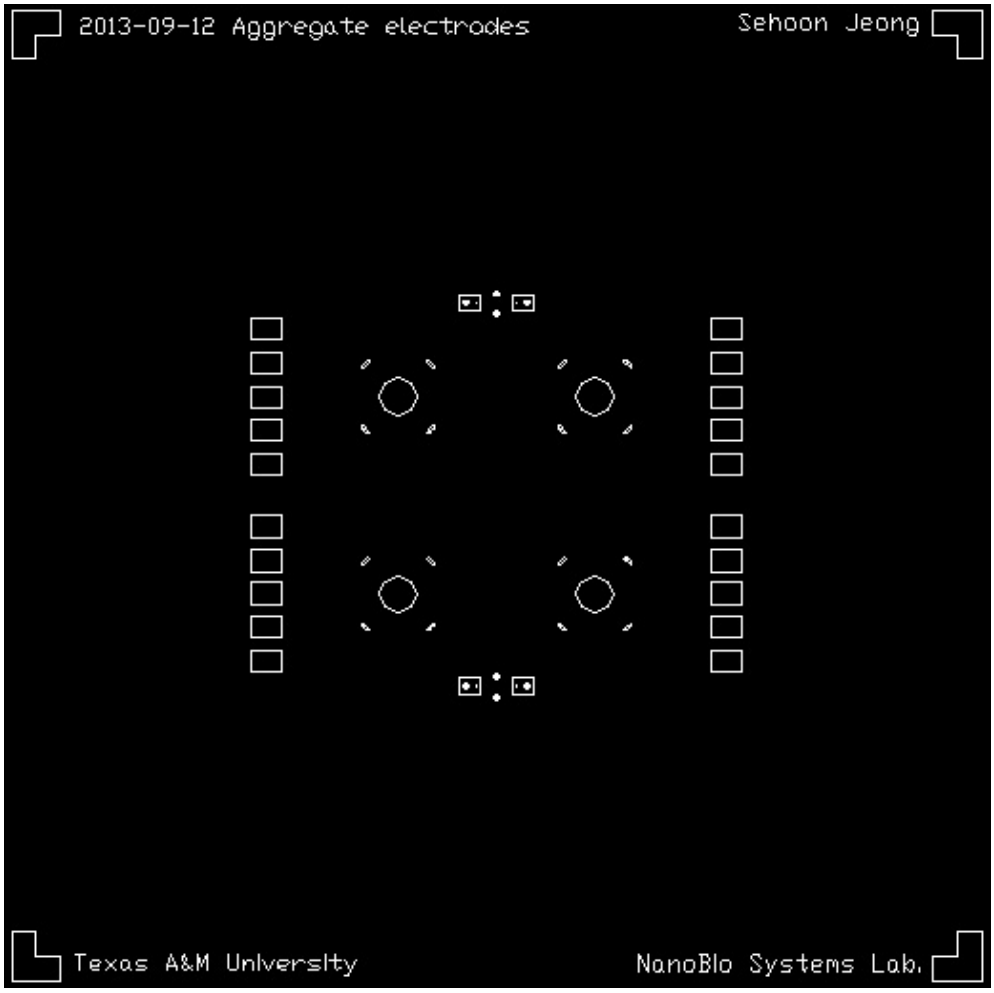


**Figure 45 Electrical stimulation-microelectrode array site opening for 3D neuron aggregate culture system**

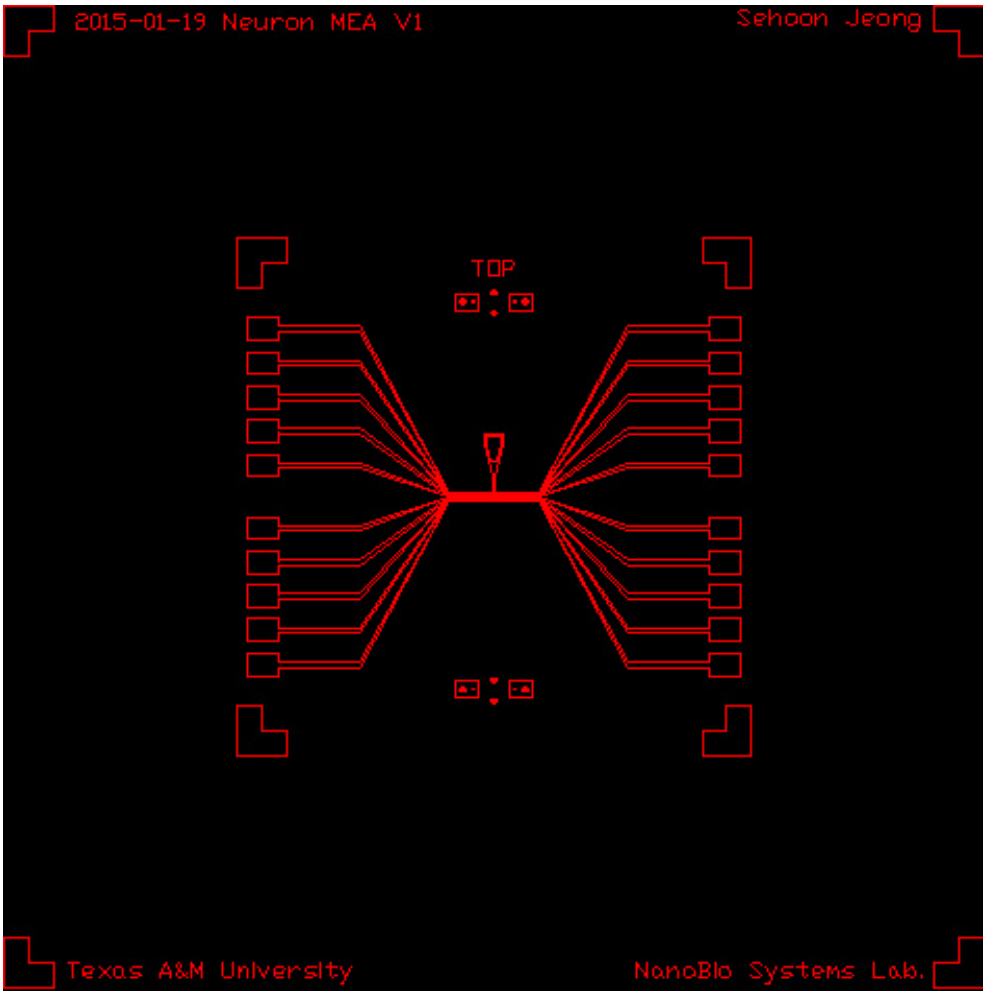


**Figure 46 Neuron signal recording microelectrode array**

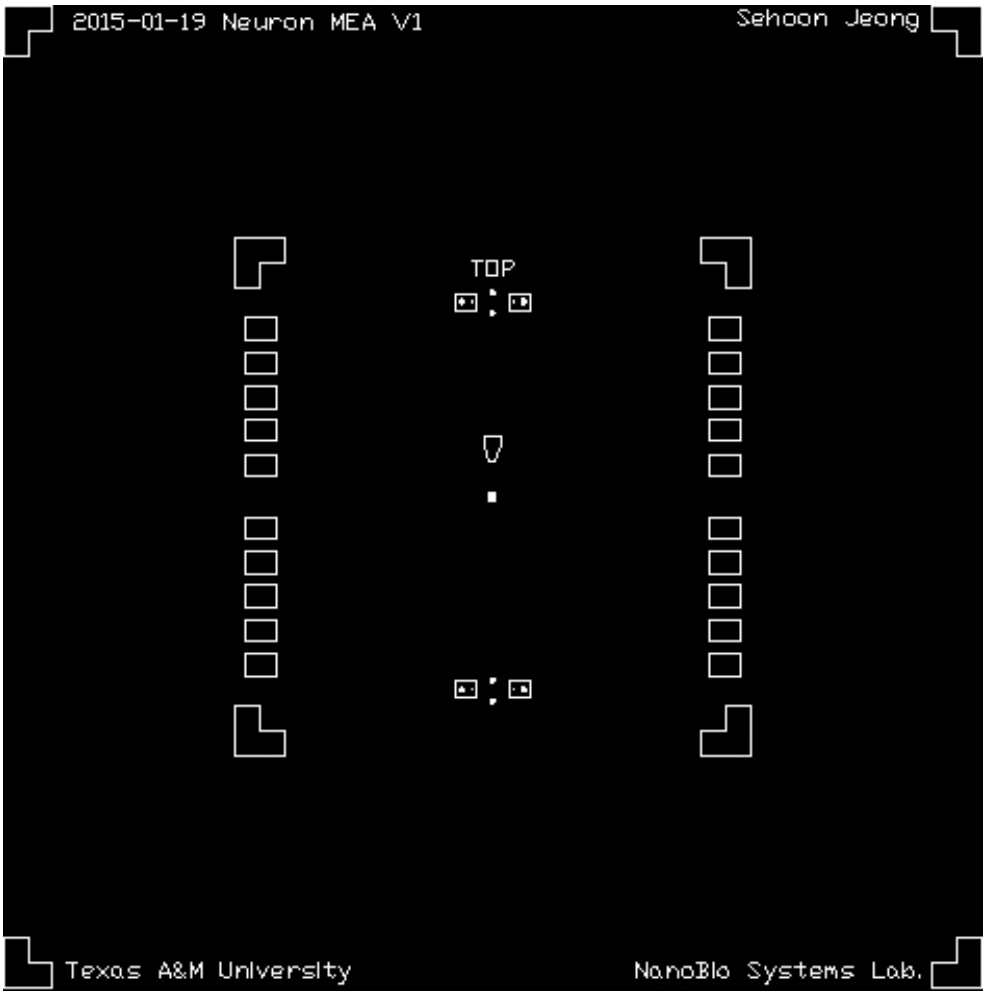


**Figure 47 Neuron signal recording microelectrode array site opening**

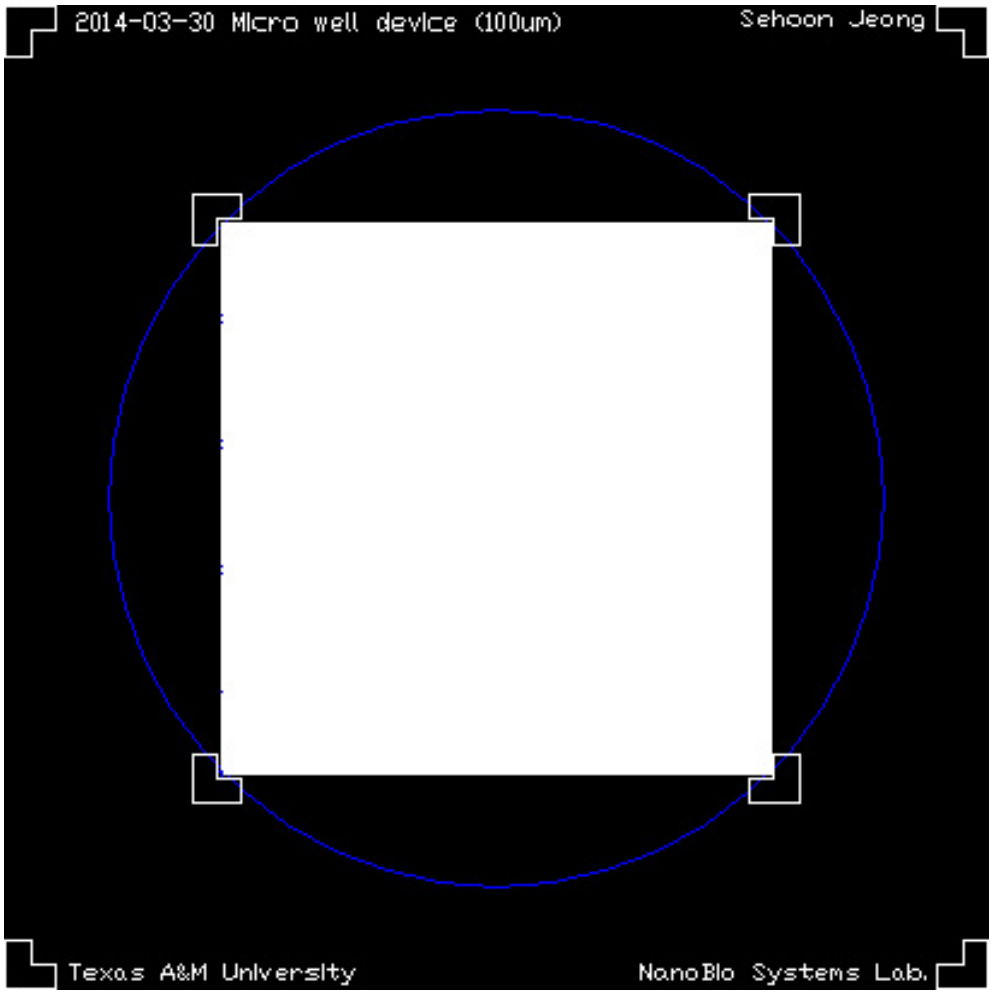


**Figure 48 Microwell array for Ø100 µm sized neural aggregate**

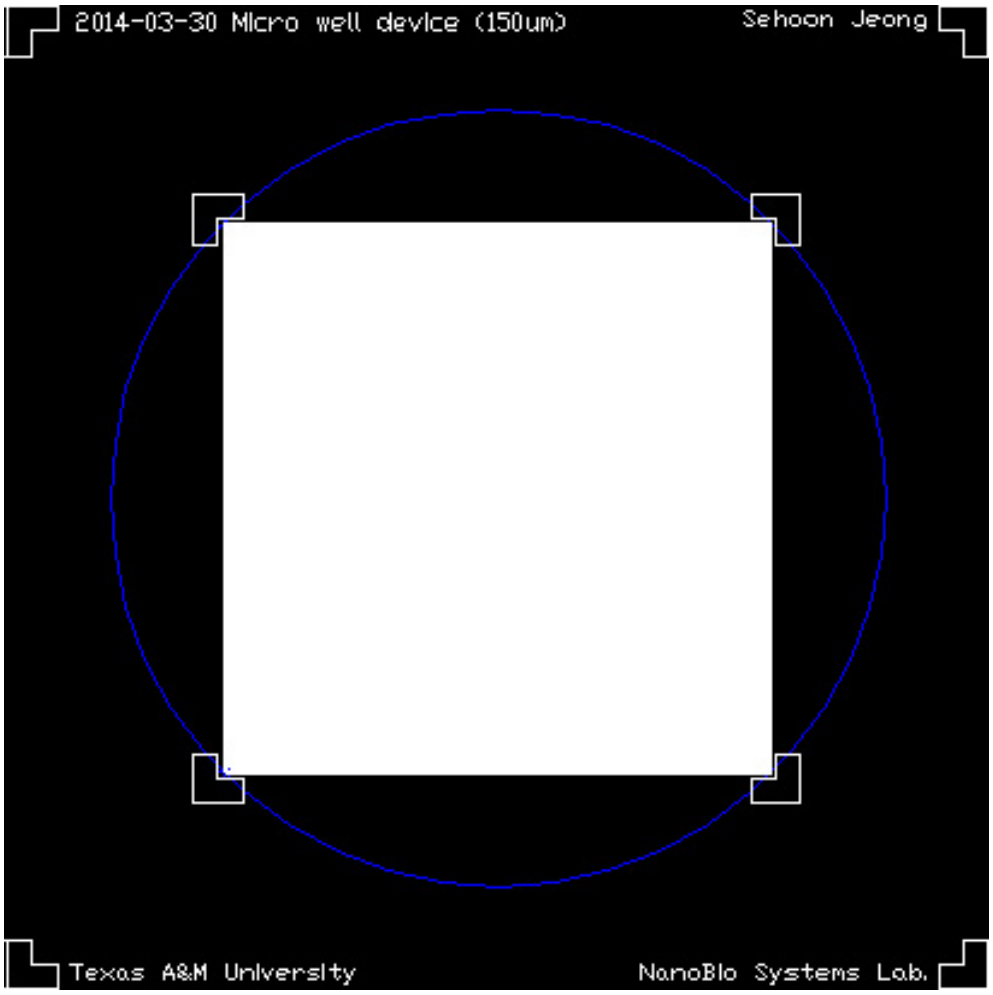


**Figure 49 Microwell array for Ø150 µm sized neural aggregate**

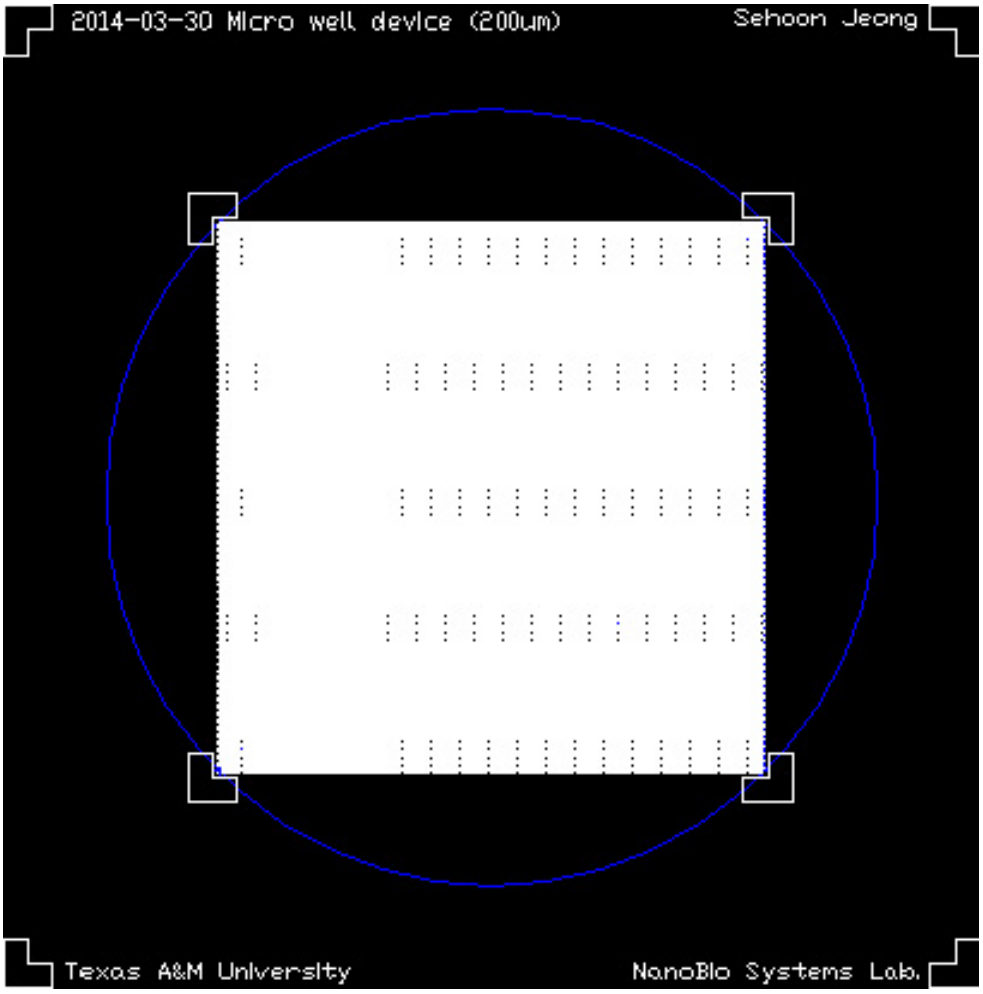


**Figure 50 Microwell array for Ø200 µm sized neural aggregate**

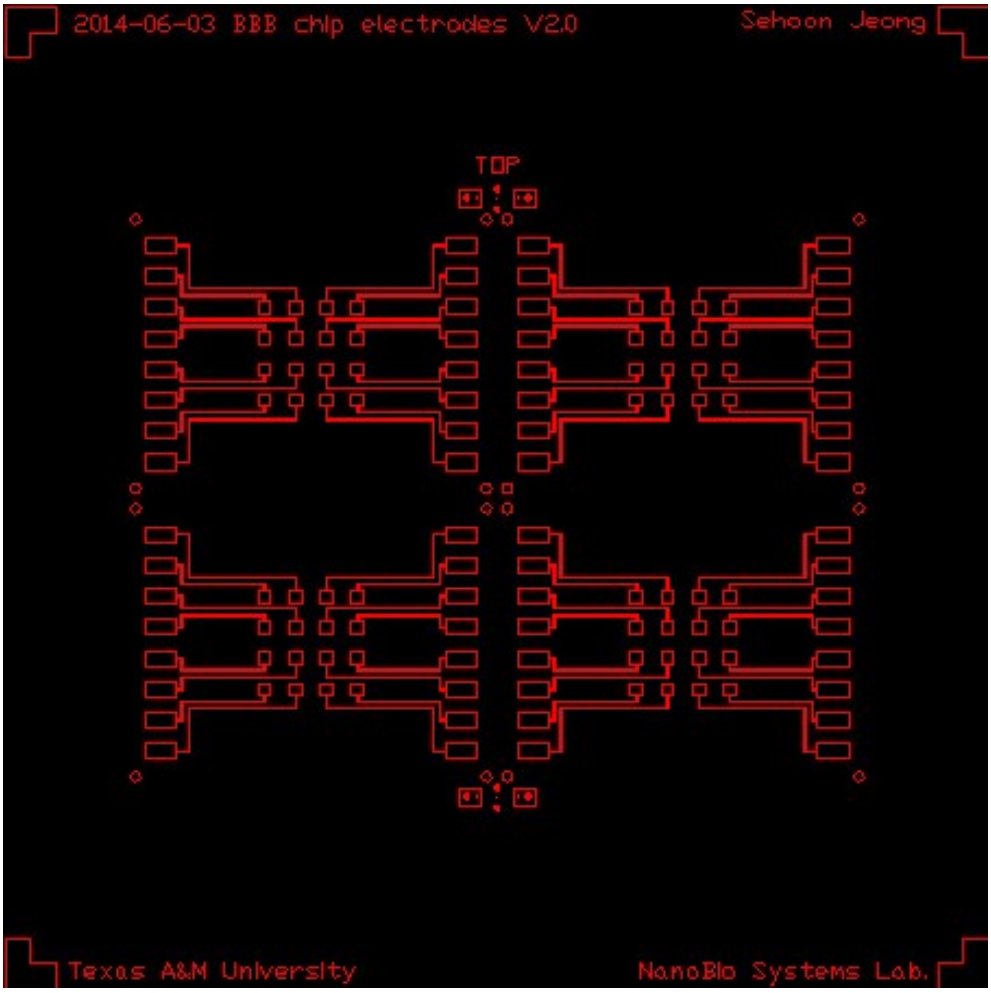


**Figure 51 TEER signal recording microelectrode array**

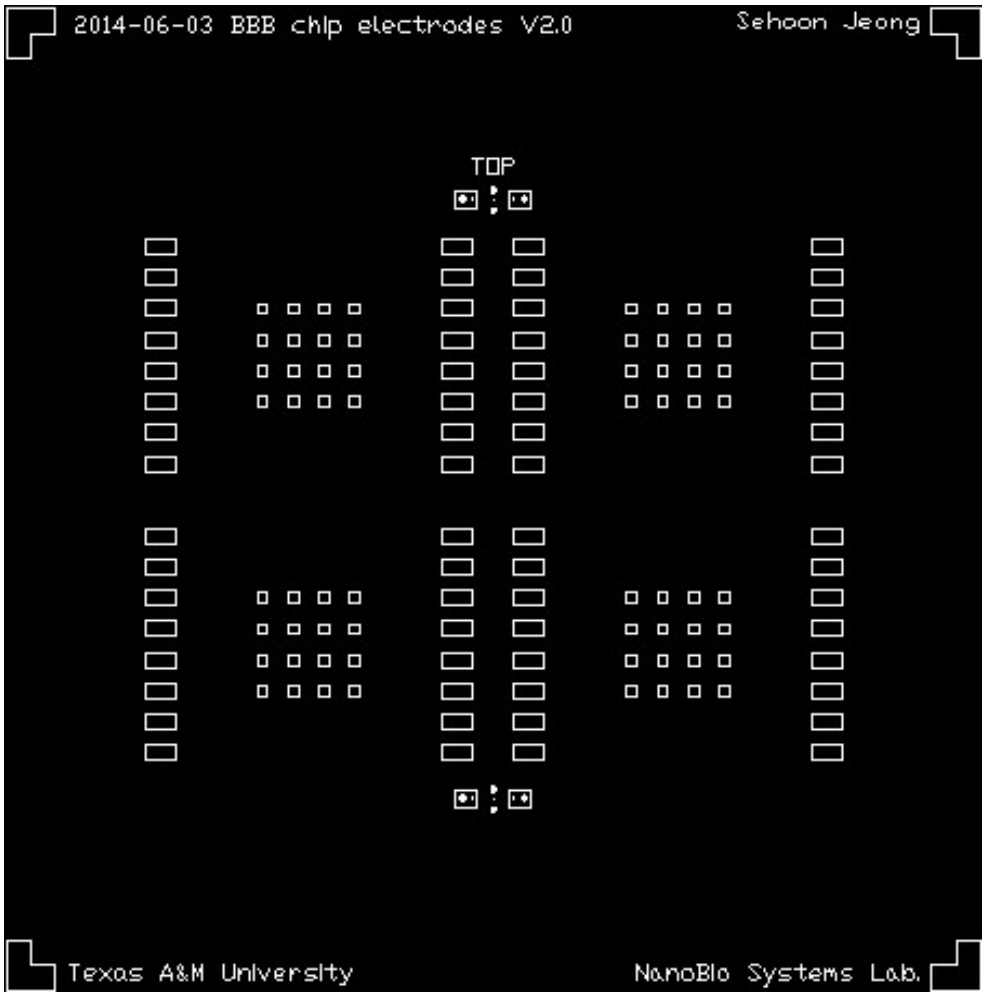


**Figure 52 TEER signal recording microelectrode array site opening**

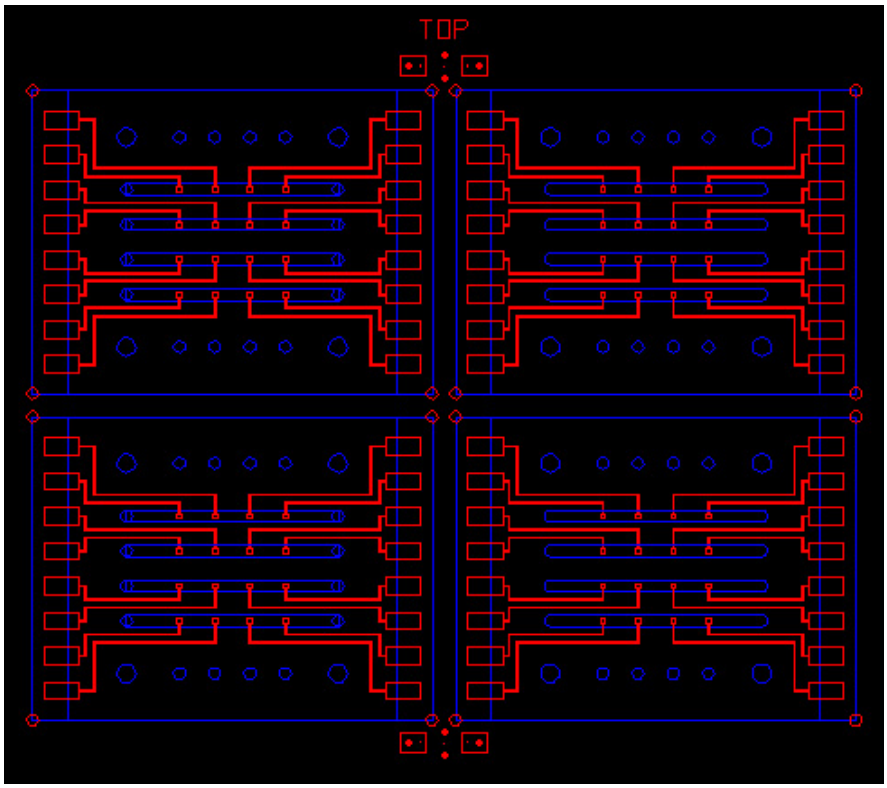


**Figure 53 Laser cutting design for total BBB chip electrode substrates.**

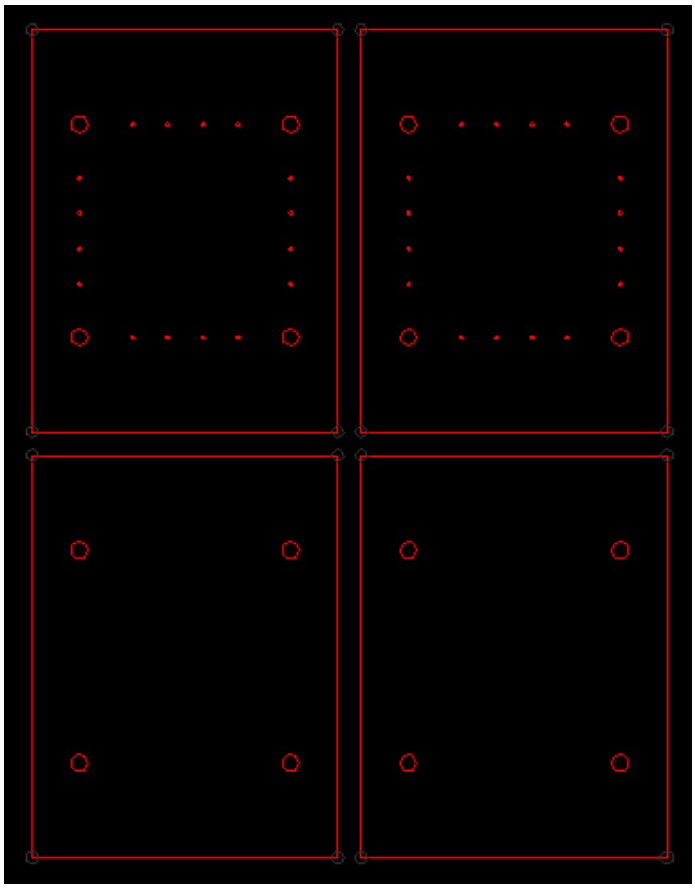

**Figure 54 Laser cutting design for BBB chip PC electrode substrates.**

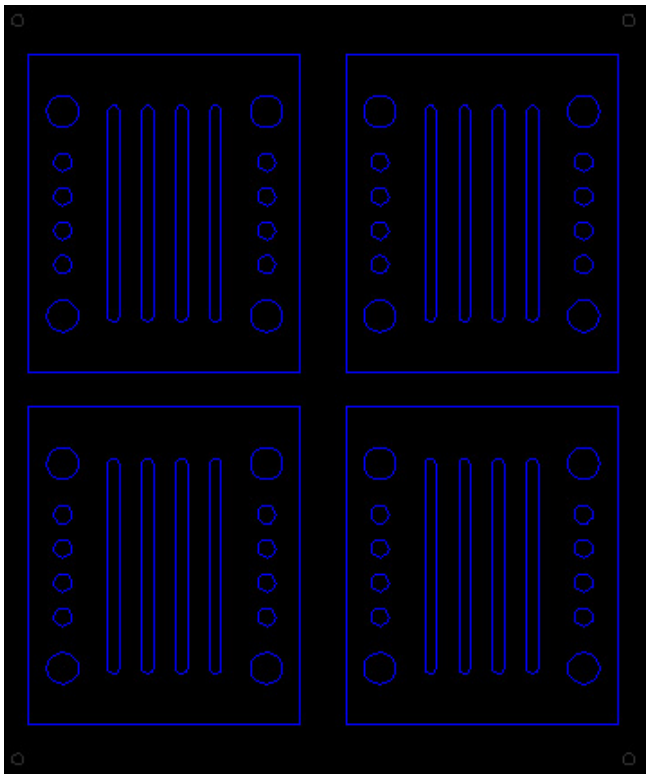

**Figure 55 Laser cutting design for BBB chip PDMS channel layers.**

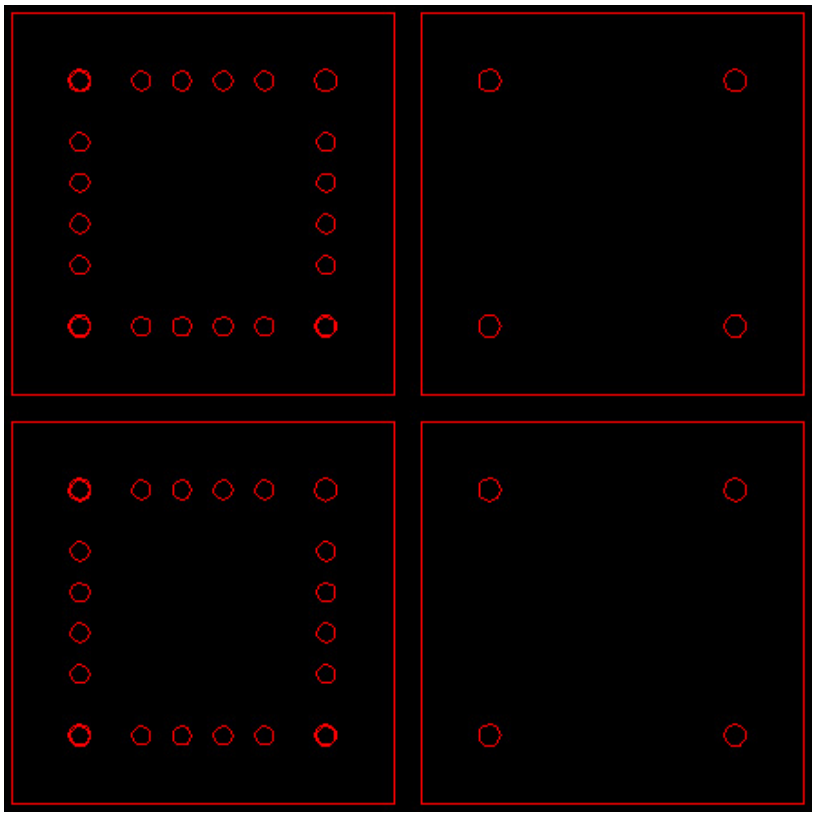

**Figure 56 Laser cutting design for BBB chip PMMA layers.**

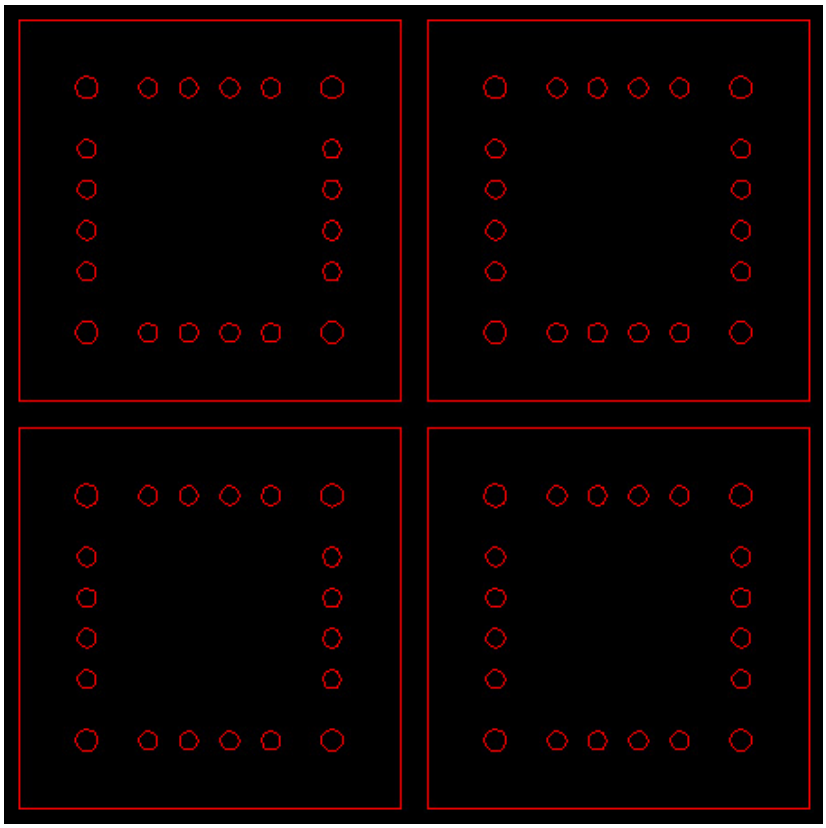

**Figure 57 Laser cutting design for BBB chip PDMS gasket layers.**

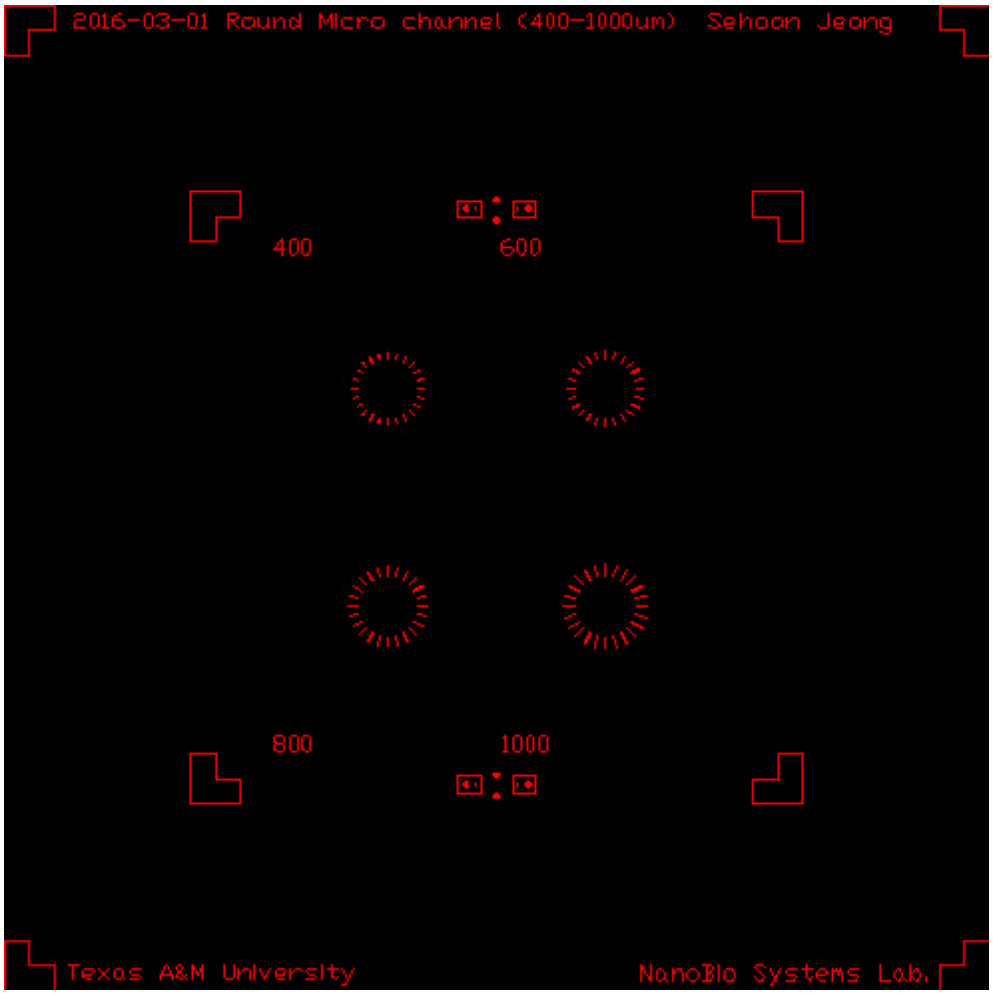


**Figure 58 Round shape SU8$^{TM}$ microchannel layer design for co-culture device.**

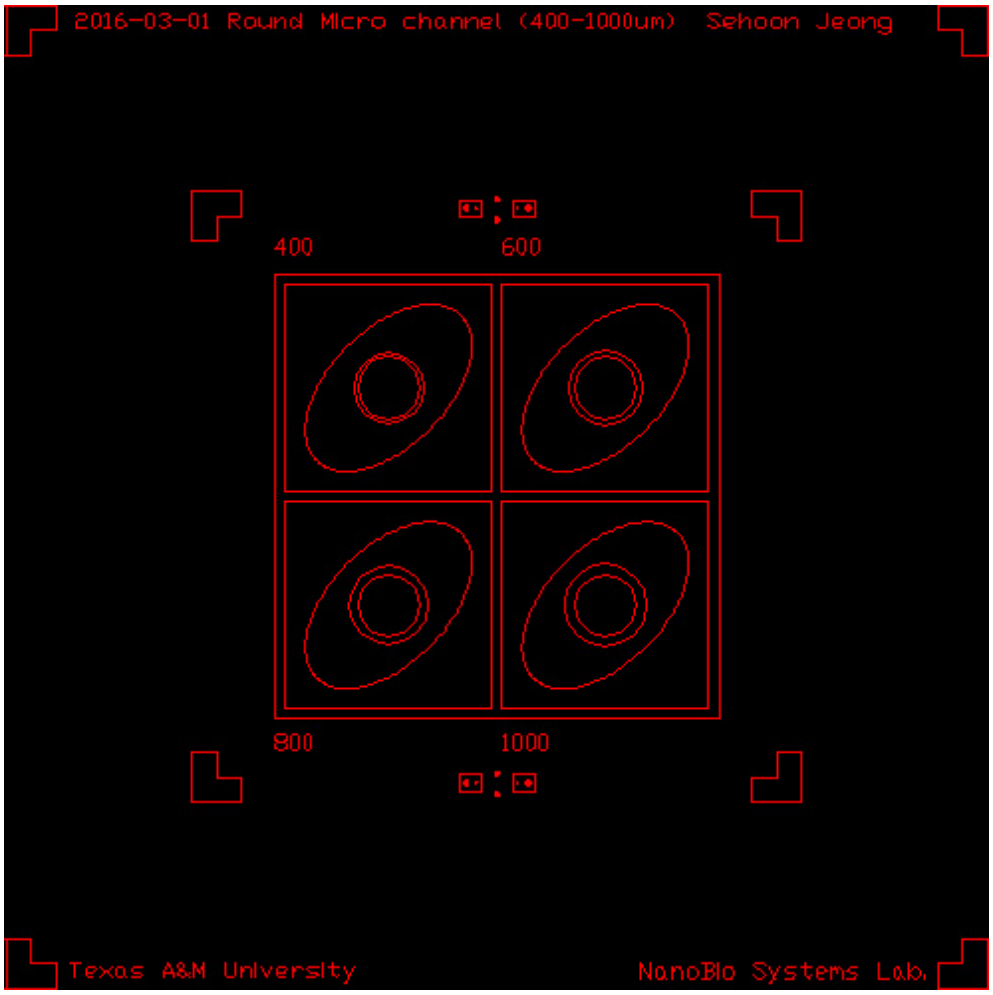


**Figure 59 Round shape SU8$^{TM}$ microchamber layer design for co-culture device.**

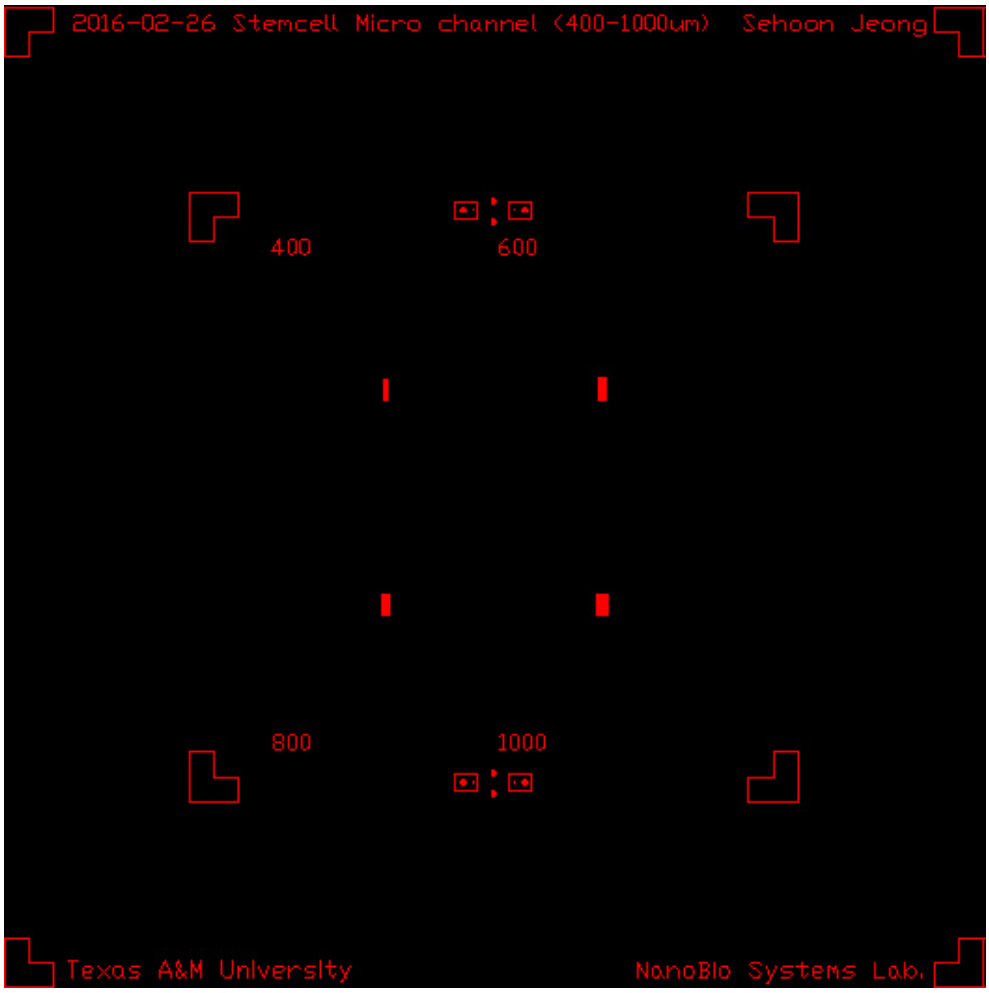


**Figure 60 Parallel shape SU8$^{TM}$ microchannel layer design for co-culture device.**


**Figure 61 Parallel shape SU8$^{TM}$ microchamber layer design for co-culture device.**

# APPENDIX B

# LABVIEW™ DESIGN

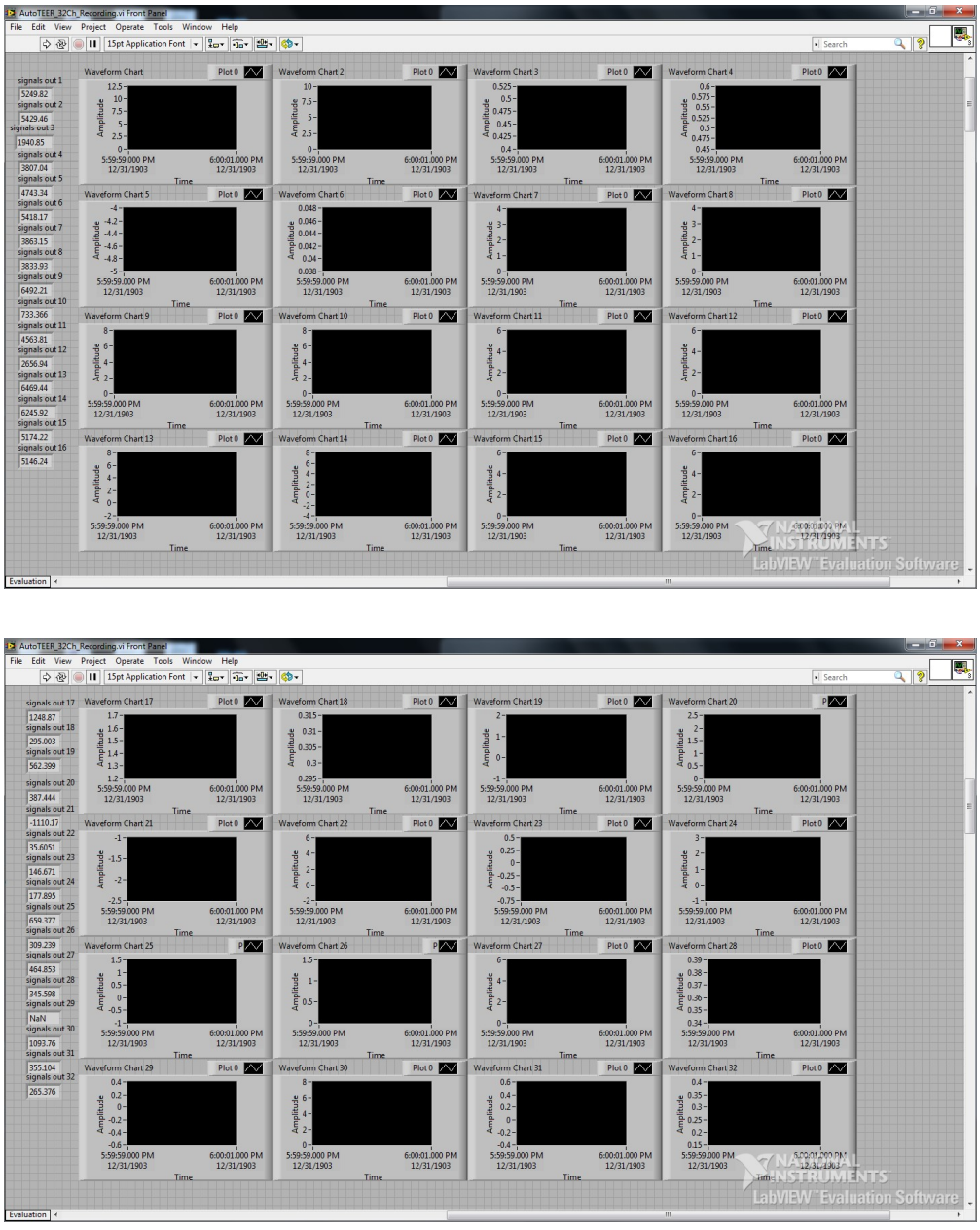





**Figure 62 Labview program for 32 channel TEER recording with the BBB chip system.**

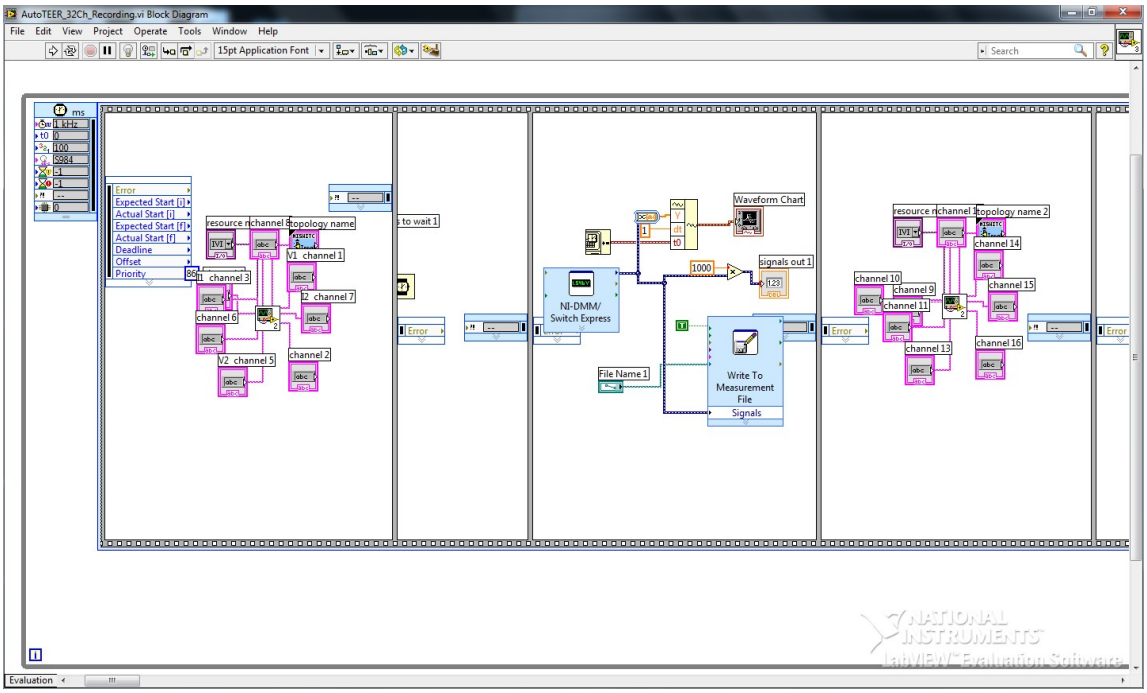


**Figure 63 Labview program block diagram for 32 channel TEER recording with the BBB chip system.**

APPENDIX C

PROTOCOL

## A. NEURAL AGGREGATE CULTURE

**Preparation**

**NBB27/DMEM**

| | |
|---|---|
| DMEM | 100ml |
| Neurobasal | 100ml |
| 1 mM Pyruvic acid | 11mg |
| 63ng/ml N-acetyl cysteine | 6.3mg |
| 0.75mM GlutaMax | 750 l of 200mM stock |
| 1xSato | 2ml of 100x stock |
| 10nM d-Biotin | 5 l of 40 M stock |
| 1xB27 | 4ml |
| (5 g/ml Insulin ((first 1st week only)) | 0.2ml of 5mg/ml stock |
| 1xPenicillin/Streptomysin | 2ml |

**1xSato**

100 g/ml Apo-Transferrin

100 g/ml BSA

16 g/ml Putrescine

60ng/ml Progesterone

5.2ng/ml Sodium Serenite

In Neurobasal

**Papain solution (make fresh before you use)**

1. Dissolve 3.2mg L-Cysteine with 4ml of 10mM HEPES/HBSS w/o $Ca^{2+}$, $Mg^{2+}$
2. Adjust pH to around 7.4 (applox. 5 l 1N NaOH, check pH )
3. Add 20-30unit/ml papain.
4. Filter sterilize, and place in water bath at 37℃.

**Trypsin Inhibitor (make fresh before you use)**

1. Sterilize by filtration 0.2g trypsin inhibitor with 20ml of 10mM HEPES/HBSS w/o $Ca^{2+,}$ $Mg^{2+}$
2. Adjust pH to around 7.4 (applox. 6 l 1N NaOH, check pH)
3. Filter sterilize, and place in water bath at 37℃

**15mm coverslips**

1. Soak all coverslips in 1L grass beaker in 33% HCl for 24 hr.
2. Wash with running water for 10min.
3. Rinse with Millipore water.
4. Drain the water off.
5. Soak coverslips in 95-98% EtOH
6. Transfer coverslips to a flat plate and dry them
7. Autoclave

**Coat plate/coverslips**

1. Coat coverslips with Poly-D-lysine (100 g/ml) for 2hr.
2. Wash 3 times with sterile dd $H_2O$ and dry completely.
3. Dilute BD-matrigel growth factor reduced to 1:20 with medium in ice.
4. Coat coverslips with 300 l/well of diluted matrigel for overnight at 37℃.
5. Wash with warm PBS.
6. Wash the plate with warm sterile dd$H_2O$
7. Let it dry briefly before you use.

   Put a coated plate for 5min at the back of the hood.

   (one side at 2'30" and turn round to the other side)

   *Do not scratch by pipette when you vacuum excess water.

**Dissection**

1. Take brains from E16 Sprague-Dawley rat to dissection media (DM: 10mM HEPES/ HBSS without $Ca^{2+}$ and $Mg^{2+}$) on ice pack.
2. Remove the meninges on each brain.
3. Remove hemispheres from midbrain/hindbrain, and transfer the cleaned forebrain to new a plate with DM on ice pack.
4. Remove DM from forebrain and add 4ml of papain/ L-cystaine solution.
5. Transfer to a 50ml tube and incubate in a 37℃ water bath for 5min.
6. Remove the papain/L-cysteine solution by pipette.
7. Add 5ml Trypsin inhibitor solution and incubate for 2-3 min at 37℃ water bath.

8. Remove Trypsin inhibitor solution.

9. Repeat 7 and 8 3 times

10. Add 20ml NBB27/DMEM.

11. Triturate 20 times after clumps have disappeared.

12. Centrifuge at 100 x g for 7min.

13. Remove supernatant and wash pellet with 20ml NBB27/DMEM

14. Centrifuge at 100 x g for 7min.

15. Remove supernatant and add 10-15ml NBB27/DMEM.

16. Suspend cells and sieve through a 70 m mesh.

**Aggregate culture**

17. Suspend neurons in NBB27/DMEM- medium with 1xSato, 10ng/ml CNTF and 10M forskolin to a final density of ~$2x10^6$ cells/ml, and place 2ml into each well of a 6-well plate (uncoated).

18. Incubate overnight.

19. Use a 1ml pipette to gently resuspend once per day for 3 days, allowing the cells to form aggregates.

20. 3 days later, sieve aggregate suspension through a 200 m mesh into a 50ml tube and allow them to settle (3min).

21. Remove supernatant by pipette.

22. Wash several times with medium to remove small aggregates and dead cells.

23. Gently resuspend the aggregates in NBB27/DMEM-1xSato +10ng/ml CNTF + 10mM forskolin

24. Count aggregate density and adjust to approx. 25-30 aggreggates/50ul.

    1plate of 6well plate in 4ml DMEM/NBB27 ------approx.100agg

    50agg/10ul in count---- 30-40agg/10ul in actual number

25. Transfer to 2ml tubes (ex. make 1:5 dilution---------50agg/50ul)

    2ml tubes should be put in the hood. Do not put into the incubator.

26. Inverse the tube containing aggregates to the aggregates are distributed evenly before loading. Before plating aggregates to the coverslip, suspend up and down twice by 200ul pipette each time and load 50ul of aggregates into the center of each well. Let cells attach 4-6hr to facilitate adhesion.

27. Add additional medium (500 μl) 6hr later or the following morning.

28. Culture the neuron aggregates 12 days, changing 1/2 volume medium every 3-4 days.

29. Purify OPCs and add $4x10^4$ cells to each well of the aggregates on a 24-well plate.

## B. CNS NEURON AND OL MYELINATION CO-CULTURE

**Embyronic cortical/hippocampal neuronal culture**

***PREPARATION (1-5 days before dissection)***

**Surgical tools:** sterilize all dissection scissors, forceps by autoclave

**Wash coverslips**

Clean all cover slips as following:

-Soak all coverslips in a 1L glass Beaker in 33% HCl for at least 24 hr, optimally over the weekend. And place the Beaker (securely) on a low speed orbital shaker in hood. May save the HCl.

-Rinse with copious amounts of Millipore water. And the wash with 700ml ddH2O for three times and shake periodically to clean out all residual HCl.

-Wash with 200proof Ethanol once

-Drain excess ethanol. Can transfer to smaller Beaker here or after autoclave

-Autoclave

-Store covered with Aluminum foil in Hood

-Ready for coating

**Coat plate/cover slips:**

Coat enough plates/coverslip with *poly-D-lysine (PDL)* for 1 dissection. This is an important step otherwise neurons tend to clump.

-Dilute the 100x PDL stock with PBS and filter to a final concentration of 100ug/ml.

-Spread PDL over the surface to be coated. Use about 0.15ml/$cm^2$. Around 0.3ml/well, 1.3ml/35mm dish, 1.2ml/6well overnight in incubator.

-Coat for 2 hr at 37ºC in incubator

-Remove solution and wash 3 times with sterile $ddH_2O$

-Stored in $ddH_2O$ at 4°C or dry at RT

For PDL-laminin coating:

-After wash PDL-coated plates with ddH2O three times, let them dry

-Coat plates/coverslpis with laminin (20ug/ml in HBSS) for 2 hr at 37°C or overnight at 4°C. (do this just the day before or the same day of dissection)

-Wash with HBSS 3x and kept in HBSS at 4°C or 37°C in culture medium.

Note: *Do **NOT** let coverslip/plate dry out during the coating/washing process.*

**Equilibrate plates.devices:**

Equilibrate all coated plates and assembled devices in NB medium in incubator o/n.

**Plating Media (PM):**

PM#1 ***MEM10S:*** Minimum Essential Media (MEM), 2 mM Glutamine, 10% FBS, Pen/Strep.

Establish *mixed neuronal-glial cultures* (Tim) (Need to use AraC 5uM to block glia proliferation once astrocytes are confluent at ~1wk for 2days. Then when OLs are added, use myelination culture medium.

PM#2 ***NBB27/Glutamate:*** Neurobasal Medium, 2% B27, 1mM Glutamine, Pen/strep, 25uM glutamic acid.

Culturing fetal and cortical neurons (cell density @ 160-640cell/$mm^2$).

***DISSECTION***

**Dissection Medium (DM): HBSS+HEPES**

Use sterile ice cold Hank's Balanced Salt Solution(w/o $Ca^{2+}$, $Mg^{2+}$…) supplemented with 10mM HEPES.

Note: HEPES is better buffer for culture exposed to air.

**Sources:** E18 Sprague-Dawley rat fetuses.

1. Incubate coated plate/coverslip with Neurobasal only (no B27 etc) and incubate at 37ºC.

2. Make papain digestion solution:

-In a 15ml conical tube add a few grains (3.2mg) of L-cysteine (Sigma C-7352) to *4 ml DM*.

-Add 1N NaOH (pH7.4, test with 5ul of solution on pH test strip) and place in water bath at 37ºC.

-*Do the following step right before dissociation, i.e. after STEP 7*)

-Add 100mg papain to a final concentration of 10units/ml, and sterilize by filtration. And place in water bath at 37ºC.

3. Make trypsin inhibitor solution:

In a 50ml conical add 0.2g trypsin inhibitor (Sigma T7295) to *20ml DM* (i.e., 0.1g trypsin inhibitor for every 10ml DM (10mg/ml final conc), pH by test strip (add 1N NaOH (about 5-8ul) until pH~7.4. Fliter sterilize, and place in water bath at 37ºC.

4. Warm enough PM

5. Setup for dissection:

2 buckets of ice

Fresh tissue paper and diaper pad on bench

10cm Petri dish for uterus on bench

10cm dish with DM on ice at bench

Ice platform at microdissection scope

4-5 6cm dishes with DM on ice at scope

Sterilized scissors and forceps

95% ethanol

**Dissection**

6. Removing the embryos

-Asphyxiate rat with $CO_2$ (or dry ice in a dish and add water. Cover the cage with foil). Immediately after rat becomes motionless, take it out of cage.

-Grabbing the base of the tail and pinching the neck behind the ears, break the rat's neck

-Holding the rat by the neck, shake the animal allowing the embryos to fall downward

-Spray alcohol the abdominal region and moving up.

-Make an inch long incision starting from around the vaginal opening upwards the chest, only cutting through the skin trying not to cut through into the innards. (in a "V" pattern)

-Spread apart the skin to expose the area where the embryos are. Cut through the layer of tissue to expose the embryos and extract the chain of embryos. Place them in a dish of ice old DM.

-Using the micro dissecting scissors cut out the fetus carefully from the embryonic sacs by making an incision between the placenta and the fetus. Cut the cords attaching the fetuses to the placenta and place the "free" fetus into one of the 60mm dishes containing DM.

-Once all the fetuses have been removed and placed into the dish of DM switch them all to a fresh dish containing DM to keep as clean as possible (not bloody)

7. Under dissecting scope

-Transfer one head at a time to fresh DM in 6cm dish on ice platform

-Peel away skin and skull, scoop out brain and discard the scull

-Transfer brain to fresh DM in 6cm dish in ice bucket

-Repeat for each head

-Remove meninges for all the brains at once, remove hemispheres from midbrain/hindbrain, and transfer the cleaned cortices/hippocampus to a new plate with DM on ice.

8. Dissociation and plating

-Add 20mg/ml papain to the L-cysteine solution and place in water bath at 37ºC for a couple of minutes (until papain dissolves)

-Use 10ml pipette to transfer cortices/hippocampi to 15ml conical

-Filter sterilize papain/L-cysteins solution into fresh 15ml conical

-Remove excess 1x DM from cortices/hippocampi

-Add 4ml the papain/L-cysteine solution

-Invert Falcon

-Place in water bath for ***5 min EXACTLY***

-Remove papain/L-cysteine solution from cortices/hippocampi

-Add 5ml Trypsin Inhibitor solution

-Invert falcon

-Remove trypsin inhibitor solution

-Add 5ml fresh Trypsin Inhibitor solution

-Invert falcon

-Place in water bath for 2-3 minutes

-Repeat 2-3 min water bath wash for additional 2 washes (+5ml Trypsin solution ea time)

-Remove trypsin inhibitor solution

-Add 5ml warm PM#2

-Triturate with a 5ml pipette or a glass Pasteur pipette (narrowed by flaming) until all clumps have disappeared

- ✓ Triturate 10-20 times after clumps have disappeared

- ✓ Add 10 ml warm PM#2 for a total volume of 10ml
- ✓ Pass through 70um cell sieves
- ✓ Count live cells
- ✓ Dilute cells in warm PM#2 to appropriate density for plating:

*For a 24well plate:*

160cell/mm$^2$ => 0.3x10$^5$/0.5ml/well => 0.6x10$^5$ cell/ml

640cell/mm$^2$ => 1.28x10$^5$/0.5ml/well => 2.5x10$^5$ cell/ml

*For microfluidic platform (square)*

3x10$^6$ cell/ml => 3000cell/ul (density still low, could double)

Use 6x10$^6$ cell/ml

-suck out medium, but do not dry up the main chamber.

-add 20ul cell suspension into one reservoir and put device in incubator for 10-15min to facilitate cell attachment,

-add 150ul of PM#2 to the same reservoirs. Then fill all other reservoirs.

*For PDMS microdevice (circular)*

Inner circle d=4mm punched hole d=3.5mm, area=9.62mm$^2$

Barrier, w=800um

Overhang connecting to open culture wells d=7mm (punched 6mm)

Height of the ring device, h=3mm

High density neurons, 640cell/mm$^2$,

i.e., 6200cell/hole/10ul, $6.2x10^5$ cell/ml

(after cells are attached, fill the hole with 10-20ul medium)

*For PDMS mirodevice (tricircle, center circle)*

Inner circle, d=8mm, area=50.24 $mm^2$

Very low density neurons, 80cell/$mm^2$, use 10 ul of the $4x10^5$cell/ml

Low density neurons, 160cell/$mm^2$, i.e., 8000cell/well/20ul, $4x10^5$cell/ml

High density neurons, 640cell/$mm^2$,

i.e., 32000cell/well/20ul, $1.6x10^6$ cell/ml

(after cells are attached, fill the well with 10-20ul medium)

- Replace media with fresh, warm PM 1-1.5 hours after plating

-If culturing for extended periods of time, replace half of the media with fresh, warm culture medium on day3-4 with NBB27 (no glutamate), pulse treat with 10uM FUDU when change medium.

-Thereafter, half change medium every 3-4 days (twice a week, and once per week for 160cell/$mm^2$ density) with one or two more cycle of pulse treatment with FUDU.

-AraC (5uM final; 1mM stock); treat for 3d (72hrs) and change to NBN27 (wo glutamate) media

Use *DMEM10S* for mixed glia+neuron, up to 4days, then add 10uM 5-fluoro-2'-deoxyuridine for 2 days to pulse block glial cells and fibroblasts (complete medium change for 1st FUDU treatment). Do total three cycles of pulse (1/2 medium changes) with each 2 days (so neurons are in culture for total ~2wks, but at least 4-6 days before OLs) before adding OLs, at which time change medium to *D/N* medium.

Use *NBB27* for neuron culture, after 4days use FUDU to purify neurons, after which one more cycle of pulse treatment (but at least 4-6 days before OL plating so pre-OLs will not be exposed to too much FUDU). After addition of preOLs use *DMEM/NBB27 (D/N)*

Use *DMEM/NBB27* for myelination co-cultures

***PreOL PLATING***

- Prepare OLs as per protocol. 1-2wk after Neuron culture
- After Petri dish absorption, wash and counting,
- Plate $8x10^4$/ml=$4x10^4$/24well or circular PDMS devices or 1-$1.5x10^4$/well with PDGF.
- Plate $6x10^6$/ml, 20 ul/ea reservoir for regular square devices in DMEM/NBB27 w/ or w/o growth factors.

***MAINTENANCE***

-Check devices everyday to ensure enough medium in the reservoir, if not add medium back

-Half change media with fresh, warm culture medium, twice a week or once a week depending on cell density (once per week for 160cell/mm$^2$ density)

Use *DMEM/NBB27* for mixed glia+neuron+OLs (half medium change)

Use *DMEM/NBB27* for neuron+OL myelination co-culture

-Various growth factors or other compounds will be added to medium based on experimental design.

***MEDIUM RECIPE***

**Plating Culture Media:**

*1)* ***DMEM10S*:** DMEM, 1mM pyruvate and 1mM Glutamine, 10% FBS, Pen/Strep.

After Adding preOLs, use D/N medium

***DMEM10S*:**

| | |
|---|---|
| DMEM (with 1mM pyruvate and with 1mM glutamine) | 200ml |
| GluMAX | 2ml of 100x stock |
| FBS | 21ml |
| Pen/Strep | 2ml of 100x stock |

Mix, store at 4ºC.

**2)** ***NBB27/Glutamate (D/N):*** Neurobasal Medium, 2% B27, 1mM GluMAX, 60ug/ml NAC (N-acetyl cysteine, 100x stock 6.3mg/ml in H2O, prepare fresh or at least weekly)

***NBB27/Glutamate:***

| | |
|---|---|
| Neurobasal Medium | 200ml |
| B27 | 4ml (50x stock aliquots in -20ºC) |
| L-glutamine 2mM | 2ml (filtered 100x stock) |
| L-Glutamic acid 25uM | 2ml (filtered 100x stock) |
| Pen/Strep | 2ml of 100x stock |

Mix, store at 4ºC.

**Maintenance Culture Medium:**

Use sterile techniques.

***NBB27:***

| | |
|---|---|
| Neurobasal Medium | 20ml (use 20ml aliquots in -20ºC) |
| B27 | 400ul 50x stock (400ul aliquots in -20ºC) |
| GluMax (0.5mM) | 50ul 100x 200mM stock (-20ºC) |
| N-acetyl cysteine | 200ul of fresh 100x stock (filter sterilize, 6.3mg/ml in $ddH_2O$) |

Mix, store at 4ºC.

***Note****:* NB and B27 are not very stable, only make enough for 1-2 week.

***DMEM/NBB27:*** DMEM/Neurobasal (1:1 vol:vol), 2% B27, SATO, 0.5mM GluMAX, 60ug/ml NAC and 10nM D-Biotin.

For 20ml:

| | | |
|---|---|---|
| DMEM (with 1mM Pyruvate, 1mM GluMAX) | 10ml | (see below) |
| Neurobasal | 10ml | |
| B27 | 400ul | 50x stock (aliquots in -20ºC) |
| N-acetyl cysteine | 200ul | of fresh 100x stock (described above) |
| Sato | 200ul | of 100x stock (see below) |
| Insulin 5ug/ml | 20ul | of 1000x stock |
| D-Biotin | 5 ul | of 4000x stock |
| Pen/Strep | 0.2ml | of 100x stock |

Mix, store at 4ºC.

***DMEM with Pyruvate and gluMAX***

Similar as for making BDM except that glutamine concentration is lower here.

| | |
|---|---|
| DMEM (w/o pyruvate, w/o glutamine) | 200ml |
| Sodium pyruvate(1mM) | 22mg/200ml |
| GluMAX (1mM) | 1ml (of 100x, 200mM stock) |

Mix and filter, store at 4ºC.

***Sato 100X Stock Solution (from Li)***

Substance Add to 40 ml Neurobasal medium (NB) to prepare 100X stock:

| | | |
|---|---|---|
| 1) Transferrin (Sigma T2252) | 100 ug/ml | 400 mg |
| 2) Crystalline BSA (Sigma A9647) | 100 ug/ml | 400 mg |
| 3) Progesterone(Sigma P8783) | 60 ng/ml (0.2 uM) | 10 ul of stock |
| (stock is 2.5 mg/100 ul ethanol) | | |
| 4) Putrescine (Sigma P7505) | 16 ug/ml | 64 mg |
| 5) Sodium selenite (Sigma S5261) | 5.2 ng/ml | 52 ul of stock |
| (stock is 4 mg/100 ul 0.1 N NaOH plus 10 ml NB) | | |
| Not added (Barres) 6) Thyroxine (T4; Sigma T1775) | | 40 ng/ml |
| | 10 ul of stock (stock is 0.8 mg/100 ul of 0.1 N. NaOH) | |
| Not added (Barres)7) Tri-idothyronine (T3; Sigma T6397) | | 30 ng/ml |
| | 10 ul of stock | |
| (stock is 0.8 mg/100 ul of 0.1 N. NaOH) | | |

The working stocks for substances 3,5,6, and 7 are thrown out and prepared fresh each time a new batch of 100X Sato is made. Gently dissolve all of the above in 40 ml of NB and aliquot at 400 ul in small eppendorf tubes. Freeze and store at -20$^{o}$ C. This is 100x Sato.

## C. CELL IMMUNOSTAINING

### Preparation

Coverslip preparation:

# 1.5 coverslip. In general you should use #1.5 coverslips as most microscope objectives are designed to work optimally with these.

Size of coverslip. Round 18 mm coverslips in a 12 well plate work well, or 12 mm coverslips in a 24-well plate, or 22 mm square coverslips/25mm round coverslips in a 6-well plate/35mm culture dishes.

Sterile coverslip.

Coating of coverslip. Many cell lines will grow well on uncoated coverslip but some do better with coated coverslips.

### Cell preparation:

Transfer your cells on the coverslip in plates/culture dishes and culture them (e.g. overnight) so they are well adhered and reach 50-70% confluency.

### Reagents preparation:

Note: Always filtration or centrifuge solutions before use to avoid precipitation.

Phosphate-buffered saline (PBS)

Serum from the species that the secondary antibody was raised in

Fixatives: 4% Paraformaldehyde

Triton

Permeabilization helps the antibodies get into the fixed cells. Cell surface proteins don't require much/any permeabilization. If the target protein is expressed intracellularly, it is very important to permeabilize the cells.

Triton X-100 is the most popular detergent for improving the penetration of the antibody. However, it is not appropriate for the use of membrane-associated antigens since it destroys membranes.

Prepare 0.3 % PBS-T by mixing with 0.3% Triton X-100 in PBS

Prepare primary-antibody in 5% goat-serum/PBS-T, dilute antibodies according to the recommended manufacturer specification data sheet.

Selection of the secondary antibody is depended on the donor species of the primary antibody and the desired fluorochrome.

**Procedure**

It is advisable to run the appropriate negative controls. Negative controls establish background fluorescence and non-specific staining of the primary and secondary antibodies.

- Rinse cells with PBS 3 times

- Fixation: fix the cells in 4% paraformaldehyde (PFA) (20 min) in PBS (freshly prepared) at RT.

- Wash the samples with PBS 10 min x3

- Permeabilization & Blocking: incubate the cells for 60min with 5% goat-serum in PBS-T to block unspecific binding of the antibodies.

- Primary Ab: Incubate cells the primary antibody dilution in 5% goat-serum in PBS-T (keep cells dark in a humidified chamber) overnight at 4°C.

If it is desirable to examine the co-distribution of two different antigens in the same cell, a double immunofluorescence procedure may be used. Cells may be incubated simultaneously with two primary antibodies, provided they are monospecific and can be distinguished with secondary antibodies conjugated to different fluorochromes (or with primary antibodies directly conjugated to different fluorochromes).

- Wash the samples with PBS 10min x3 on shaker

- Secondary antibody: incubate cells with the secondary antibody in 5% goat-serum in PBS-T for 60 min at RT (keep cells dark in a humidified chamber). Most secondary antibodies can be used after 1:200-1:1000 dilution

Note: If the primary antibodies are already conjugated to a fluorochrome, incubation with secondary antibody is not necessary.

- Wash the samples with PBS 10min x3.

- Counter staining: stain nuclear with DAPI or Hoechst for 5-10min.

- Wash the samples with PBS 10min x3.

For long-term storage, after sealing, store the slide upright in a covered slide box at 4°C.

## D. SU-8™ FABRICATION PROCEDURE

**For SU-8™ 2075**

**Spin-coating procedure**

-Pour Ø 3-4 cm size of volume of SU-8 2075 on Si wafer

Do not pour a lot of SU8. Due to the high viscosity of SU8, after finishing a step of spin-coating there may be unwanted SU-8 remaining in the area on the edge of the Si wafer, which can cause uneven coating later.

-Start spin coating RIGHT AFTER pouring SU-8.

*-Properly spread it out on the Si wafer by slowly rotating the wafer by hand until making SU-8 about Ø 6-7 cm sized round.*

-Spin-coating: Based on spin-coater in Lithobay 2 room

| | | |
|---|---|---|
| 100 um thickness | 10+10s 500 rpm | → 0+60s 1800 rpm |
| 150 um thickness | 10+10s 500 rpm | → 0+60s 1200 rpm |
| 200 um thickness | 10+10s 500 rpm | → 0+60s 950 rpm |

**Soft-Baking procedure**

-Slowly increase the hot plate temperature from 30 °C to 65 °C by each 5 °C. Do not increase the temperature drastically as it may cause cracking or bubble formation. Check the real hotplate temperature with thermometer.

-Keep the wafer on the hotplate at 65 °C for 24hrs.

-Slowly increase the hot plate temperature from 65 °C to 95 °C by each 5 °C. Again do not increase the temperature drastically.

-Keep the wafer on the hotplate at 95 °C for more than 40 min.

**UV Exposure (with Karl Suss MA6) based on film mask**

| | | |
|---|---|---|
| 100 µm thickness | → 270 mJ/cm$^2$ | |
| 100 µm thickness | → 300 mJ/cm$^2$ | over exposure |
| 150 µm thickness | → 365 mJ/cm$^2$ | over exposure |
| 200 µm thickness | → 400 mJ/cm$^2$ | over exposure |

Do measure exposure power with the UV meter and use a handheld timer to confirm the correct exposure time.

The MA6 built in timer is inaccurate for long times (more than 1min).

**Post-Exposure Baking procedure**

-Slowly increase the hot plate temperature from 30 °C to 65 °C by each 5 °C. Do not increase the temperature drastically.

Confirm the real hotplate temperature with thermometer.

-Keep the wafer on the hotplate at 65 °C for 20 min.

-Slowly increase the hot plate temperature from 65 °C to 95 °C by each 5 °C. Do not increase the temperature drastically.

-Keep the wafer on the hotplate at 95 °C for 40 min.

-Slowly cool down the exposed wafer to room temperature. Rapid cooling may cause cracking. A long delay between PEB and development may allow diffusion and reduce the resolution of the pattern.

**Developing procedure**

-Developing the wafer with Thinner type P (→EBR-10A)

-Approximate times listed below (Over developing); confirm complete development with a microscope

| | |
|---|---|
| 100 μm thickness, distance 100 μm pattern between each structure | 12 min 30s |
| 150 μm thickness, distance 150 μm pattern between each structure | 21 min 30s |
| 200 μm thickness, distance 200 μm pattern between each structure | 25 min |

-Wash the wafer with fresh Thinner type P

-Wash the wafer with IPA (Isopropyl alcohol) (White residue is an indicator of incomplete development)

-Blow dry with $N_2$ gun